CHAPTER 15

TRACE GAS EFFECTS ON CLIMATE

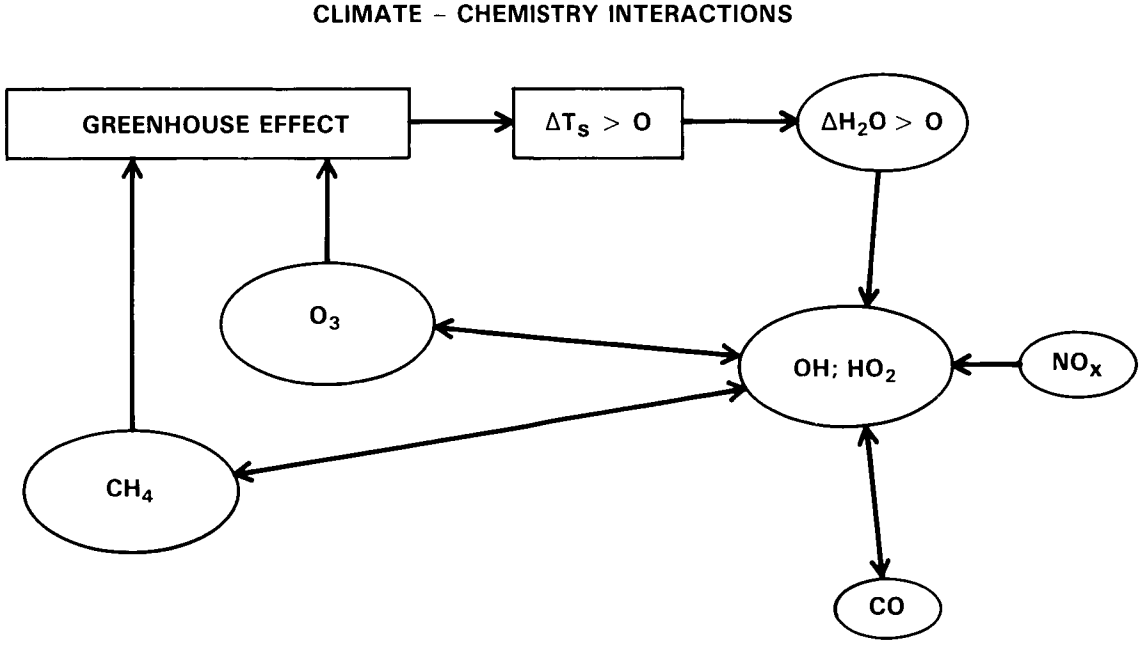

Panel Members

V. Ramanathan, Chairman

L.B. Callis, Jr.
R.D. Cess
J.E. Hansen
I.S.A. Isaksen
W.R. Kuhn
A. Lacis
F.M. Luther
J.D. Mahlman
R.A. Reck
M.E. Schlesinger

CHAPTER 15

TRACE GAS EFFECTS ON CLIMATE

TABLE OF CONTENTS

TABLE OF CONTENTS (Continued)

15.0 INTRODUCTION

15.0.1 Background and Objectives

It is now generally recognized that anomalies in radiative forcings induced by trace gases of anthropogenic origin can become the dominant factor governing climate change on decadal to longer time scales. One particular example is the greenhouse effect of CO_2 increase which has been the subject of scientific curiosity since the latter half of the nineteenth century (Tyndall, 1863; Arrhenius, 1896 and Chamberlin, 1899). Interest in the CO_2 problem gained tremendous momentum during the last two decades; this time period witnessed the development of a hierarchy of climate models with interactive clouds, oceans and cryosphere to examine the climate change that might result from CO_2 increase in the atmosphere. The last two decades also witnessed an unprecedented surge of interest in understanding the sensitivity of the ozone layer to chemical perturbations. The combination of these two developments gave rise to a series of scientific discoveries (see WMO, 1982).

First was the finding that the greenhouse effects of many polyatomic trace gases (e.g., CFCs,) were greater than that of CO_2 increase on a molecule per molecule basis. To cite one example, addition of one molecule of $CFCl_3$ (CFC11) or CF_2Cl_2 (CFC12) to the atmosphere was calculated to have the same surface warming effect as that due to an addition of 10^4 molecules of CO_2. Subsequently, it was uncovered that perturbations in stratospheric ozone can have perceptible effects on tropospheric climate through radiative-dynamical interactions between the stratosphere and troposphere. Furthermore, tropospheric ozone, which until recently was assumed to have negligible climate impact, was shown to be very effective in enhancing the greenhouse effect. Over the years, other gases (CH_4, N_2O, to cite a few) were added to the list of important greenhouse gases, and the list is still growing. Finally, it has been estimated that if the present rates of growth in the concentration of numerous trace gases continue unabated for the next several decades, the surface warming due to trace gases could surpass the observed temperature changes of the past century. In such estimates, the combined effect of increases in trace gas amounts (other than CO_2) was comparable to the greenhouse effect of CO_2 increase. The estimated effects on stratospheric climate were also substantial and far exceed the decadal scale natural variations. General circulation model studies suggested that the tropical tropopause temperatures are sensitive to perturbations in ozone and CFCs.

In effect, these unexpected developments forced the scope of the problem dealing with the greenhouse theories of climate change to be broadened from the CO_2-climate problem to the trace gas-climate problem. This broadening of the scope of the problem posed a number of new theoretical, modeling and observational challenges that could be largely ignored when dealing with the CO_2-climate effects alone. For example, we can no longer ignore the interactions between radiation, chemistry and dynamics, since these determine the stability of the O_3 layer to chemical perturbations. Radiative/dynamical interactions in the troposphere and stratosphere, as well as exchange of trace gases between these two regions, have emerged as key issues because of the potential importance of stratospheric H_2O and O_3 to climate. On the observational front, it became clear that long-term trends in CH_4, N_2O, CFCs, stratospheric and tropospheric O_3, and H_2O are just as important as the trend in CO_2 for understanding long-term climate trends. These requirements have placed extremely stringent demands on the observational platforms both with respect to instrument precision and sampling accuracies.

The two primary objectives of this report are (1) to describe the new scientific challenges posed by the trace gas-climate problem and to summarize current strategies for meeting these challenges, and (2) to make an assessment of the trace gas effects on troposphere-stratosphere temperature trends for the period covering the pre-industrial era to present and for the next several decades. We will rely heavily on the

numerous reports published on the CO_2-climate problem with respect to climate modeling issues, such as: model sensitivity; uncertainty in model results; role of feedback processes such as cloud and ice-albedo feedback. We will discuss in some detail the role of the oceans in governing the transient climate response to time varying CO_2 concentrations. Although the issue of transient climate response is discussed extensively in published reports dealing with the CO_2-climate problem, recent work has shed some new light onto this issue. Furthermore, the transient climate response is a crucial issue for assessing the trace gas effects on past and future temperature trends.

15.0.2 Observed Temperature Trends and Theories of Climate Change

The most frequently used index of climate change is the observed trends in surface-air temperature over the land areas of the globe. The instrumental record of surface-air temperature has recently been extended backwards in time to the year 1860 by Kelly *et al.* (1984). Kelly *et al.'s* time series of annual land averaged (Northern Hemisphere only) surface-air temperature is shown in Figure 15-1. The coldest decades in the record occur prior to the 1900's and the warmest decades are centered around the 1940's. The cooling trend that began around the 1940's ended in the 1970's, and temperatures during the early 1980's are comparable to the peak temperatures registered during the 1940's. Overall, the post-1940 period has been consistently warmer than the pre-1900 period. This tantalizing feature has given rise to numerous theories and plausibility arguments of climate change, most of which involve the observed increase in CO_2 and its greenhouse effect.

Various factors that govern climate change on decadal to longer time scales have been uncovered. Many of the factors fall under the category of externally (external to the climate system) induced variations in the climate forcing terms. The first set of factors involves global scale changes in the radiative heating such as due to: trace gases including CO_2, frequency of volcanic events and variations in solar insolation. Factors involving regional scale changes include changes in radiative forcing (turbidity, deforestation and desertification), thermal forcing (urban heat island) and thermodynamic forcing (alteration of evaporation and precipitation by deforestation is one example). Decadal scale climate change may also result from internal fluctuations in the interactions within the land-ocean-cryosphere-atmosphere system. Such internal fluctuations include variations in ocean heat storage, sea-ice and glaciers.

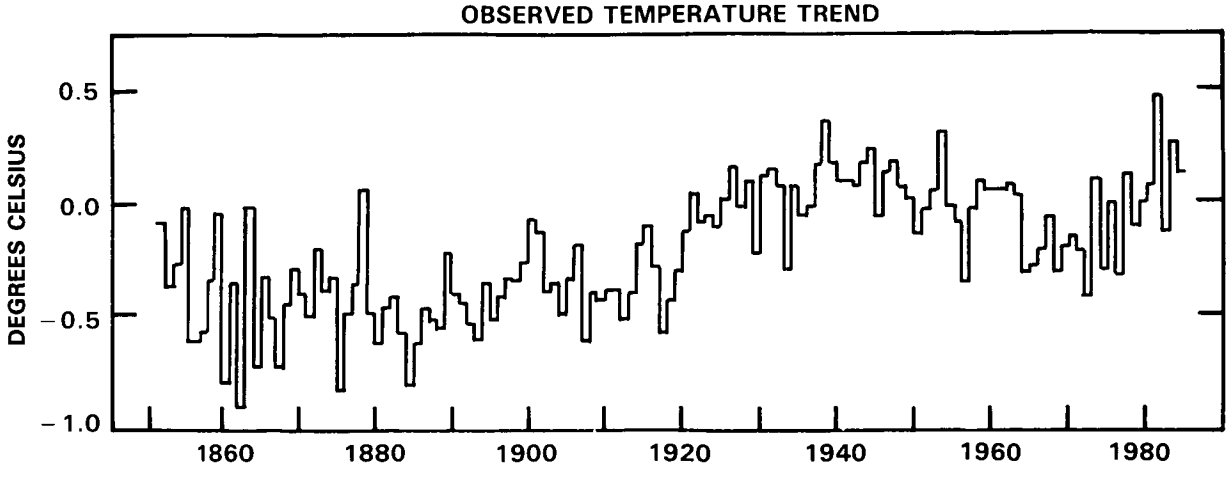

Figure 15-1. Observed surface-air temperature trends for land masses of the Northern Hemisphere (Kelly *et al.*, 1984).

Of the various factors mentioned above, accurate determination of trends has been possible only for CO_2 concentrations (at least since the 1950's). The greenhouse effect of CO_2 has received the most attention (in the literature) as a mechanism for climate change. For all other climate forcing terms, the measurements are either non-existent or, when they exist, the accuracies are insufficient to determine decadal trends. The lack of measurements has prevented identification of the causal factors for the temperature trends of the last 125 years. Nevertheless, the magnitude of the temperature variations revealed in Figure 15-1 provides a valuable measure for assessing the importance of trace gas effects.

Stratospheric temperature trends are discussed in Chapter 14 of this report. The stratospheric temperature records that are representative of hemispheric averages are available only for the past two to three decades. This limited temperature record indicates significant decadal variations of the order of 2-5 K in the mid- to upper-stratospheric temperatures.

15.0.3 Greenhouse Theory

The greenhouse effect is best illustrated by considering the annual and global average radiative energy budget of the earth-atmosphere system. The incoming solar radiation, the reflected solar radiation and the outgoing longwave radiation at the top of the atmosphere have been determined by satellite radiation budget measurements and the values inferred from these measurements are shown in Figure 15-2. The surface-atmosphere system emits to space roughly 236 W m^{-2}, which balances the absorbed solar radiation. The emitted radiation is mostly contained in wavelengths longer than 4 μm and hence, it is referred to as longwave, infrared (IR) or terrestrial radiation.

At a surface temperature of 288 K, the longwave emission by the surface is about 390 W m^{-2}, whereas the outgoing longwave radiation at the top of the atmosphere is only 236 W m^{-2} (see Figure 15-2). Thus, the intervening atmosphere causes a significant reduction in the longwave emission to space. This reduction in the longwave emission to space is referred to as the greenhouse effect. The most important radiatively active atmospheric constituents that contribute to this greenhouse effect are H_2O, CO_2 and clouds. Together these three constituents contribute roughly 90% of the total effect and the H_2O contribution is the largest. The remaining 10% is due to O_3, CH_4 and N_2O. Climate model estimates, as well as simple back-of-the-envelope type calculations, suggest that without the greenhouse effect but with the solar absorption held fixed (at the present-day value) the global average surface temperature would be about 254 K (WMO, 1982).

The radiatively active constituents absorb as well as emit longwave radiation, but the net effect is to reduce the longwave radiation to space. The fundamental cause for the reduction is the decrease in tropospheric temperature with altitude. The radiatively active gases absorb radiation emitted by the warmer surface but emit to space at the colder atmospheric temperature; hence, the net effect is to reduce the radiation to space.

The stratospheric emission and absorption of longwave radiation make an appreciable contribution to the total greenhouse effect and, furthermore, add a considerable degree of complication to the simplified picture presented above. These complications arise because of the increase in temperature with altitude in the stratosphere and because of the non-uniform ozone mixing ratio.

When the concentration of a radiatively active gas is increased, the longwave radiation to space is diminished, which upsets the global energy balance shown in Figure 15-2. If the increase in the gas concentration does not alter the solar absorption, then the greenhouse effect will lead to an increase of radia-

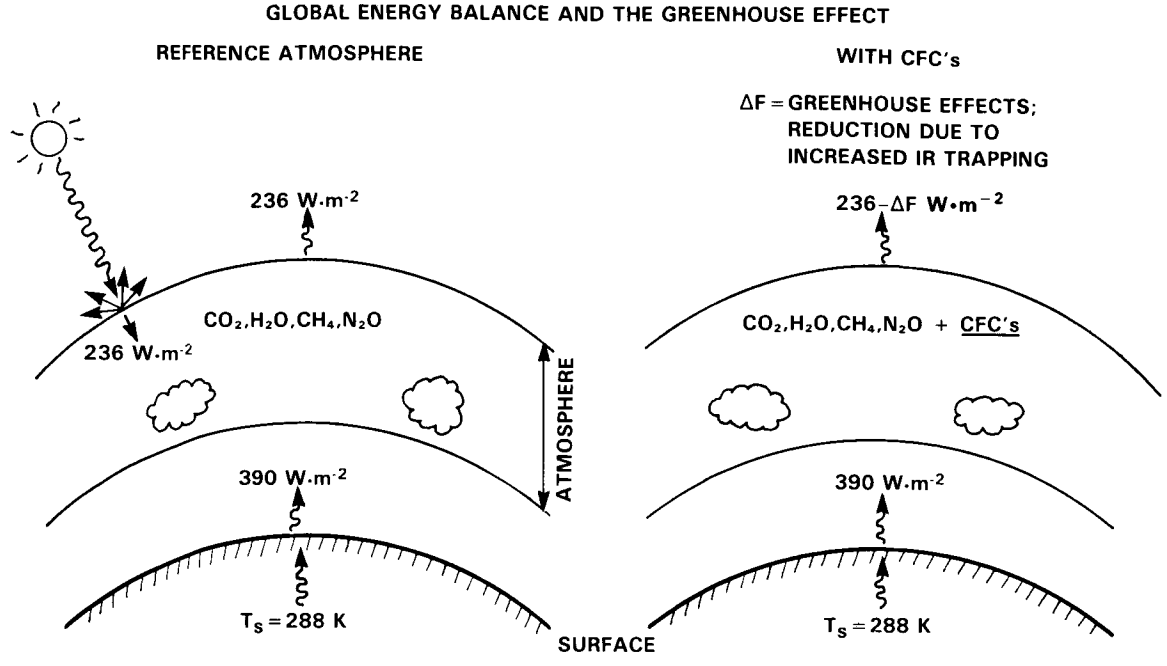

Figure 15-2. Global energy balance and the greenhouse effect.

tive energy available to the surface-atmosphere system. To maintain a balance with the net incoming solar radiation, the surface-troposphere system should warm (in response to the excess radiative energy, i.e., radiative heating) and radiate more longwave radiation to space until the longwave emission to space balances the absorbed solar radiation (i.e., until the energy balance at the top-of-the atmosphere is restored). Hence, the greenhouse theory is based on this fundamental concept of global energy balance for the surface-atmosphere system as a whole. Almost all of the modern day climate models (since the pioneering study of Manabe and Wetherald, 1967) are built around this concept of global-annual energy balance for the surface-atmosphere system. Numerous studies undertaken prior to the Manabe and Wetherald study, and a few recent studies, have misunderstood the implication of this concept of surface-atmosphere energy balance and have made erroneous interpretations of the surface temperature change due to CO_2. These studies infer surface temperature change from surface energy balance alone and ignore the energy balance of the surface-atmosphere system.

15.0.3.1 Effect of Solar Absorption

There is a frequently held misconception about the greenhouse effect. In order to draw an analogy between the CO_2-warming effect and the actual greenhouse, it is frequently mentioned that CO_2 increase enhances the greenhouse effect because it allows solar radiation to penetrate to the surface while absorbing longwave radiation. While it is true that CO_2 is nearly transparent to solar radiation, the transparency to solar radiation is not a necessary condition for enhancing the atmospheric greenhouse effect. For example, H_2O absorbs solar radiation very strongly longwave of 0.9 μm yet it is the strongest greenhouse gas. This is because almost all of H_2O solar absorption occurs within the troposphere (almost entirely within the first 5 km from the surface). Since the troposphere and surface are efficiently coupled by convection, large-scale motions and radiation, energy deposited within the lower half of the troposphere warms the troposphere as well as the surface. Hence, gaseous absorption of solar radiation in the lower troposphere

will have a surface warming effect. However, solar absorption that occurs within the stratosphere (as in the case of O_3) would have a surface cooling effect by reducing the energy available to the surface troposphere system. In summary, solar absorption by a radiatively active gas will add to or ameliorate the greenhouse effect depending on the altitude of solar absorption.

The role of climate models in the greenhouse theory is to estimate the climate response to the excess radiative heating induced by the greenhouse effect. The response, of course, depends on feedback processes involving the land, ocean, and atmosphere (including clouds). In addition to models, empirical studies based on observed satellite data (Cess, 1976) have played an important role in estimating the climate response.

15.0.4 The Trace Gas-Climate Problem

Chemical pollutants in the atmosphere can modify the climate through one or more of the following processes:

(i) Radiatively active gases: If the pollutants are radiatively active in the longwave region, they will enhance the atmospheric greenhouse effect. In particular, several polyatomic trace gases (of anthropogenic origin) have strong absorption features in the 7-13 μm (Figure 15-3). This spectral region is referred to as the atmospheric "window" since in this region the atmosphere is relatively transparent. In the 7-13 μm

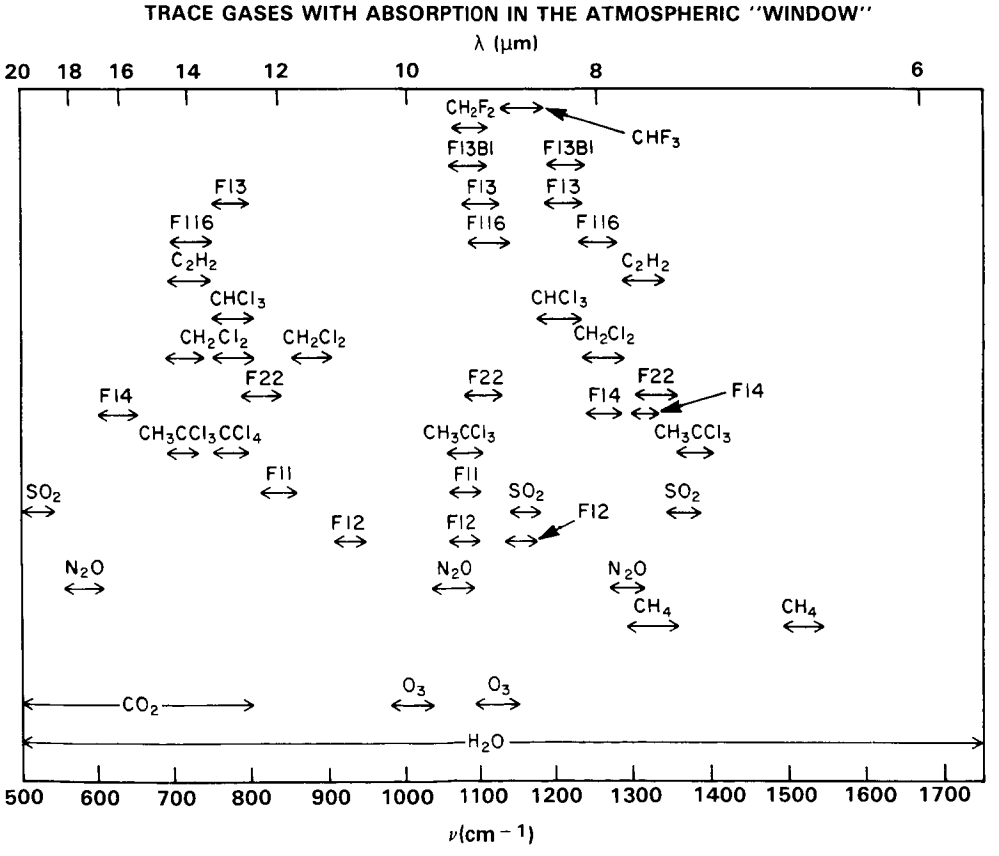

Figure 15-3. Spectral locations of the absorption features of various trace gases. (Kiehl, private communication). The spectral region between 7 to 13 μm is referred to as the atmospheric "window".

C.3

region, roughly 70-90% of the surface and cloud emission escapes to space. Consequently, pollutants with strong absorption features in the 7-13 μm region are quite effective in enhancing the greenhouse effect. In addition, perturbing gases such as CO_2 and O_3, which govern the magnitude of stratospheric longwave emission and absorption, have significant impacts on stratospheric climate.

(ii) Chemically active gases: Gases such as CO and NO, which by themselves have negligible radiative effects, can alter the concentrations of radiatively active gases such as CH_4 and O_3 by chemical interactions.

(iii) Radiatively and chemically active gases: Gases such as CH_4, are chemically active as well as radiatively active. Methane oxidation in the troposphere can lead to increased tropospheric O_3, and the greenhouse effect of the increased tropospheric O_3 can be comparable to that of CH_4 increase. Likewise, breakdown of CFCs in the stratosphere produce reactive chlorine which destroys O_3, and the effect of the O_3 decrease can either amplify or ameliorate the CFC greenhouse surface warming depending on the vertical distribution of the O_3 decrease.

(iv) Ozone change and stratosphere-troposphere radiative interactions: O_3 absorbs solar radiation in addition to absorbing and emitting longwave radiation; hence, stratospheric O_3 modulates the solar and longwave radiation reaching the troposphere. Stratospheric O_3 influences tropospheric climate through a complicated set of stratospheric-tropospheric radiative interactions in both the solar and longwave radiation regimes. The greenhouse effect of tropospheric O_3 also plays a significant role in determining the sensitivity of climate to O_3 change. Consequently, it is very difficult to generalize the nature, the sign, or the magnitude of the potential climate change due to O_3 perturbations.

(v) Radiative-chemical interactions: These effects arise because of the strong temperature dependence of the reaction rates of the various chain reactions in the stratosphere that ultimately govern the stratospheric O_3 concentration. The net effect of this dependence is such that a temperature increase (decrease) in the upper stratosphere leads to O_3 decrease (increase). Hence, stratospheric cooling due to increased CO_2 leads to an increase in O_3 which tends to compensate some of the CO_2 induced cooling. This O_3-temperature feedback results in a negative feedback on temperature perturbations in the stratosphere. Furthermore, a local O_3 decrease allows deeper penetration of sunlight and permits enhanced O_3 production at lower levels. This interaction between O_3 change and penetration of sunlight has a significant impact on the profile of O_3 change.

(vi) Interactions involving stratospheric dynamics: Large-scale motions in the stratosphere have a strong impact on some of the climate change processes described earlier. First, the climate effect of O_3 change depends crucially on the vertical and latitudinal distribution of O_3 change in the lower stratosphere which is determined by the interactions between transport and chemistry. The second interaction concerns the effect of altered dynamics due to changes in stratospheric diabatic heating (from O_3 change) on the transport of constituents. Perhaps the most important dynamics-transport effect concerns the interaction between trace gas perturbation, tropopause temperature, and stratospheric H_2O.

(vii) Climate-chemistry interactions: The greenhouse warming of the surface causes an enhancement in the evaporation of moisture from the land and oceans resulting in an increase in the tropospheric H_2O. This, in turn, through photolysis and H_2O chemistry can perturb OH in the troposphere. Since OH plays a dominant role as a cleansing and oxidizing agent for tropospheric gases (including pollutants), the altered OH can potentially perturb the concentration of radiatively active species such as CH_4 and O_3 (and possibly others).

The above description basically gives the scope of the problem that we will be dealing with in this report. The nature of the various interactive processes and the potential surface temperature effect of various radiative perturbations are described schematically in Figure 15-4. The surface temperature change shown in Figure 15-4 for O_3 is for a uniform change in O_3 within the troposphere and stratosphere. Since the surface temperature effects of O_3 depend very strongly on vertical distribution of the O_3 change, the results shown in Figure 15-4 can not be scaled for non-uniform O_3 change. Finally, the climate sensitivity to radiative perturbation depends on feedbacks involving temperature, H_2O, clouds, ice and snow cover, and on feedbacks between the ocean and the atmosphere (and possibly the biosphere). A comprehensive discussion of these topics is beyond the scope of this report and, furthermore, is unnecessary since several detailed reports (Charney, 1979; Smagorinsky, 1982) are available on this topic.

15.0.5 The Need for Model Studies

The nature of the radiative forcing arising from the myriad of interactive processes mentioned earlier is so complex that numerical models with varying degrees of complexity are needed to identify the magnitude of the various processes. The array of models needed for the trace gas-climate problem include:

(i) 1-D radiative-convective models to identify the important greenhouse effects and tropospheric-stratospheric radiative interactions.

(ii) 1-D radiative-convective chemistry models to examine the role of radiative-chemistry interaction in the stratosphere.

(iii) 2-D transport-chemistry models to estimate the magnitude of seasonal and latitude variations of O_3 change.

(iv) 2-D "fixed dynamical heating rate" models to examine the possible magnitude of temperature changes in response to trace gas perturbations.

(v) 3-D stratospheric models: These models with comprehensive treatment of radiation and dynamics can play a central role in elucidating the role of dynamics in governing the interaction between radiative perturbations and temperature perturbations. Furthermore, these models are necessary to examine the potentially important problem of how alterations in stratospheric meridional and vertical thermal gradients impact tropospheric dynamics through stratosphere/troposphere dynamical interactions. There is also another important class of 3-D models concerned primarily with atmospheric transport and chemistry. Such models are essential for evaluating the robustness of the conclusions of the 1-D and 2-D models concerning O_3 perturbations as well as for understanding the nature of interactive chemistry and transport. These 3-D models should ultimately lead to the development of self-consistent 3-D models that account for the interactions between radiation, chemistry and dynamics.

(vi) 3-D climate models with and without interactive oceans: In these models, the perturbations in trace gases are prescribed. The model determines the climate change (troposphere and stratosphere) due to the imposed perturbations. These models, in conjunction with the 1-D radiative-convective models, play a central role in the assessment of trace gas effects on climate.

More detailed discussions of these models are given in Section 15.2.

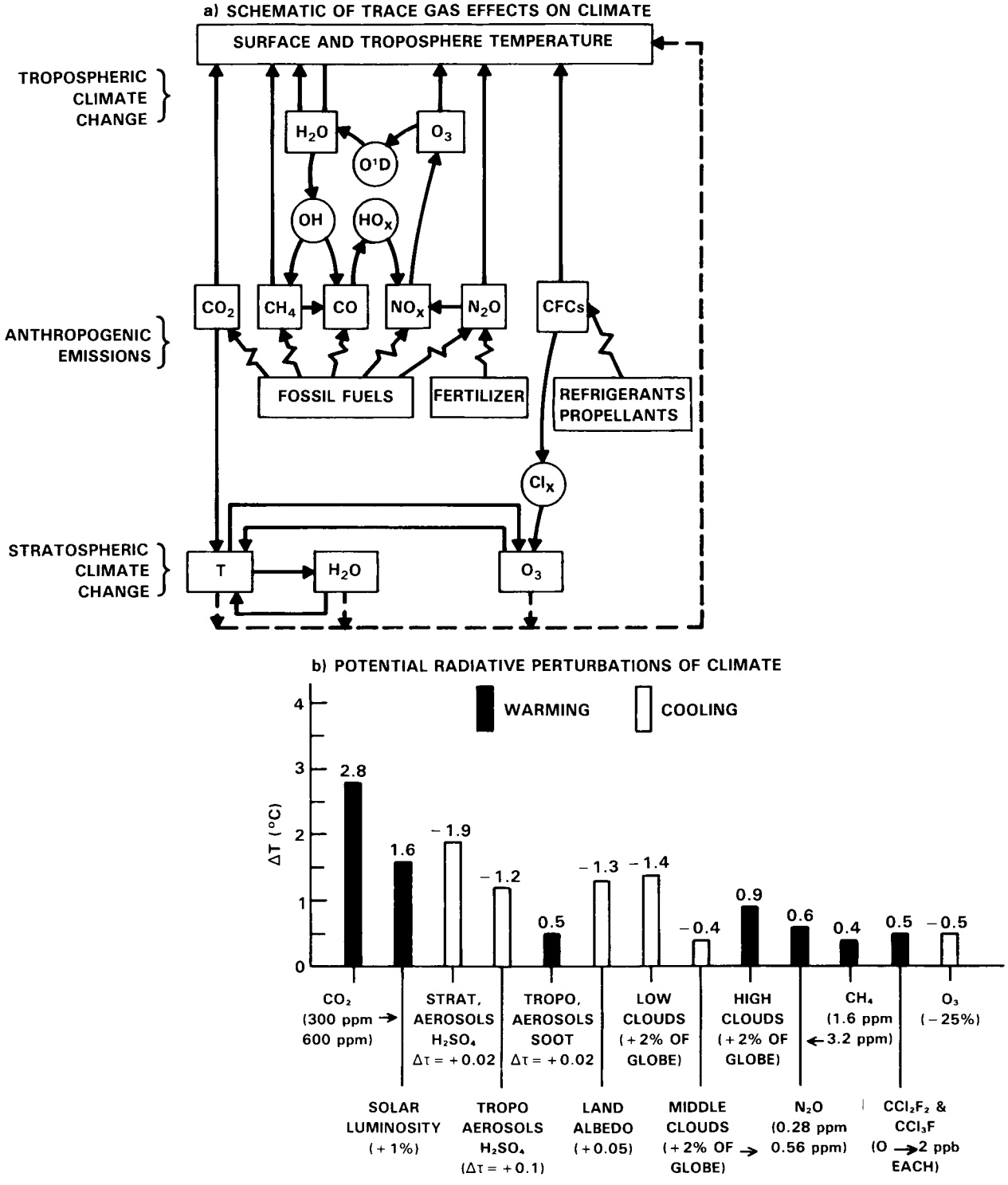

Figure 15-4. (a) Examples of climate effects due to chemically and radiatively active gases (Ramanathan, 1980). (b) One dimensional radiative-convective model estimates of surface temperature effects of various global radiative perturbations. All of the results, except for CH_4, and the figure are adapted from Hansen *et al.*, 1981. The CH_4 result was obtained as follows: The radiative forcing of doubled CH_4 as given in WMO (1982) is multiplied by the climate sensitivity of Hansen *et al.* (1981) model to obtain ΔT_S.

15.1 NATURE OF RADIATIVE FORCING

Radiative forcing due to trace gases can be considered either in terms of the changes in the fluxes of radiative energy into and out of the entire system (i.e., surface-troposphere system) or in terms of the change in the vertical distribution of the radiative heating rates. The choice between the two quantities depends on the region of interest. Within the troposphere, the vertical mixing of sensible and latent heat by convection and large scale motions is considered to be quite rapid compared to the time scales associated with radiative adjustments. As a result, the vertical distribution of the tropospheric temperature change is largely governed by dynamical processes while the mass weighted tropospheric temperature change is governed by the radiative forcing of the column. Hence, as a first approximation, we can ignore the details of the vertical distribution of the tropospheric radiative forcing and focus, instead, on the radiative forcing of the entire surface-troposphere system. Since the surface-troposphere radiative forcing is simply the change in the net radiative flux at the tropopause, it is rather straightforward to assess the importance of trace gas radiative forcing. The only minor complication is that we have to account for changes in stratospheric temperature and longwave emission in order to compute the flux changes at the tropopause. Within the stratosphere, however, time scales associated with radiative adjustments are comparable to, or faster than, those associated with dynamical processes. As a result, the magnitude of the stratospheric climate change is influenced strongly by the vertical distribution of the radiative heating rate perturbation within the stratosphere.

The trace gas radiative forcing is estimated from radiation model calculations by fixing all other parameters (e.g., temperature, humidity) in the model and then computing the changes in the radiative flux due solely to the change in the constituent of interest. Such estimates are fundamental to a proper understanding of the temperature response yielded by climate models. The longwave absorption features of the trace gases that are considered in this report are shown in Tables 15-1a and 15-1b.

15.1.1 Greenhouse Gases With Weak Solar Absorption

With the exception of H_2O, O_3 and NO_2, all other gases shown in Tables 15-1a and 15-1b have either weak or no absorption bands in the solar spectrum. Increasing the concentration of the gases with weak solar absorption subjects the troposphere to a net radiative heating accompanied by either a strong (e.g., CO_2) or weak (e.g., CH_4) longwave cooling of the mid to upper stratosphere.

15.1.1.1 CO_2 - Current Understanding and Recent Findings

The best known example of tropospheric heating/stratospheric cooling is the radiative forcing due to doubling of CO_2 (Figure 15-5). The significant enhancement of the cooling rate from the middle stratosphere to lower mesosphere shown in Figure 15-5 is due to the increase in emission to space from the wings of the non-overlapping Lorentzian lines within the CO_2 15 μm band system. The vertical distribution of the cooling rate perturbation (Figure 15-5a) is largely governed by the vertical temperature gradient (the temperature increases with altitude from 15 to about 50 km and decreases above 50 km). Since the 15 μm Planck function (i.e., CO_2 emission) increases exponentially with temperature, the cooling rate perturbation follows the temperature profile.

As opposed to the stratospheric effects, the CO_2 increase enhances the tropospheric radiative heating (Figure 15-6). The surface-troposphere radiative heating (flux change at the tropopause) has strong latitudinal gradient varying from about 4.5 to 5 W m^{-2} in the tropics to about 2 W m^{-2} in the polar region. The

Table 15-1a. Summary of Spectroscopic Data As Given in WMO (1982). More Recent Compilation Can Be Found in Smith *et al.* (1985).

Molecule	Band[1]	Rough spectral range (cm^{-1})	Band Strength[2] at 296 K (cm^{-2} atm^{-1})	Comments[3]
H_2O	rotation	0 - 1650	1306	Current improvements underway —
	υ_2	640 - 2800	257	problem of the continuum absorption
CO_2	15 μm system?	550 - 800	$\simeq$ 220	Current improvements underway
	10 μm system?	850 - 1100	0.04	
	4-3 μm system?	2100 - 2400	$\simeq$2440	
O_3	υ_3		312	V_3 band intensity to be multiplied by
	υ_1?	950 - 1200	13	1.11?. Problem of the half-widths
	$\upsilon_2+\upsilon_3-\upsilon_2$?		10	(constant with quantum?)
	υ_2	600 - 800	16	
N_2O	υ_2	520 - 660	24	Current improvements underway
	υ_1	1200 - 1350	218	Line intensities re-examined
	υ_3?	2120 - 2270	1247	
CH_4	υ_4	950 - 1650	134	Current improvements underway
CH_3D	υ_3 and υ_6	1000 - 1425	105	
SO_2	υ_3	1300 - 1400	763	Current improvements underway for
	υ_1?	1000 - 1200	87	these three bands
	υ_2?	400 - 600	97	
NO_2	υ_3	1550 - 1650	1515	Current improvements underway for
	υ_2?	600 - 900	92	these three bands
NH_3	υ_2	500 - 1350	534	Data recently revised
	rotation?	20 - 400	440	
HNO_3	υ_4	1330	680	A difficult molecule. Requires additional
	υ_2	1670 - 1750	500	work
OCS	υ_3?	1950 - 2100	1954	The fundamental υ_2 band is not compiled
	υ_1	810 - 890	27	and should be
H_2CO		compilation starting at 270 cm^{-1} plus far infrared		Bands active in the thermal IR should be compiled
HOCl	υ_1	compilation starting at 3400 cm^{-1}		Bands active in the thermal IR should be compiled
CH_3Cl	υ_1, υ_4, $3\upsilon_6$	compilation starting at 2900 cm^{-1}		Bands active in the thermal IR should be compiled. The data does exist
H_2O_2		1200-1350	318	Preliminary
C_2H_2	υ_5	640 - 810	951	Should be developed
	$2\upsilon_5 - \upsilon_5$?	640 - 820	112	
HCN	υ_2	580 - 850	822	Other bands available
C_2H_6	υ_9	700 - 950	36	Other bands available
C_2H_4	υ_7	900 - 1100	455	Preliminary
C_3H_8		735 - 760	2	Preliminary
CFCs		800 - 1200		Not yet compiled in data catalogs —
F11		850 - 1250		Laboratory spectra available
F12		1070 - 1250		
F13				

[1] A question mark indicates bands less important than the main bands but which could eventually play a role in radiation modeling (to be checked).
[2] Actually, the sum of the strengths of the lines present in the compilation (296 K). Isotopic band intensities are not added except for the estimate of a band system intensity (e.g., the 15 μm CO_2 system).
[3] Most comments were taken from L.S. Rothman (private communication).

Table 15-1b. Absorption Features of Atmospheric Trace Gases — More Recent Compilations.

Molecule	Rough Spectral Range (cm^{-1})	Band Intensity (cm^{-1} (atm cm)$^{-1}$ 296K) Measurement Range	Recent Value	Reference*
1. CFCs				
$CFCl_3$ (F11)	800–900	1540–1828	1828	K,P,S
	1050–1100	531–721	679	
CF_2Cl_2 (F12)	875–950	1265–1490	1446	K,P,S
	1060–1125	1141–1226	1141	
	1125–1175	728–821	767	
CF_3Cl (F13)	750–825	116–145	116	P
	1075–1125	1758–2311	1758	
	1175–1240	2116–2767	2116	
CF_4 (F14)	600–650	39–57	39	P,S
	1250–1300	3850–5472	5472	S
$CHClF_2$ (F22)	780–840		219	N;R
	1080–1140		637	
	1280–1340		101	
C_2F_6 (F116)	880–740		135	P
	1080–1150		975	
	1220–1280		3374	
2. Others				
CCl_4	730–810	1214–1869	1325	P
$CHCl_3$	740–820	797–1107	930	P
	1190–1250	129–190	129	
CH_3CCl_3	700–750		277	N;R
	1050–1110		154	
	1360–1410		13	
CHF_3	1110–1160	2224–3540	2693	P,S
CH_2F_2	1060–1120	1230–1485	1230	P,S
$CBrF_3$	1060–1110		1908	P
	1180–1240		1914	
PAN	570–620		72	N;R
	760–820		296	
	1130–1190		301	
	1270–1330		251	
	1700–1760		531	

*K: Kagan *et al.* (1983); P: Pugh, L.A., and K. Narahari Rao (1976); N;R: Measured values by Niki (Ford Motors, Dearborn, MI) and cited in Ramanathan *et al.* (1985); S: Smith *et al.* (1985).

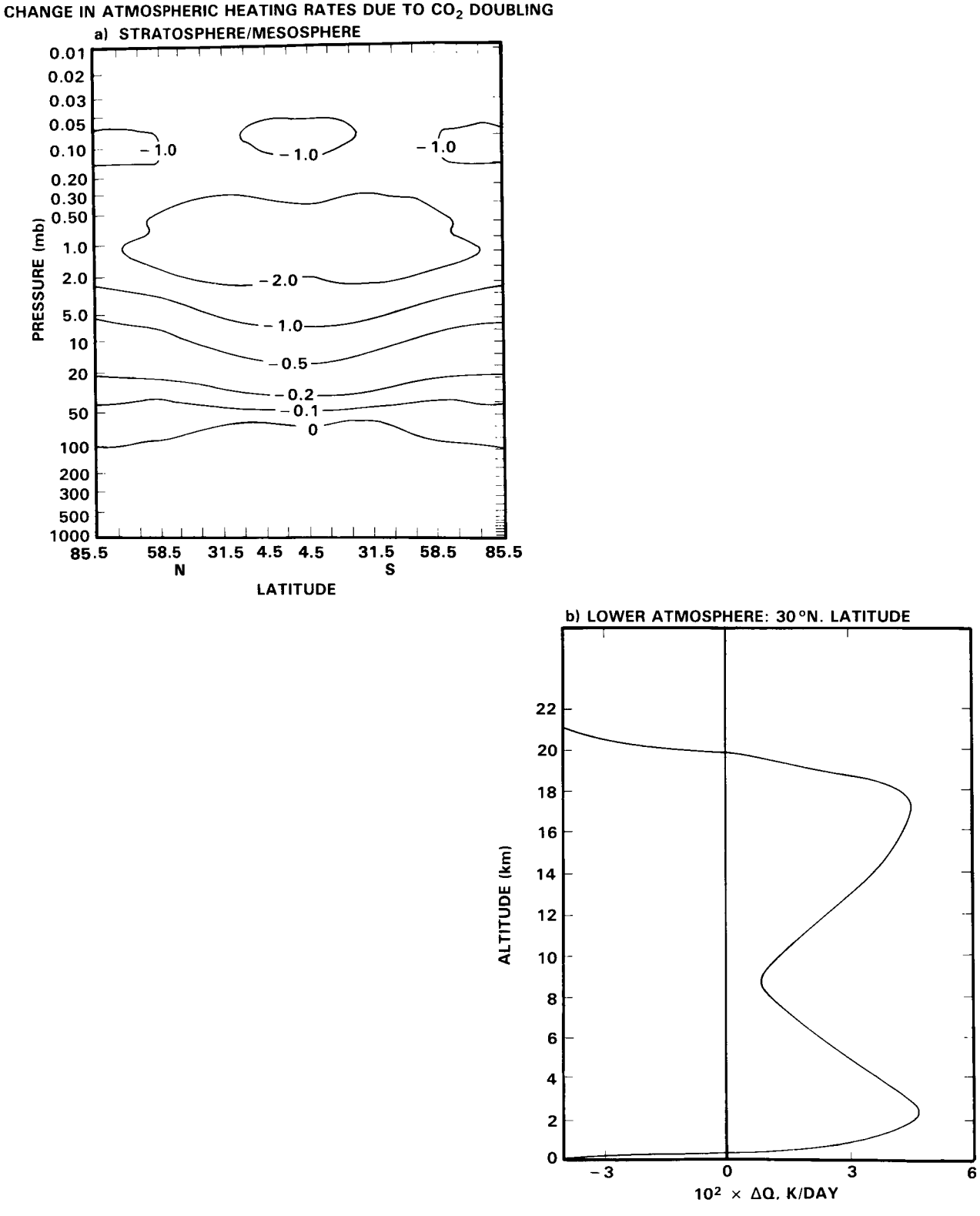

Figure 15-5. Computed change in radiative heating rates for a doubling of CO_2: (a) Stratosphere-mesosphere; Fels *et al.,* 1980; (b) troposphere & lower stratosphere; Ramanathan, 1981

global average value of the surface-troposphere heating (ΔQ) is about 4.2 W m^{-2} (for a CO_2 doubling) and ΔQ scales roughly as:

$$\Delta Q = c \ln F$$

where c is a constant and F is the ratio of CO_2 concentration to a reference value. For a doubling of CO_2, the global average ΔQ consists of roughly 1.6 W m^{-2} due to enhancement in downward emission from the stratosphere (mostly due to CO_2) and about 2.6 W m^{-2} due to decrease in the upward flux at the tropopause, and both these quantities vary significantly with latitude (Figure 15-6).

In addition to the 15 μm bands, CO_2 has absorption features in the 7.6 μm and 10 μm (2 bands) region and also has several bands in the solar spectrum (Table 15-2). The 7.6 μm and 10 μm bands have frequently been ignored by climate models. For CO_2 doubling, the 7.6 μm bands have a negligible effect

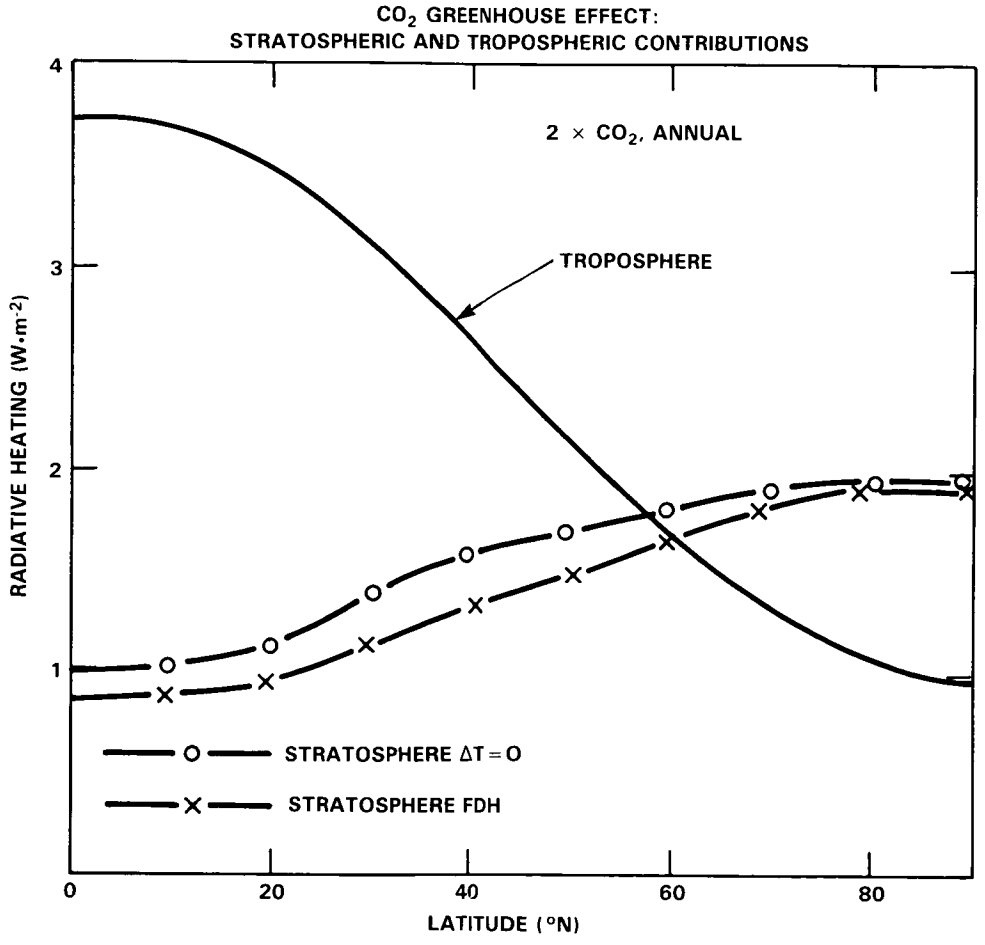

Figure 15-6. Separate contributions from the troposphere and the stratosphere to the total heating of the surface-troposphere system, due to doubled CO_2, for annual mean conditions. The stratosphere contribution is given by the increase in the downward radiative flux from the stratosphere. Stratospheric temperatures are held fixed as CO_2 is increased for the $\Delta T = 0$ curve, whereas they are allowed to change according to the fixed dynamical heating assumption (See Section 15.2.1) for the FDH curve. (Ramanathan *et al.*, 1979).

and the two bands in the 10 μm region contribute roughly 5 to 10% (of the 15 μm greenhouse effect). The solar bands have negligible impact on the stratospheric heating rates and on the surface-troposphere radiative forcing. However, they have a non-negligible impact on the partitioning of the forcing between the surface and the troposphere. For example, for a doubling of CO_2, the increased CO_2 solar absorption within the troposphere reduces the surface absorption of solar radiation by about 0.3 W m^{-2} and enhances the tropospheric solar absorption by about 0.4 W m^{-2} (Hansen *et al.*, 1981). In the 15 μm region, H_2O also has strong absorption features, and the overlapping of H_2O absorption with CO_2 bands ameliorates the greenhouse effect. Most climate models include the overlapping effect of H_2O lines but ignore the strong H_2O continuum absorption (in the 15 μm region) which was only discovered in the early 1970's. Table 15-3 illustrates the influence of H_2O-CO_2 overlap on the CO_2 radiative forcing for midlatitude summer conditions when the ameliorating effect of H_2O-overlap is expected to be large. The H_2O absorption reduces the surface heating (i.e., enhanced CO_2 downward emission) by an order of magnitude but ameliorates the surface-troposphere heating by only 15%, half of which is due to the continuum absorption. The model results in Table 15-3 are for clear-sky conditions, and the inclusion of clouds (accounted for in most climate models) ameliorates the surface-troposphere heating by another 10 to 20%.

In summary, the radiative forcing due to CO_2 arises from a complex chain of processes, and it is reasonably straightforward to account for most of these processes. However, attempts (in the published literature) to oversimplify the radiative calculations have led to significant errors and misinterpretations of the greenhouse effects (e.g., Newell and Dopplick, 1979; Idso, 1980).

Table 15-2. Long-Wave and Solar Bands of CO_2

Spectral Region, μm	Band Type
	Long-Wave Bands
12–18	Fundamental, isotopic, and hot bands (Total of 76 bands)
10	Two hot bands (9.4 and 10.4 μm region)
7.6	Isotopic bands
	Solar Bands
4.3	Fundamental, isotopic, and hot bands (see Dickinson [1972] for a listing of the number of bands in each spectral region)
Others	There are numerous combination and overtone bands between 1 and 3 μm. See Dickinson (1972) for more details.

Table 15-3. Effects of 12-18 μm H_2O Absorption on the Radiative Forcing Due To CO_2 Doubling. Clear-sky Tropical Atmosphere Conditions. (Kiehl and Ramanathan, 1983)

	Radiative Forcing (W m^{-2})	Comments
(i) Surface-troposphere heating		
CO_2 only	6.4	Change in the net
CO_2 + H_2O lines	5.9	longwave flux at
CO_2 + H_2O lines + continuum	5.4	the tropopause
(ii) Surface heating		
CO_2 only	6.9	Increase in the
CO_2 + H_2O lines	3.6	downward emission
CO_2 + H_2O lines + continuum	0.4	

15.1.1.2 Gases with Absorption Bands in the 7-13 μm Region

The atmosphere is relatively transparent in this spectral region as revealed dramatically in the spectral distribution of the longwave emission to space measured by the NIMBUS 3 IRIS instrument (Figure 15-7). The maximum emission by the planet occurs in the 7-13 μm region where roughly 70-90% of the radiation emitted by the surface and clouds escapes to space. CH_4, N_2O and most other anthropogenic trace gases (in particular, the polyatomic trace gases) have strong absorption features in this spectral region and, hence, are effective in enhancing the greenhouse effect. CH_4 and N_2O, in their present-day concentrations of 1.65 and 0.30 ppmv, respectively, contribute about 3.5 W m^{-2} to the radiative forcing of the surface-troposphere system, which is comparable to the greenhouse effect due to a doubling of CO_2.

The vertical distributions of the forcing due to increases in CH_4, N_2O and CFCs are shown in Figure 15-8. The corresponding radiative forcing of the surface-troposphere system and that of the surface alone are shown in Table 15-4 for comparison purposes. The model results shown in Figure 15-8 and Table 15-4 are clear-sky estimates computed with tropical atmospheric profile. The tropical profile is chosen since CFC effects on atmospheric radiative heating rates are a maximum in the vicinity of the tropical tropopause (e.g., see Dickinson *et al.*, 1978). The surface-troposphere radiative forcing for globally averaged conditions is also significantly smaller than the tropical clear-sky values shown in Table 15-4; for example, for CO_2 doubling, the clear-sky tropical profile yields a value of 5.4 W m^{-2} (see Table 15.3 and also Table 3 of Kiehl and Ramanathan, 1983) as opposed to about 4.2 W m^{-2} for globally averaged conditions.

The CH_4 and N_2O effects shown in Figure 15-8 are similar to those of CO_2 in many respects. They all show tropospheric heating and stratospheric cooling. Furthermore, the surface radiative heating (i.e., downward emission at the surface) is only a small fraction of the total greenhouse effect, as in the case

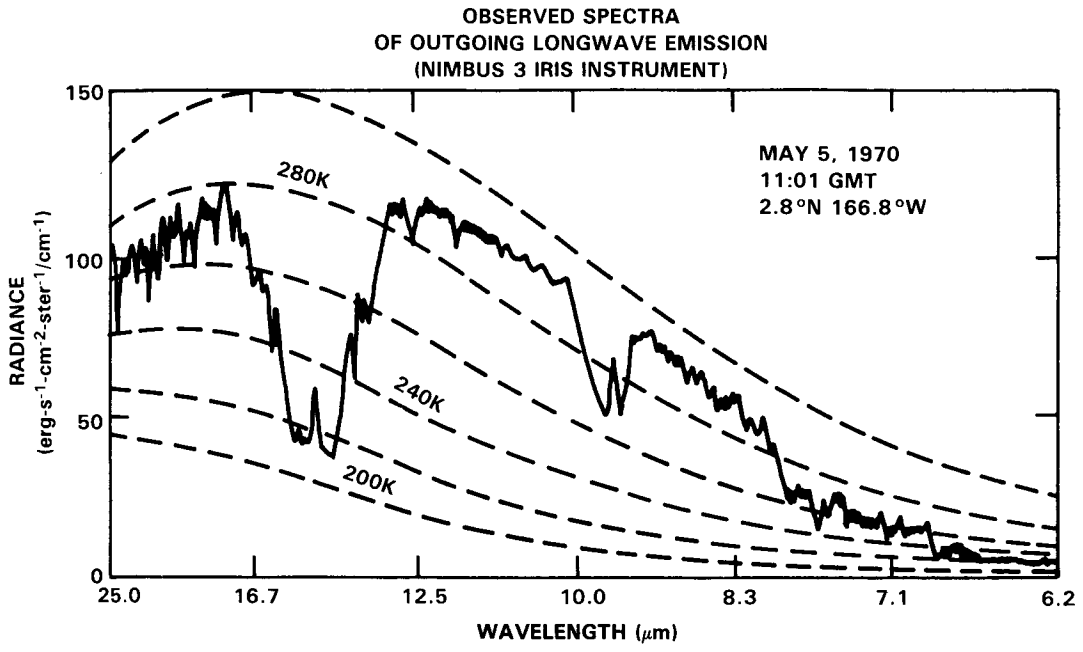

Figure 15-7. Sample spectra from the IRIS instrument on board NIMBUS-3 satellite. The dashed lines indicate the effective radiation temperature for different wavelengths. Source: Hanel *et al.,* 1972.

Table 15-4. Surface-Troposphere Radiative Forcing Due To Increase in CH_4, N_2O and CFCs for Clear-sky Tropical Profile (Source: Kiehl, 1985).

Units: W m^{-2}

	$2 \times N_2O$	$2 \times CH_4$	CFC 11 & 12 (0 → 2 ppb)	$2 \times CO_2$**
Surface-troposphere forcing*	0.7	0.9	1.2	5.38
Surface forcing	0.12	0.15	1	0.4

* Downward stratospheric emission contributes about 10% for N_2O; and about 2% for CH_4 and CFCs.

** The CO_2 results are taken from Kiehl and Ramanathan (1983). The values given here are taken from their narrow band Malkmus model results (see Table 3 of Kiehl and Ramanathan, 1983).

of CO_2. However, the enhancements in stratospheric cooling rates for CH_4 and N_2O doubling are an order of magnitude smaller than that of a doubling of CO_2.

The CFC effects differ significantly from CH_4, N_2O and CO_2 in the following aspects: (a) the maximum in the local heating rate occurs at the tropopause and (b) the CFC surface heating (i.e., downward

TRACE GAS INCREASE AND ATMOSPHERIC RADIATIVE HEATING RATES
(TROPICAL ATMOSPHERE); SOURCE: KIEHL (1985)

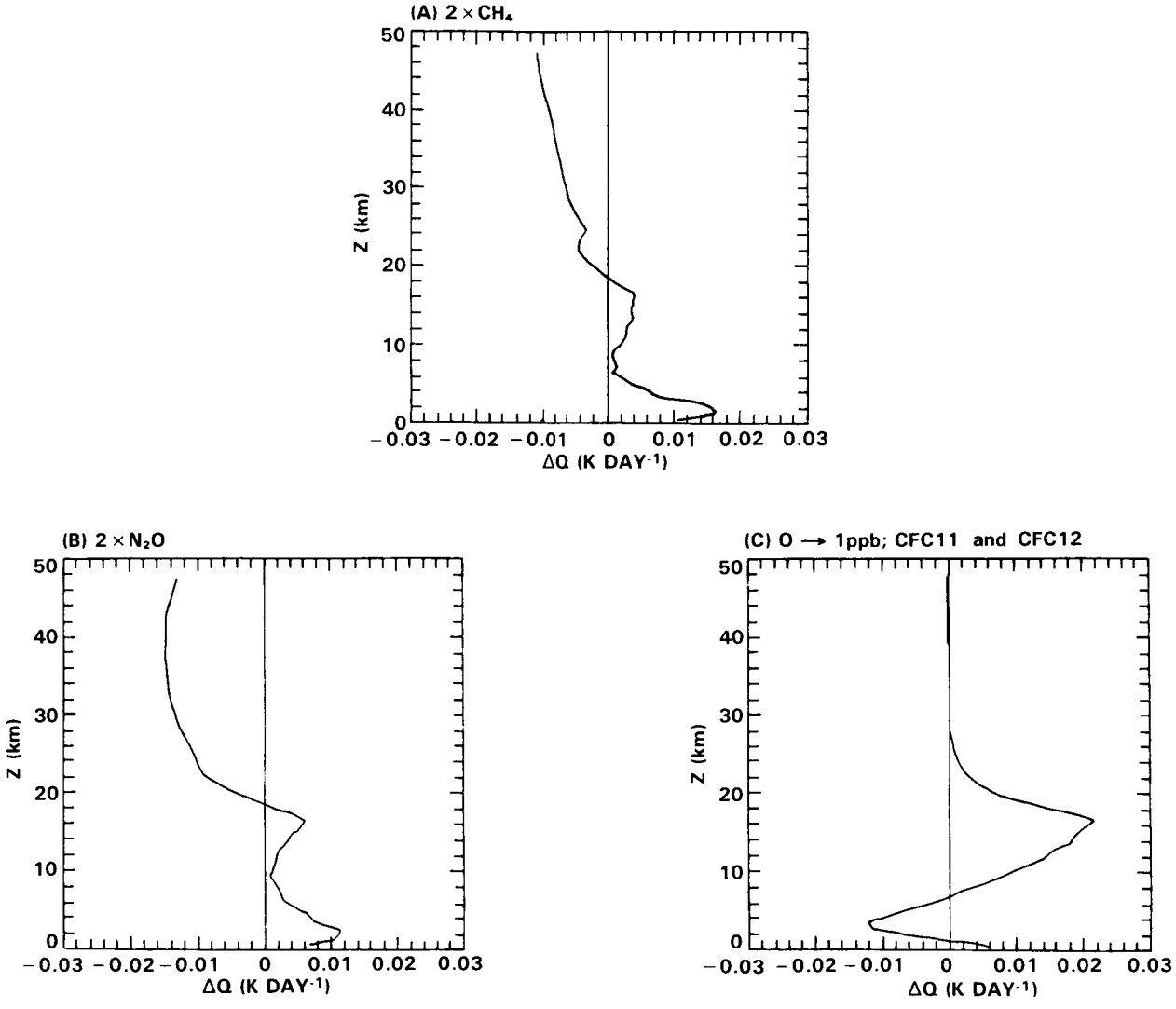

Figure 15-8. Computed change in radiative heating rates (ΔQ) due to trace gas increase. The calculations are for clear-sky conditions and employ tropical profile.

emission at the surface in Table 15-4) is almost equal to the surface-troposphere forcing, whereas, for the other gases the surface heating is only a small fraction of the total effect. By scaling the CFC greenhouse effect of about 1.2 W m^{-2} at the tropopause for a 0 to 1 ppbv (each of CFC11 and 12) increase with that (5.4 W m^{-2}; see Table 15-3) for a CO_2 doubling, we see that the radiative forcing resulting from the addition of 1 molecule each of CFC11 and 12 is more than that due to the addition of 10^4 molecules of CO_2. The principal reasons for the extreme efficiency of CFCs are: CFC band strengths are several times stronger than those of CO_2 (see Tables 15-1a and 1b); CFC absorption increases linearly with its concentration, whereas the CO_2 greenhouse effect scales logarithmically with the CO_2 amount; and CFC absorption occurs in the atmospheric window (see WMO, 1982, for further discussions).

15.1.2 Greenhouse Gases with Strong Solar Asorption: O_3

On a global-annual average, stratospheric O_3 absorbs about 12 W m^{-2} of solar radiation and about 8 W m^{-2} of 9-10 μm radiation emitted by the surface-troposphere system. It also emits about 4 W m^{-2} (2.5 W m^{-2} up to space and 1.5 W m^{-2} down to the troposphere). Thus, stratospheric O_3 contributes to a net heating of the stratosphere which is balanced by longwave cooling due to CO_2 and H_2O. In effect, stratospheric O_3 helps modulate the solar and longwave fluxes to the troposphere.

The largest impact of stratospheric O_3 change is felt in the stratosphere itself (Figure 15-9). The solar heating rate perturbation peaks in the vicinity of the stratopause. With respect to the longwave heating rate perturbation (Figure 15-9b), O_3 reduction causes a decrease in the lower stratospheric heating rates (due to decreased absorption of surface emission) and an increase in the mid to upper stratosphere heating rates (due to decreased emission).

Reduction in stratospheric O_3 can modify the surface temperature via two competing processes: more solar radiation is transmitted to the surface-troposphere system, thereby contributing to a surface warming; on the other hand, the cooler stratosphere (due to decreased solar and longwave absorption) emits less to the troposphere which would tend to cool the surface. The solar warming and the longwave cooling effects are comparable in magnitude, and the magnitude as well as the sign of the net effect depends very critically on the magnitude of the stratospheric temperature change which in turn depends strongly on latitude and season.

The magnitude of the longwave cooling effect depends on the altitude of O_3 reduction, whereas the magnitude of the solar warming effect depends solely on the reduction in total column amount. Consequently, changes in stratospheric O_3 can have different effects on the surface temperature depending on the vertical distribution of the O_3 change. This dependence is revealed in Figure 15-10 which shows the computed change in surface-troposphere radiative heating for two different profiles of O_3 change. While the uniform O_3 reduction leads to a net radiative cooling, the non-uniform O_3 change profile (denoted by CFM; Figure 15-10b) leads to a net increase in the heating. For the CFM perturbation, most of the decrease in O_3 occurs in the upper stratosphere and, hence, the reduction in longwave emission (due to stratospheric cooling) is not "felt" by the troposphere with the result that the solar warming dominates over the longwave cooling effect. The profile shown in Figure 15-10a is the ozone change vs. altitude calculated by models using the photochemistry which was current in 1979. Today's (1985) one-dimensional models show significantly less ozone change in the lower stratosphere (see Chapter 13). Two-dimensional models show a highly latitude-dependent ozone change in the lower stratosphere with increases predicted at low latitudes and decreases at high latitudes. (see Chapter 13).

Since the net effect on tropospheric radiative forcing is obtained as a difference between solar and longwave effects, it depends strongly on latitude and season. In middle to higher latitudes, even the sign of the effect depends on season (e.g., see the CFM curve in Figure 15-10).

Although the troposphere contains only about 10% of the total O_3, the longwave opacity of present tropospheric O_3 amounts is nearly the same as that of present stratospheric O_3 amounts (due to the pressure broadening effects on the O_3 9.6 μm band line shape). Furthermore, both solar and longwave effects of tropospheric O_3 change influence the surface temperature in the same direction in contrast to the opposing solar and longwave radiative effects induced by stratospheric O_3 change. As a result, surface temperature is significantly more sensitive to changes in tropospheric O_3 than to stratospheric O_3 changes. In fact,

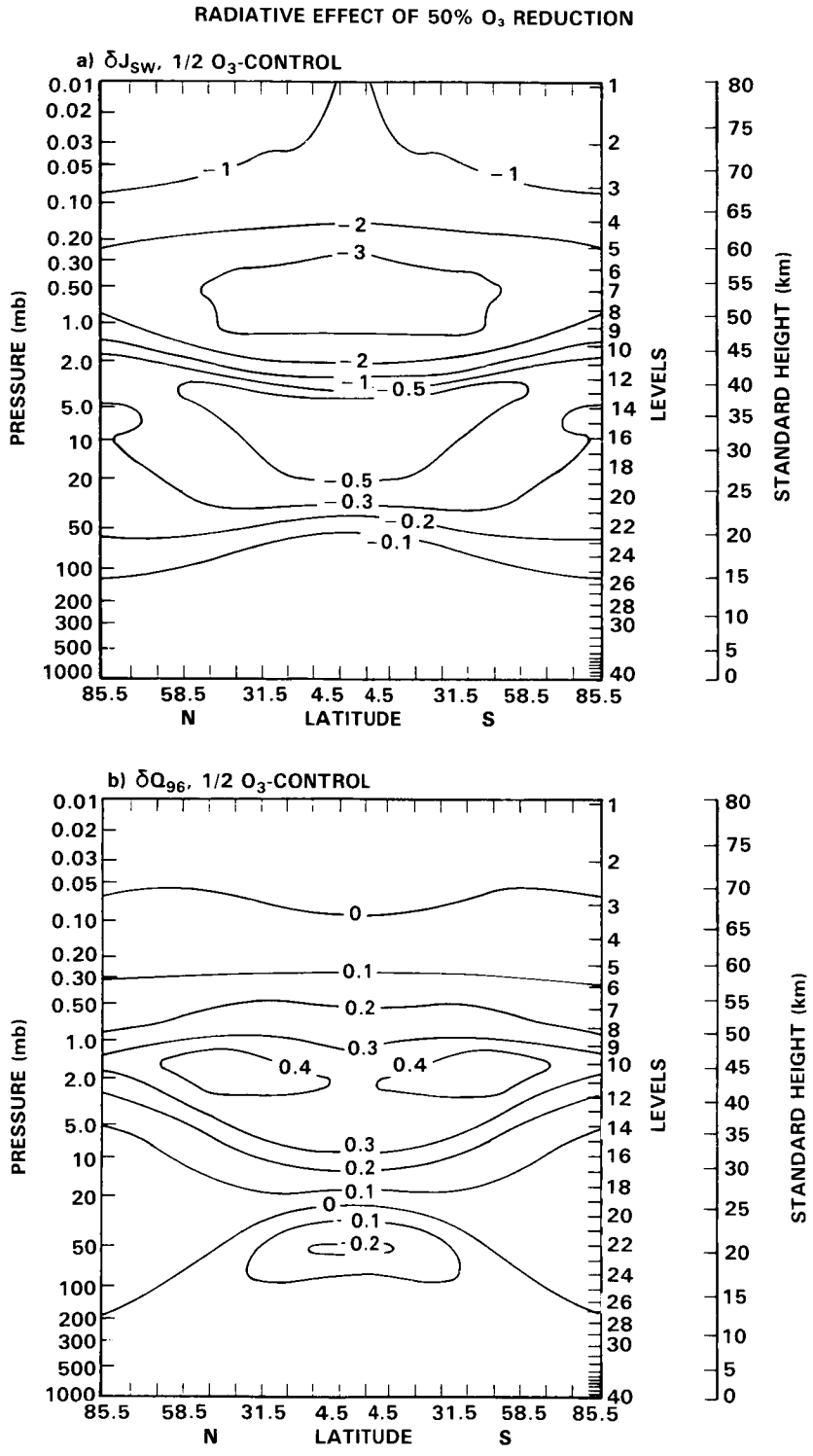

Figure 15-9. Radiative drives (K day^{-1}) for the ozone reduction experiments: (a) δJ_{SW}, the change in shortwave heating due to a 50% ozone reduction; and (b) $\delta Q_{9.6}$, the change in 9.6 μm O_3 band heating rate due to a 50% ozone reduction, with the temperatures in all cases held fixed at the control values. Source: Fels *et al.*, 1980.

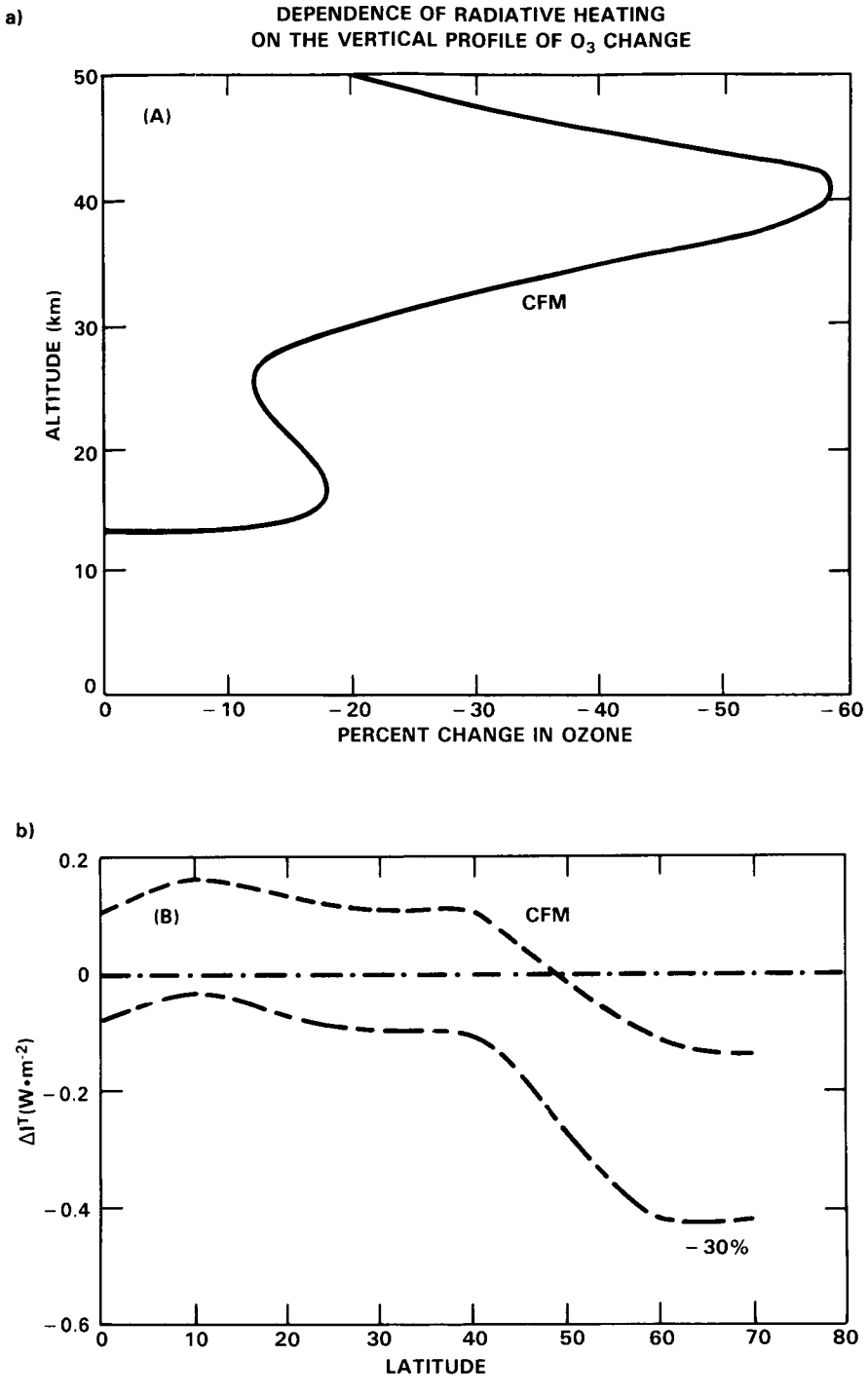

Figure 15-10. The dependence of computed change in the net radiative flux at the tropopause to assumed vertical profile of O_3 change. (a) The CFM profile is similar to the profile yielded by photo-chemical models which were current in 1979 for the effect of adding CFC's while holding other gases constant. Present models show less effect in the lower stratosphere and even give increases especially at low latitudes; (b) the computed change in the net flux at the tropopause for the CFM profile and for a 30% uniform O_3 reduction. Source: Ramanathan and Dickinson, 1979.

for a uniform O_3 change, tropospheric O_3 change is about two to three times as effective as stratospheric O_3 change in altering the radiative forcing (e.g., see Table 15-5).

The strong dependence of the computed surface temperature change to the altitude and latitude of of O_3 perturbation is summarized in Figure 15-11 (adapted from Wang *et al.*, 1980). This figure shows the computed surface temperature change (per cm-atm of O_3 change) as a function of the altitude at which O_3 is perturbed. For both the tropical and mid-latitude profile, the computed surface temperature change is most sensitive to ozone change (on a per molecule basis) within the upper troposphere and lower stratosphere. The larger sensitivity of the tropical profile is mainly due to the warmer tropical surface temperature and the colder tropical tropopause temperature both of which tend to maximize the greenhouse effect of O_3.

15.1.3 Additiveness of the Greenhouse Effects

The question to be addressed here is: would the computed change in tropospheric radiative forcing due to the simultaneous addition of two or more gases to the atmosphere be the same as that of summing up the effects of adding each gas separately? This question arises because the absorption features of several gases appear in the same spectral region. For example, the CF_4, CH_4 and N_2O bands occur in the 6-8 μm region; N_2O bands in the 15 μm region overlap with CO_2 bands; CFC bands overlap with O_3 bands; etc. To a large extent, model calculations show that the error involved in the additive assumption is less than 5% or so.

The above conclusion becomes invalid once one or more of the added gases alters a radiatively active constituent through chemical interactions. For example, both CFCs and CH_4 influence O_3 through chemistry. CH_4 is estimated to lead to an increase in O_3 in the upper troposphere and lower stratosphere, whereas

Table 15-5. Computed Surface-Troposphere Radiative Forcing Due To Uniform Reduction in O_3; Globally Averaged Conditions with Average Clouds.

O_3 Perturbation	Radiative Forcing[1] ($W\ m^{-2}$)	Source
−25% in the total column	−0.6 to −0.7 $W\ m^{-2}$	Inferred from Hansen *et al.* (1981)[2]
−25% in the stratosphere	−0.1 to −0.2 $W\ m^{-2}$	Ramanathan and Dickinson (1979)
−25% in the troposphere	−0.4 to −0.5 $W\ m^{-2}$	Fishman *et al.* (1979a)

[1] The values cited here account for stratospheric temperature changes to the imposed perturbations.

[2] These authors give results for surface temperature change and the radiative forcing was inferred by multiplying the temperature change with their model sensitivity (i.e., λ as given by Eq. 1 defined in Section 15.2.2) which is about 1.4 $W\ m^{-2}\ K^{-1}$.

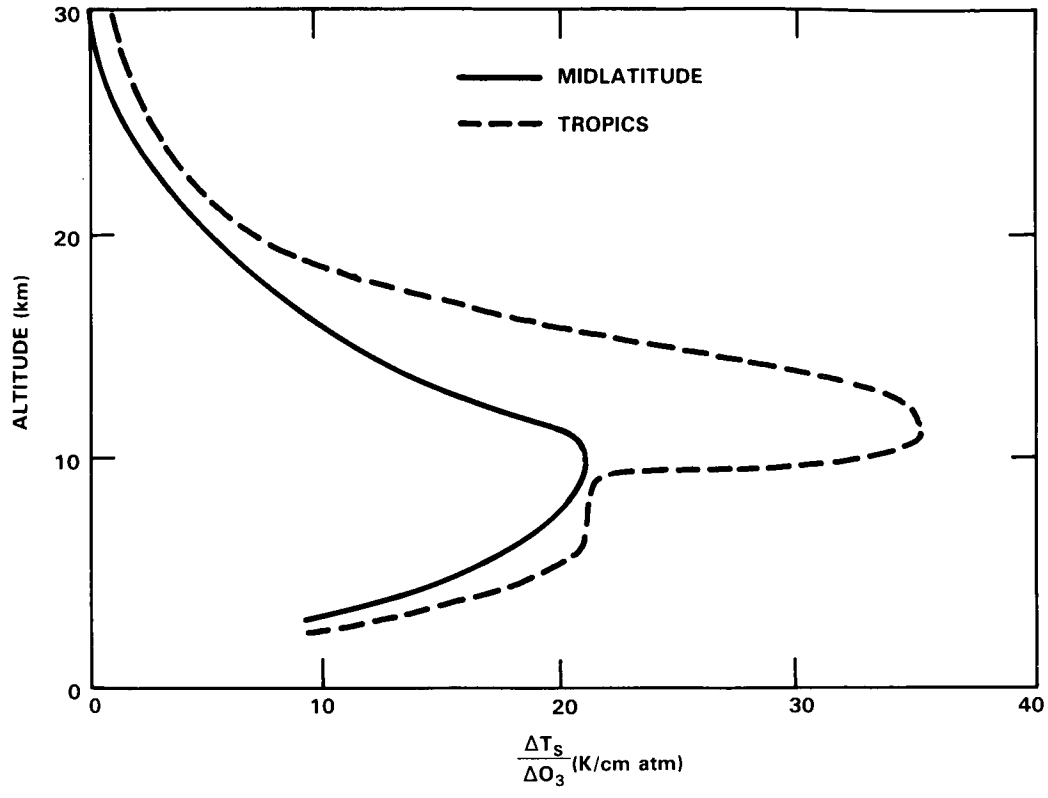

Figure 15-11. Computed change in surface temperature (per unit local O_3 change) as a function of altitude at which O_3 is perturbed. The surface temperature sensitivity curve is shown for midlatitude (solid) and tropical (dashed) atmosphere conditions. Source: Wang *et al.*, 1980.

an increase in CFCs would lead to a decrease in O_3 in the stratosphere. Simultaneous addition of CH_4 and CFCs may not produce the same change in the vertical profile of O_3 as that obtained by superposition of the individual O_3 changes produced by CH_4 and CFCs. Since the tropospheric effects depend on the vertical distribution of the O_3 perturbation, the validity of the additiveness assumption needs to be examined in the case of trace gases that chemically impact other radiatively active gases.

15.1.4 Effects of Aerosols

Stratospheric aerosols of volcanic origin undergo episodic variations while tropospheric aerosols can undergo episodic or secular variations. It is necessary to understand the nature and magnitude of the "signature" of aerosols on the observed trends of surface-troposphere-stratosphere temperatures before we can identify the role of trace gases on long term (decadal) climate trends. The above necessity is the primary motivation for including a brief discussion on aerosols in the present chapter.

A detailed description of our current understanding of aerosol effects on climate can be found in WCP (1983). Aerosols can impact climate either directly by absorption and scattering of solar and longwave radiation or indirectly by altering optical properties of clouds (Lenoble, 1984). Aerosols can influence cloud optical properties in one of the following two ways (Lenoble, 1984): (1) Aerosols lodged within a water droplet or ice crystal can alter the radiative properties of the cloud; (2) aerosols can also serve

as condensation or freezing nuclei and influence the size and concentrations of droplets or ice crystals which in turn govern the radiative properties of clouds (Twomey *et al.*, 1984). The aerosol-climate problem is so complicated that after decades of research, it is still difficult to make any general statements about whether aerosols cool or warm the climate. However the direct radiative effects are relatively better understood than the indirect effects and hence we will focus on the direct radiative effects of aerosols.

The visible optical depth of the background stratospheric aerosols is of the order of 0.01 or less, and hence, has a negligible impact on climate (WCP, 1983). The background tropospheric aerosol is estimated (by climate models) to cause a global surface cooling of about 1 to 3 K (see Table 2.2 of WCP, 1983). However, small changes in the assumed optical properties of aerosols (e.g., single scattering albedo and/or backscattered fraction; also see Lenoble, 1984) can change the computed effect from cooling to warming.

With respect to climate change, aerosols of volcanic origin in the stratosphere and of anthropogenic origin in the troposphere have the potential for influencing temperature trends within the stratosphere and troposphere on time scales ranging from a few years to several decades.

The stratospheric volcanic aerosols have been shown to affect the tropospheric climate in the following way. Aerosols produce two competing effects: (1) the scattering and absorption of solar radiation by the aerosols reduce the solar radiation reaching the troposphere and (2) they increase the atmosphere's longwave opacity. By decreasing the direct solar radiation and increasing the scattered radiation, the aerosol contributions can cool the troposphere. The increased longwave opacity and solar absorption can also heat the stratosphere. As the volcanic cloud ages, some SO_2 is oxidized to sulfuric acid to produce more aerosols (Hofman and Rosen, 1983); existing aerosols increase in mean radius (Hofman and Rosen, 1982), which in turn increases the Mie scattering in the visible spectral region. To account fully for aerosol effects upon climate, it is necessary to follow the cloud dispersion, the oxidation of SO_2, the change in the size distribution, the geographical location, the height and vertical structure of the aerosol cloud. To use this information effectively in a model, it is also necessary to know the aerosol refractive index (Reck and Hummel., 1981), from which the aerosol extinction, single scattering albedo and the asymmetry factor may be calculated.

One of the best documented and better understood effects of volcanic aerosols is their effect on stratospheric temperatures. Stratospheric temperature statistics recorded over the last two decades clearly reveal the low latitude warming in the lower stratosphere following the eruption of Agung in 1963 and El Chichon in 1982 (WCP; 1983). In the special case of the effects of the El Chichon eruption of 4 April 1982 (McCormick *et al.*, 1984; Michalsky *et al.*, 1984), isolation of its stratospheric signal from the thermal effects of the El Niño event and the quasibiennial oscillation indicates that a temperature increase of 1-3 °C at 30 mb occurred between the equator and 35 ° latitude (Labitzke *et al.*, 1983; Quiroz, 1983a). Harshvardhan *et al.* (1983) used a nine-layer zonally averaged energy balance model with ice-albedo feedback to estimate that the maximum surface cooling should have been 0.3-0.4 °C, 2.5 years following the eruption. They expected the largest zonal temperature change to occur around 70 °N with a value 0.5-0.6 °C. Their model also predicted an increase in the reflected solar radiation at the top of the atmosphere of about 3-4 W m^{-2}.

Episodic aerosol disturbances in the troposphere have also been shown to lead to regional climatic effects. The most important of these disturbances are arctic haze (Leighton, 1983), Saharan dust (Fouquart *et al.*, 1984) and urban aerosols (Galindo, 1984). Amongst these disturbances, arctic haze may turn out to be an important issue for the trace gas-climate problem for several reasons. First, observations indicate that arctic haze contains large amounts of anthropogenic compounds like soot and sulfuric acid (Blanchet and List, 1984). Secondly, it has been shown recently (Wilkness and Larson, 1984) that con-

tinental air masses (containing soot and other anthropogenic gases) can be transported over very long distances (e.g., from Asia to Arctic). Hence, the arctic haze can exhibit a secular trend in the future. Thirdly, the arctic haze has a substantial impact on the springtime solar heating rates (Porch and MacCracken, 1983). Under clear-sky conditions, the haze layer can enhance the heating rate by as much as 50%. The climatic effects of the haze are expected to be concentrated in the arctic region and might change with time (since the haze is of anthropogenic origin). Since the trace gas effects on tropospheric climate are also expected to be large in the arctic region (see Sections 15.4 and 15.5), the potential effects of the haze on arctic climate can make it difficult to infer the trace gas effects.

In summary, aerosols can produce a sizeable "noise" in meteorological data which makes it very difficult to establish a direct relationship between trace gas increases and climate change. While some models exist (Lenoble, 1984) to predict the climatic consequences of stratospheric aerosols, more research needs to be done in measurements and in modeling to establish the role of tropospheric aerosols in climate. In particular, we need to establish trends (if any) in the tropospheric aerosols and their radiative properties. Perhaps, the best hope for assessing aerosol effects is to monitor the albedo of the planet from satellites with a high degree of precision (within 0.1%).

15.1.5 Current Status in Trace Gas Radiative Treatment

Numerous approximations are invoked within climate models to simplify the treatment of the radiative effects of trace gases (e.g., the use of band models). For example, an international study entitled "the intercomparison of radiation codes used in climate models (ICRCCM)" undertook the task of comparing clear-sky longwave fluxes and cooling rates computed by about 40 radiation models including line-by-line, narrow-band and broad-band models (see the appendix for further discussion of the band models). The results of this study have been published as a World Climate Research Programme report by Luther and Fouquart and this report will be referred to as ICRCCM (1984). The principal findings of the ICRCCM (1984) study, which focused on clear-sky longwave calculations for H_2O, CO_2 and O_3 are given below:

(1) The line-by-line models are in very good agreement with each other (within 1% in the computed fluxes). (2) The radiation codes used in climate models differ significantly from each other. For example, the net radiative flux change (for clear-sky mid-latitude summer condition) at the tropopause due to CO_2 doubling (i.e., the radiative forcing of CO_2 doubling) yielded by the models ranged from 4.5 to 7.5 W m^{-2}. To give another example, the range in the computed downward flux at the surface for a mid-latitude summer atmosphere (with only water vapor) is about 60 W m^{-2}. (3) Because of large uncertainties in H_2O line shapes and in the physics of the H_2O continuum, there is an urgent need to validate line-by-line calculations with accurate laboratory data and with flux measurements in the atmosphere.

Since H_2O, CO_2 and O_3 are discussed in great detail in the ICRCCM study, the present discussion will focus on the other trace gases listed in Table 15-1. Climate models generally employ narrow-band or broad-band models for CH_4 and N_2O and employ various versions of the optically thin approximation for all other gases in Table 15-1.

The validity of the optically thin approximation is discussed in detail in WMO (1982; see the appendix by Cess in that report). For concentrations of CFC's (and others in Table 15-1) of several ppbv or less, the optically thin approximation when employed in conjunction with the exponential sum-fitting method has been shown (Ramanathan *et al.*, 1985) to yield the same accuracy as the more detailed narrow-band model. The next step is to assess the accuracy of the approaches used in narrow- and broad-band models.

The effect of simplified model approaches can be evaluated by intercomparing models of varying complexity. This technique for evaluating models is illustrated in Annex 1 for the ν_4 band of CH_4 (located at 1300 cm^{-1}). The following is a summary of the analyses given in the Appendix:

(a) It is possible to define and derive a self-consistent narrow-band or broad-band model that agrees excellently with line-by-line calculations both for homogeneous and for inhomogeneous optical paths (i.e., atmospheric path);

(b) The choice of spectral interval for the narrow-band model is quite arbitrary. The spectral interval has to be chosen by comparing with line-by-line calculations.

(c) Line half-width and its temperature dependence are available for only a minor fraction of the several thousand lines within each band. The lack of this data is a major source of uncertainty in line-by-line calculations.

For CFC's and all other gases except CH_4 and N_2O, the relevant narrow-band model parameters are unavailable. Even the integrated band strengths are unavailable for many potentially important gases such as CFC113 and 114. Furthermore, for many of the gases the hot bands (i.e., bands for which the lower vibrational state is an excited state) overlap strongly with the fundamental bands (e.g., see Varanasi and Ko, 1978 for CFC11 and 12). In such instances, it is important to determine the strengths of the hot bands for accurate modeling of the opacities in band models.

15.2. THEORY AND MODELS

15.2.1 Stratospheric Response to Perturbations

The study of climatic impacts *within* the stratosphere due to added trace constituents is of special interest for several reasons. First, for reasonable projections of future trace constituent distributions, the expected temperature changes in the upper stratosphere are nearly an order of magnitude greater than the expected surface changes. Second, these expected temperature changes are essentially independent of ocean temperature changes and cloud feedback effects. Both processes are a source of considerable uncertainty in assessing tropospheric climate change.

Climate change in the stratosphere is also different because temperature change there is coupled directly with photochemical processes. The strongest link is with the temperature dependence of the equilibrium ozone. For example, the cooling effect of increasing CO_2 in the upper stratosphere superficially involves virtually no chemistry. However, as temperatures drop, ozone amounts increase, leading to a local *heating* effect. This is an important *negative* feedback. In addition, increases of the trace gases, particularly CH_4, H_2O, N_2O and chlorofluorocarbons, tend to lead to O_3 decreases (and cooling effects) in the upper stratosphere. However, such local decreases of O_3 affect the incoming solar ultraviolet radiation such that greater penetration into the lower stratosphere would be allowed. This acts to increase local *heating* there, but more importantly, increases production of O_3 below. This process produces a very significant "self-healing" effect on the total O_3 column, while leading to significant changes in the *shape* of the ozone profile. This, in turn, affects the local temperature.

The almost bewildering array of interactive feedback processes in the stratosphere implies that they can be understood only through careful, self-consistent modeling of the radiative-photochemical-dynamical

system. Ultimately, this modeling must be done with fully interactive, time-dependent, three-dimensional models.

For a number of reasons, such complete models remain impractical today. The most well known reason is the tremendous computational requirements for a fully comprehensive model. However, even if such resources were now available, the current strategy of using a hierarchy of models ranging from the very simple to the very complex would still be the appropriate one. This is because there remain significant uncertainties in our understanding of many aspects of the radiative-photochemical-dynamical system. Useful reductions of such uncertainties require a wide range of considerably more focused research activities. Without improved understanding and modeling capability in all components of the problem, the power of more comprehensive modeling treatments tends to be diminished.

These difficulties are amplified by the very serious uncertainties in the projected changes in atmospheric trace constituent amounts. To explore such problems, typically a generous range of possibilities (scenarios) is considered.

This situation has led to a wide variety of modeling approaches, all of which work to reduce the complexity of the problem and emphasize various sets of scientific questions. Some of these modeling approaches are surveyed below.

15.2.1.1 Role of Radiative-Photochemical-Diffusive Models

The simplest approach that comes close to allowing an understanding of the complex interactions among radiation, photochemical and transport processes is the so-called one-dimensional (1-D) model. These models allow no horizontal variations and thus may logically be considered to represent globally averaged (in the horizontal) conditions. Historically, however, they often have been used to represent local conditions, usually at some appropriate "midpoint" latitude such as 30°. Historically, the 1-D models have usually considered only photochemical problems, with the required transport being parameterized by carefully chosen but empirical "eddy" diffusion coefficients (e.g., McElroy *et al.*, 1974, Hunten, 1975).

Such 1-D models have been shown to be very powerful tools for understanding complex chemical feedbacks in spite of their simplicity. Moreover, they have served as the basic tool for most of the previous assessments of the expected impacts on stratospheric ozone changes due to various anthropogenic activities (e.g., National Research Council, 1979). Typically, these models have prescribed temperatures and thus have only indirect implications for stratospheric climate changes.

More recently, some investigators have begun efforts to couple these chemically oriented 1-D models with the Manabe and Wetherald (1967) type radiative-convective 1-D climate models. These include Luther *et al.* (1977) and Boughner (1978).

To date, the main concern has been with including the effects of climatic feedback on calculated ozone changes. As the effects of radiatively important trace species other than CO_2 become the object of more serious climatic attention, the inclusion of photochemical feedbacks in the climate system will gain more research attention. However, in such cases the limitations of the 1-D model framework will become more severe. This is particularly so for the calculation of chemical/climatic feedbacks through stratospheric water, a trace substance whose spatial distribution seems to be fundamentally dependent upon 3- D processes.

15.2.1.2 Two-Dimensional Effects

In both climatic and chemical problems, there are many physical processes that at best are poorly represented in 1-D models. The next logical step is to construct a 2-D model in the meridional-vertical plane. This allows inclusion of many important sun-angle dependent processes. Most models in this category have prescribed transport processes in various combinations of zonally symmetric and "eddy" mechanisms.

In the past, the main concern has been with the problem of self-consistent prescription of mean and eddy transport processes. Recently, conceptual progress (Plumb and Mahlman, 1985) and semi-empirical successes (e.g., Garcia and Soloman, 1983; Ko *et al.*, 1985; Guthrie *et al.*, 1984) have been achieved. This progress has been mainly in the "transport/chemistry only" models in which the transport doesn't really change as the constituents or the climate of the stratosphere change.

Early attempts to produce self-consistent dynamical response in 2-D models were given in Vupputuri (1978) and Pyle and Rogers (1980a). In these models the eddy fluxes are essentially specified (usually through local eddy diffusion coefficients), but the meridional circulation is calculated self-consistently in response to these fluxes. In a more fundamental sense, these models are not really climate models either since the fundamental eddy forcing remains prescribed through large changes in constituents. They might, however, capture an important part of the 2-D "non-dynamical" part of the climatic response to trace constituent changes. Such models can yield temperature changes that are very close to the "fixed dynamical heating" (FDH) limit described in the next section.

15.2.1.3 Three-Dimensional and Dynamical Effects

Since it is clear that both chemical and dynamical processes are inherently three-dimensional, it is inevitable that 3-D climate/chemical models will play an increasing role in analysis of such trace gas/climate problems. However, even as such models are employed, they can provide information which at times may show ways in which full 3-D processes may not have to be modeled explicitly once they are well understood. For example, the work of Mahlman *et al.* (1985) indicates that all long-lived stratospheric gases exhibit predictable structure provided that the complete 3-D structure is solved for one of them and the chemistry of each of the gases of interest is known. In this context, it is likely that full 3-D solutions will not be required for each of the ever growing list of radiatively active gases that may influence climate.

In the context of predicting stratospheric climate change, it is of interest to inquire whether 3-D models are really required. The answer to this probably can be supplied only with a properly posed 3-D model. An early attempt in this regard was offered by Fels *et al.* (1980). They pointed out that there are two possible extremes of stratospheric climatic responses to changes in trace constituents. These are (1) "dynamical adjustment" and (2) "radiative adjustment." For dynamical adjustment, the net dynamical heating (sum of adiabatic heating mechanisms in the thermodynamic equation) adjusts so that the temperature doesn't change. For radiative adjustment (see also Fels and Kaplan (1975), and Ramanathan and Dickinson (1979)) the temperature changes so that the *net dynamical heating* doesn't change.

Since the net dynamical heating is a function of the degree to which the stratosphere is dynamically forced, "radiative adjustment" means in this context that *no further changes* in dynamical forcing occur as a result of changing trace constituents. This is why Fels *et al.* (1980) refer to this as the "fixed dynamical heating" (FDH) limit. The attractive feature of the FDH limit (if valid) is that, in principle, climatic calculations can be performed with purely radiative models. However, this requires that such radiative models perturb about *realistic* atmospheric structure (either real or modeled). The experiments of Fels

et al. (1980) suggest strongly that mid and high latitudes of the stratosphere are rather well described by the FDH limit. For *tropical* wind systems, however, considerable dynamical adjustment is expected. They offer a mechanistic model that explains why significant dynamical adjustment is expected mainly in the tropics.

The calculations of Fels *et al.* (1980) pertain to annual mean conditions and may not necessarily reflect the validity of the FDH model for other seasons (in particular, the winter polar regions where dynamical processes play a crucial role in maintaining the thermal structure). Nevertheless, it seems safe to conclude that, on an annual mean basis, the stratospheric temperature response to radiative heating perturbations is governed to a large extent by longwave radiative adjustment processes.

15.2.2 Troposphere Response and the Role of Feedbacks

One of the fundamentally important concepts which has emerged out of the numerous 1-D, 2-D and 3-D climate model studies is that the surface temperature change is largely determined by the radiative forcing of the surface-troposphere system (i.e., net flux change at the tropopause). The computed surface temperature change is neither strongly dependent on the vertical distribution of the radiative heating within the troposphere nor does it depend strongly on the manner in which the radiative heating is partitioned between the surface and the troposphere. The reason for the insensitivity of the computed surface temperature change to the vertical heating distribution has been explained in the introduction to Section 15.1.

The model results that helped forge this concept are numerous and only a few examples will be given below: (a) The radiative forcing of the surface-troposphere system due to a 2% increase in solar insolation and due to a CO_2 doubling agree within about 10%. But, the partioning of this forcing in terms of surface forcing and tropospheric forcing is vastly different. Yet, almost all climate model studies, including the general circulation model studies (e.g., Wetherald and Manabe, 1975; Hansen *et al.*, 1984) show that the computed surface temperature change for the 2% solar radiation increase is within 10% of that due to CO_2 doubling; (b) Likewise, as shown in Section 15.1, the vertical distribution of the radiative heating due to CFCs and CH_4 or CO_2 are drastically different. Yet, the computed surface temperature change due to the individual gases scales almost linearly with respect to their radiative forcing of the surface-troposphere system. The conclusions derived from these studies apply only to small deviations from the observed climate and should not not be generalized to large perturbations.

Three different types of climate models have been used to compute the climate change due to trace gas perturbations: energy balance models (EBMs), radiative-convective models (RCMs) and general circulation models (GCMs).

15.2.2.1 Energy Balance Models: the Zero Climate Feedback Limit

The concept of surface-troposphere radiative forcing is particularly useful for inferring the role of feedback processes since it enables the problem to be formulated in terms of a zero-dimensional climate model. Denoting the perturbation in surface/troposphere radiative heating (i.e., the radiative forcing) as ΔQ, the surface temperature change ΔT_s can be related to ΔQ by the relation (Dickinson, 1985):

$$\Delta T_s = \frac{\Delta Q}{\lambda} \tag{1}$$

where λ is referred to as the climate feedback parameter. The net (solar + longwave) radiative forcing, ΔQ, is the net (down minus up) radiative flux change at the tropopause due to the trace gas change. The change in the net flux is computed by holding the surface and tropospheric temperatures fixed at the reference value but allowing the stratospheric temperatures to come to equilibrium with the radiative heating perturbation. These subtle requirements of computing ΔQ have been ignored at times (in the literature) with catastrophic errors. For example, Equation (1) has been applied by estimating ΔQ at the surface which tends to underestimate ΔT_s by a factor of two to four (see Ramanathan, 1981) or by estimating ΔQ at the top of the atmosphere without allowing the stratosphere to come to equilibrium which tends to underestimate ΔT_s by a factor of two (see the discussions in Schneider, 1975)

In general, λ estimated by the hierarchy of simple and sophisticated climate models lies in the range of:

$$1 < \lambda < 4 \text{ Wm}^{-2}\text{K}^{-1}.$$

For the simplest case in which the earth-atmosphere system radiates as a black body with an effective radiating temperature of 254 K, $\lambda = 4\sigma T^3$ ($=3.7$ W m^{-2} K^{-1}). For this case, a doubling of CO_2 (note $\Delta Q \approx 4.2$ W m^{-2}) would yield a surface warming of about 1.1 K. This simple model implicitly assumes that the troposphere and surface are coupled so that the same temperature change occurs in the troposphere or at the surface, i.e., the lapse rate is assumed to be an invariant of climate. More importantly, this model ignores all climate feedback processes involving temperature, humidity, clouds and others. The only feedback this model includes is the negative feedback between temperature and longwave emission (Dickinson, 1982). Hence, the climate response obtained from a model with fixed lapse rate, fixed atmospheric composition and fixed planetary albedo is referred to as zero climate feedback case and the change in surface temperature for this case is denoted by $(\Delta T_s)_0$.

The EBM given by (1) imposes the energy balance at the top-of-the tropopause. There are also surface energy balance models (SEBMs) which solve for ΔT_s by imposing surface energy balance. A recent review by Schlesinger and Mitchell (1985) shows that a wide range of values for λ may be obtained (0.3 to 10 W m^{-2}K^{-1}) for SEBMs depending upon modeling assumptions. In several cases where the λ is outside the range of 1 to 4 W m^{-2}K^{-1}, the cause has been traced to the assumptions that violated the first law of thermodynamics (Cess and Potter, 1984).

There are also 1-D (latitude) and 2-D (latitude and altitude) EBMs which have played an important role in illustrating the magnitude of several climate feedbacks. These EBMs are reviewed in North *et al.* (1981).

15.2.2.2 Radiative-Convective Models

Radiative-convective models determine the equilibrium vertical temperature distribution for an atmospheric column and its underlying surface for given insolation and prescribed atmospheric composition and surface albedo. An RCM includes submodels for the transfer of solar and longwave radiation, the turbulent heat transfer between the earth's surface and the atmosphere, the vertical redistribution of heat within the atmosphere by dry or moist convection, the atmospheric water vapor content and cloud amount. The radiative transfer models used in RCMs are frequently identical to those used in GCMs. The vertical heat redistribution by convective atmospheric motions is modeled as an adjustment whereby the temperature lapse rate of the atmosphere is prevented from exceeding some given value. The amount of water vapor is detemined in RCMs either by prescribing the absolute humidity or the relative humidity; in the

latter case the amount of water vapor increases (decreases) with increasing (decreasing) temperature. Finally, the fractional cloudiness and the temperature or altitude of the cloud tops are either prescribed or predicted.

The zero-climate feedback limit in the RCM is obtained by prescribing the lapse-rate, absolute humidity and planetary albedo and by holding them fixed as surface and atmospheric temperatures vary. The computed surface temperature change for the zero climate feedback case, $(\Delta T_s)_0$, generally ranges from 1.3 K (Manabe and Wetherald, 1967; Ramanathan, 1981) to 1.2 K (Hansen *et al.*, 1984). Both of these values are reasonably close to the value of 1.1 K obtained from the zero-dimensional EBM (Section 15.2.2.1). Hence, $(\Delta T_s)_0$ is a nearly model-independent parameter and is a useful measure of the radiative forcing due to a given change in atmospheric composition.

To indicate the importance of the climate feedback processes listed in Table 15-6, we introduce a climate feedback factor, F, which is defined as:

$$F = \frac{\Delta T_s}{(\Delta T_s)_0} \tag{2}$$

where ΔT_s is the change in surface-air temperature with the feedback. The $(\Delta T_s)_0$, ΔT_s and F obtained for CO_2 doubling with various hypothesized feedbacks are shown in Table 15-6.

The water vapor feedback (second row in Table 15-6) is one of the better understood feedback processes and was introduced in the RCM by Manabe and Wetherald (1967) based on the fact that the observed zonally averaged relative humidity is quite insensitive to seasonal changes in temperatures. With fixed relative humidity, the water vapor amount increases with an increase in surface temperature according to the Clausius-Clapeyron relation. Since H_2O is the most important greenhouse constituent, the H_2O-T_s feedback increases computed ΔT_s by roughly 50 to 80% depending on the model (see Manabe and Wetherald, 1967; the review paper by Ramanathan and Coakley, 1978; F in Table 15-6). The increased solar absorption by H_2O contributes roughly 10% to the H_2O-T_s feedback.

Other parameters such as lapse rate, cloud top temperature, cloud cover will have a significant impact on λ. The numbers in Table 15-6 indicate the potential importance of these feedbacks. However, the magnitude and even the sign in some instances (e.g., clouds) of these feedbacks are not well known.

Another important feedback concerns the snow and ice albedo feedback. With an increase in surface temperature, snow and ice cover will melt which may lead to a decrease in the areal extent of snow and ice cover; this will lead to a decrease in surface albedo and a corresponding increase in the absorbed solar radiation. This positive feedback has been the subject of scores of EBM, RCM and GCM studies. Generally, according to Dickinson (1985), several models have converged to the conclusion that the ice-albedo feedback amplifies global average ΔT_s by about 15% (also see last column of Table 15-6); note, however, that the magnitude of amplification by any one feedback depends on the other feedbacks included. It should also be noted that the ice-albedo feedback has a significant impact on polar surface temperature change.

15.2.2.3 General Circulation Models

The principal prognostic variables of an atmospheric GCM are the temperature, horizontal velocity, and surface pressure, which are governed, respectively, by the thermodynamic energy equation, the horizontal momentum equation, and the surface pressure tendency equation. With the mass continuity equation and

Table 15-6. Feedback Analysis Using the Oregon State University 2-Layer RCM. (Source: Schlesinger, Private Communication)

Feedback Mechanism	T_S ($1\times CO_2$) (°C)	ΔT_S (°C)	F[2]
None $[\Delta T_S)_0]$[1]	15.28	1.35	
Water Vapor[3]	14.53	1.94	1.4
Lapse Rate[4]	9.53	0.88	0.7
Cloud Temperature[5]	15.28	1.73	1.3
Cloud Cover	15.28	1.38	1.0
Cloud Optical Depth[7]	15.28	1.39	1.0
Surface Abedo[8]	15.43	1.56	1.2
Water Vapor[3] and Lapse Rate[4]	9.38	1.19	.9
Cloud Temperature[5]	14.20	2.79	2.1
Cloud Cover[6]	15.12	1.81	1.3
Cloud Optical Depth[7]	15.39	1.70	1.3
Surface Albedo[8]	14.58	2.39	1.8
Water Vapor[3], Cloud Temperature[5], and Surface Albedo[8]	14.14	3.85	

[1] $(\Delta T_S)_0$ is calculated by the RCM without feedbacks.
[2] $F = \Delta T_S/(\Delta T_S)_0$.
[3] With the fixed relative humidity profile of Manabe and Wetherald (1967).
[4] With the moist adiabatic lapse rate.
[5] With fixed cloud temperature prescribed equal to that of the $1\times CO_2$ simulation with no feedback.
[6] With variable cloud cover prescribed similarly to that of Wang *et al.* (1981) and cloud albedo, absorptivity and transmissivity.
[7] With variable optical depth τ prescribed similarly to that of Wang *et al.* (1981) and cloud albedo, absorptivity and transmissivity parameterized in terms of τ following Stephens *et al.* (1984).
[8] With variable surface albedo prescribed as in Wang and Stone (1980).

the hydrostatic approximation and appropriate boundary conditions, these equations form a closed system for an adiabatic and frictionless atmosphere. But the general circulation of the atmosphere is the large-scale, thermally driven field of motion in which there are interactions between the heating and motion fields. Therefore, several additional prognostic variables, with corresponding governing equations and appropriate boundary conditions, must be added to simulate the heating. Of these, the most important is the water vapor, which is governed by the water vapor continuity equation. Because the atmosphere is largely heated by the underlying surface through the exchange of sensible and latent heat, and because snow lying on the ground can have a large influence on the surface albedo, the ground temperature, soil moisture, and mass of snow on the ground are prognostic variables, governed by energy, water, and snow

budget equations for the ground. In addition to the prognostic variables, GCMs have many diagnostic variables, among which clouds may be one of the most important.

The equilibrium changes in surface air temperature ΔT_s simulated by 7 selected GCMs for a doubled CO_2 concentration are presented in Table 15-7. The first four studies were performed with atmospheric GCMs coupled to a swamp ocean model which has zero heat capacity and no horizontal or vertical heat transports. These coupled atmospheric GCM/swamp ocean models are run without a seasonal insolation cycle to prevent the freezing of the ocean in the latitudes of the polar night. The last three studies were performed with atmospheric GCMs coupled to a fixed-depth mixed layer ocean model which has heat capacity, prescribed horizontal heat transports (zero except in Hansen *et al.*, 1984), and no vertical heat transports. These coupled atmospheric GCM/fixed-depth mixed layer ocean models are run with the seasonal insolation cycle.

Table 15-7 shows that the models without the seasonal insolation cycle give surface air temperature warmings of 1.3 to 3.0 K for a doubling of CO_2, while the models with the seasonal insolation cycle give annual average warmings of 3.5 to 4.2 K (also see footnote 2 in Table 15-7). It is difficult to identify the specific causes for the wide range of surface air temperature warming simulated by the models with a swamp ocean because these models differ in geographical domain, land/ocean distribution and orography as well as in their treatment of clouds, snow and sea ice (Schlesinger, 1984). It is therefore gratifying that the three simulations with the atmospheric GCM/fixed-depth mixed layer ocean model having a global

Table 15-7. Surface Air Temperature Change Induced by a Doubled CO_2 Concentration As Simulated by Selected General Circulation Models.

Study	ΔT_s (K)
Manabe & Wetherald (1975)	2.9
Manabe & Wetherald (1980)	3.0
Schlesinger (1983)	2.0
Washington & Meehl (1983)	1.3
Washington & Meehl (1984)	3.5
Hansen *et al.* (1984)	4.2[2]
Manabe & Wetherald[1]	4.0

[1] Unpublished study. See Schlesinger and Mitchell (1985).

[2] This version of the Hansen *et al.* GCM has less sea-ice than observed. They also report results with an alternate version of the GCM which has roughly 15% more sea-ice than observed and this "alternate" version yielded a ΔT_s of 4.8 K.

domain, realistic land/ocean distributions and orography, and interactive clouds produce comparable global mean surface air temperature warmings.

15.2.2.4 The Importance of Cloud Feedback

One of the least understood and potentially important feedbacks is the feedback involving clouds. The issues to be addressed are threefold. The first concerns the response of cloud cover, cloud base and cloud tops to temperature changes; the second concerns the change in cloud radiative properties (i.e., albedo and emissivity); and the last is the relationship between the above changes and the radiative forcing due to the clouds. The limited number of studies on this tough problem have led to the following conflicting inferences. Empirical studies using satellite radiation budget data in conjunction with cloud cover data have indicated that even if cloud cover changes substantially, the radiative changes would be negligible (Cess, 1976). Similar empirical studies, but using different satellite data sets (see Cess *et al.*, 1982), have suggested that an increase (decrease) in clouds would lead to a large radiative cooling (heating). The implication of these studies is that an increase (decrease) of global average clouds by about 4% i.e., from 50 to 54% (or decrease to 46%) would be sufficient to ameliorate (amplify) the CO_2 effect by a factor of 2 or more. Recent GCM studies, on the other hand, indicate that cloud feedback could amplify the CO_2 warming by about 25 to 50%.

The GCM studies have largely ignored the so-called cloud-optics feedback (Charlock, 1982; Somerville and Remer, 1984). In this feedback, the cloud liquid water increases with an increase in T_s such that the cloud albedo increases with an increase in T_s. The increase in cloud albedo provides a negative feedback. RCM calculations (Charlock, 1982, and Somerville and Remer, 1984) suggest that the cloud optics feedback may reduce ΔT_s by a factor of 1.5 to 2.

The fundamental difficulty in the way of realistic attack on the cloud problem is the fact that the processes that govern cloud formations and their radiative effects occur on scales ranging from several meters to several tens of kilometers. Theoretical, modeling and observational breakthroughs are needed to bridge the gap between the spatial scales of climate models and the scales of cloud formation. In the interim, we have to acknowledge the potentially large source of uncertainty in model estimates of climate sensitivity and explore imaginative ways of verifying model sensitivity with observations.

15.2.3 The Implications of H_2O-Climate Feedback

Most climate models and, in particular, all of the GCMs indicate that an increase in tropospheric water vapor content will accompany the greenhouse warming of trace gases. The increase in H_2O is a strong function of latitude and altitude ranging from 5 to 15% in the low latitudes to as much as 50% in the polar regions (e.g., see Washington and Meehl, 1984). As described earlier (Section 15.2.2) this H_2O feedback amplifies the surface warming by about 50 to 80%. In addition to providing the positive climate feedback, the increase in tropospheric H_2O has important implications to tropospheric chemistry (Hameed *et al.*, 1980; Callis *et al.*, 1983a; WMO, 1982).

The increase in H_2O can lead to increased production of tropospheric OH which, in turn, may lead to enhanced oxidation of CH_4, CO and O_3 (see Figure 15-4), and possibly other chemicals. Since OH plays a dominant role as a cleansing agent of tropospheric pollutants, surface-troposphere temperature changes (through the H_2O feedback) can have substantial influence on the concentrations of other greenhouse gases (e.g., O_3 and CH_4) in the troposphere. The nature and magnitude of this climate-chemistry feedback is discussed in Section 15.3.

The second important role of H_2O feedback concerns the interactions between low-latitude tropopause temperatures and stratospheric H_2O. The direct radiative forcing of trace gases such as CFCs and O_3 are particularly large in the vicinity of the tropical tropopause (Figures 15-8 and 15.9). Furthermore, GCM results reveal a large change in tropical tropopause temperatures in response to O_3 change (Figure 15-12) or to CFCs (Dickinson *et al.*, 1978). Since the stratospheric H_2O concentration is believed to depend critically on this temperature, substantial cooling (or warming) of the tropopause may lead to a substantially drier (or wetter) stratosphere.

Large changes in stratospheric water vapor have important radiative and chemical consequences. For example, a doubling of stratospheric H_2O from 3 to 6 ppm can lead to a 0.6 K surface warming (Wang *et al.*, 1976). Since H_2O is a controlling factor in stratospheric HO_x chemistry (Liu *et al.*, 1976), altered stratospheric H_2O can also influence stratospheric concentrations of O_3 and CH_4.

15.3 EFFECTS ON ATMOSPHERIC AND SURFACE TEMPERATURES

Most of the trace gases that have been detected in the atmosphere are listed in Table 15-8 together with information pertinent to their presently known sources, sinks, lifetimes, and present concentrations. The direct greenhouse effects of these gases will be discussed first, to be followed by discussions of the effects arising from chemical perturbations.

15.3.1 Direct Effects

Most of the gases shown in Table 15-8 have absorption features in the longwave spectrum (see Tables 15-1a and 15-1b). Many of the gases shown in Table 15-8 have a substantial surface warming effect at 1 ppbv level (see Figure 15-13). For reference purposes, Figure 15-13 also shows the surface warming due to uniform increases in tropospheric O_3 between 0 to 12.5 km, CH_4 and N_2O. All of the gases shown in Figure 15-13 have strong absorption features in the "window" region of 7-13 μm. Bands of gases such as CF_4 occur in the same wavelength as CH_4 and N_2O bands. Because of this band overlap, CF_4, in spite of having the strongest band (band strength of about 5000 cm^{-2} atm^{-1}, see Table 15-1b) of the gases shown in Figure 15-13, does not have as large a surface warming as some of the other CFCs. The direct greenhouse effects have also been estimated by numerous recent studies (e.g., Brühl and Crutzen, 1984; Wang *et al.*, 1985; Ramanathan *et al.*, 1985; Owens *et al.*, 1985b).

The radiative-convective model (RCM) results for ΔT_S due to increases in CFCs, CH_4 and N_2O have differed significantly among models. Recent studies (Ramanathan *et al.*, 1985 and Owens *et al.*, 1985b) have attempted to clarify the sources for the discrepancy. For CFCs, most of the differences were traced to the use of different spectroscopic data and to differences in model sensitivity. When these results were scaled to the same model sensitivity of $\Delta T_S = 2$ K for a doubling of CO_2 and to the most recent CFC band strengths of Kagann *et al.* (1983), all of the models (Ramanathan, 1975; Reck and Fry, 1978; Lacis *et al.*, 1981; Ramanathan *et al.*, 1985) except the Owens *et al.*, (1985) model, yield a surface warming of 0.52 to 0.56 K for a 0 to 2 ppbv increase in each of CFC11 and CFC12. The Owens *et al.*, model yields a ΔT_S of 0.45 K (see Owens *et al.*, 1985b for a more complete discussion of this intercomparison). A similar scaling procedure of model sensitivity (i.e., $\Delta T_S = 2$ K for CO_2 doubling) for doubling of CH_4 and N_2O shows a spread of about 0.2 to 0.3 K for doubling of CH_4 and about 0.35 to 0.45 K for doubling of N_2O (see Table 9 of Owens *et al.*, 1985b). These differences strongly suggest the need for an ICRCCM (1984) type intercomparison study for the trace gases shown in Figure 15-13.

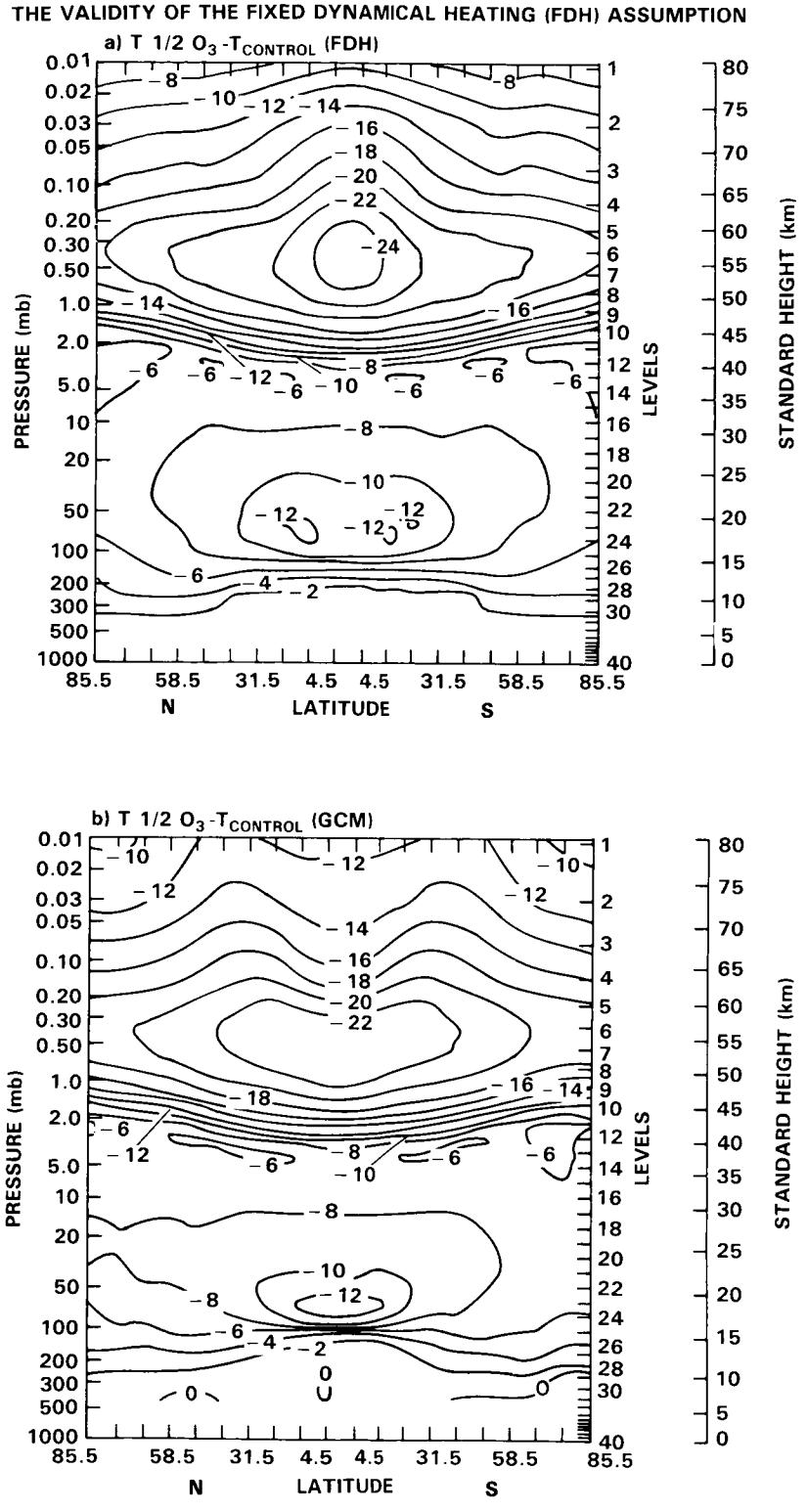

Figure 15-12. Temperature change due to 50% ozone reduction as simulated by (a) the FDH model and (b) the GCM. (Fels *et al.,* 1980).

Table 15-8. Estimates of the Abundance of Trace Chemicals in the Global Atmosphere of Years 1980 and 2030. Source: Ramanathan, Cicerone, Singh and Kiehl (1985)

Chemical Group	Chemical Formula	Dominant Source*	Dominant Sink*	Estimated Average Residence Time (τ_j) (years)	Year 1980 Global Average Mixing Ratio (ppb)†	Year 2030 probable global average concentration (ppb)*** Probable Value	Possible Range	REMARKS (also see text for details)
Carbon Dioxide	CO_2	N,A	O	2	339×10^3	450×10^3	—	Based on a 2.4% per year increase in anthropogenic CO_2 release rates over the next 50 years
Nitrogen Compounds	N_2O	N,A	S(UV)	120	300	375	350 - 450	Combustion and fertilizer sources
	NH_3	N,A	T	0.01	<1	<1	—	Concentration variable and poorly characterized
	$(NO+NO_2)$	N,A	T(OH)	0.001	0.05	0.05	0.05 - 0.1	Concentration variable and poorly characterized
Sulfur Compounds	CSO	N,A	T(O,OH)?	1(?)	0.52	0.52	—	Sources and sinks largely unknown
	CS_2	N,A	T	1(?)	<0.005	<0.005	—	Sources uncharacterized
	SO_2	A(?)	T(OH)	0.001	0.1	0.1	0.1 - 0.2	Given the short lifetime the global presence of SO_2 is unexplained
	H_2S	N	T(OH)	0.001	<0.05	<0.5	—	
Fully Fluorinated Species	CF_4(F14)	A	I	>500	0.07	0.24	0.2 - 0.31	Aluminum industry a major source
	C_2F_6(F116)	A	I	>500	0.004	0.02	0.01 - 0.04	Aluminum industry a major source
	SF_6	A	I	>500	0.001	0.003	0.002 - 0.05	
Chlorofluoro-carbons	$CClF_3$(F13)	A	S(UV),I	400	0.007	0.06	0.04 - 0.1	All chlorofluorocarbons are of exclusive man-made origin. A number of regulatory actions are pending. The nature of regulations and their effectiveness would greatly affect the growth of these chemicals over the next 50 years.
	CCl_2F_2(F12)	A	S(UV)	110	0.28	1.8	0.9 - 3.5	
	$CHClF_2$(F22)	A	T(OH)	20	0.06	0.9	0.4 - 1.9	
	CCl_3F(F11)	A	S(UV)	65	0.18	1.1	0.5 - 2.0	
	CF_3CF_2Cl(F115)	A	S(UV)	380	0.005	0.04	0.02 - 0.1	
	$CClF_2CClF_2$(F114)	A	S(UV)	180	0.015	0.14	0.06 - 0.3	
	CCl_2FCClF_2(F113)	A	S(UV)	90	0.025	0.17	0.08 - 0.3	
Chlorocarbons	CH_3Cl	N(O)	T(OH)	1.5	0.6	0.6	0.6 - 0.7	Dominant natural chlorine carrier of oceanic origin
	CH_2Cl_2	A	T(OH)	0.6	0.03	0.2	0.1 - 0.3	A popular reactive but non-toxic solvent
	$CHCl_3$	A	T(OH)	0.6	0.01	0.03	0.02 - 0.1	Used for manufacture of F22; many secondary sources also exist
	CCl_4	A	S(UV)	25 - 50	0.13	0.3	0.2 - 0.4	Used in manufacture of fluorocarbons; many other applications as well
	CH_2ClCH_2Cl	A	T(OH)	0.4	0.03	0.1	0.06 - 0.3	A major chemical intermediate (global production=10 tg/yr); possibly toxic
	CH_3CCl_3	A	T(OH)	8.0	0.14	1,5	0.7 - 3.7	Non-toxic, largely uncontrolled degreasing solvent
	C_2HCl_3	A	T(OH)	0.02	0.005	0.01	0.005 - 0.02	Possibly toxic, declining markets because of substitution to CH_3CCl_3
	C_2Cl_4	A	T(OH)	0.5	0.3	0.07	0.03 - 0.2	Possibly toxic, moderate growth due to substitution to CH_3CCl_3
Brominated and iodated species	CH_3Br	N	T(OH)	1.7	0.01	0.01	0.01 - 0.02	Major natural bromine carrier
	$CBrF_3$(F13B1)	A	S(UV)	110	0.001	0.005	0.003 - 0.01	Fire extinguisher
	CH_2BrCH_2Br	A	T(OH)	0.4	0.002	0.002	0.001 - 0.01	Major gasoline additive for lead scavenging; also a fumigant
	CH_2I	N	T(UV)	0.02	0.002	0.002	—	Exclusively of oceanic origin
Hydrocarbons, CO, H_2	CH_4	N	T(OH)	5 - 10	1650	2340	1850 - 3300	A trend showing increase over the last 2 years has been identified
	C_2H_6	N	T(OH)	0.3	0.8	0.8	0.8 - 1.2	Predominantly of auto exhaust origin
	C_2H_2	A	T(OH)	0.3	0.06	0.1	0.06 - 0.16	No trend has been identified to date
	C_3H_8	N,	T(OH)	0.03	0.05	0.05	0.05 - 0.1	No trend has been identified to date
	CO	N,A	T(OH)	0.3	90	115	90 - 160	No trend has been identified to date
	H_2	N,A	T(SL,OH)	2	560	760	560 - 1140	
Ozone	O_3 (Tropospheric)	N	T(UV, SL,O)	0.1 - 0.3	F(Z)**	12.5%		A small trend appears to exist but data are insufficient
Aldehydes	HCHO	N	T(OH,UV)	0.001	0.2	0.2	—	Secondary products of hydrocarbon oxidation
	CH_3CHO	N	T(OH,UV)	0.001	0.02	0.02	—	1980 concentration estimated from theory

*N - Natural; A - Anthropogenic; O - Oceanic; S - Stratosphere; UV - Ultraviolet Photolysis; T - Troposphere; OH - Hydroxyl radical removal; I - Ionospheric and extreme UV and electron capture removal; SL - Soil sink.

†These concentrations are integrated averages; for chemicals with lifetimes of 10 years or less, significant latitudinal gradients can be expected in the troposphere; for chemicals with extremely short lifetimes (0.001-0.3 years) vertical gradients may also be encountered.

**Varies from 25 ppbv at the surface to about 70 ppbv at 9 km. The concentration was increased uniformly by the same percentage from the surface to 9 km.

***These values are not used in the present assessment.

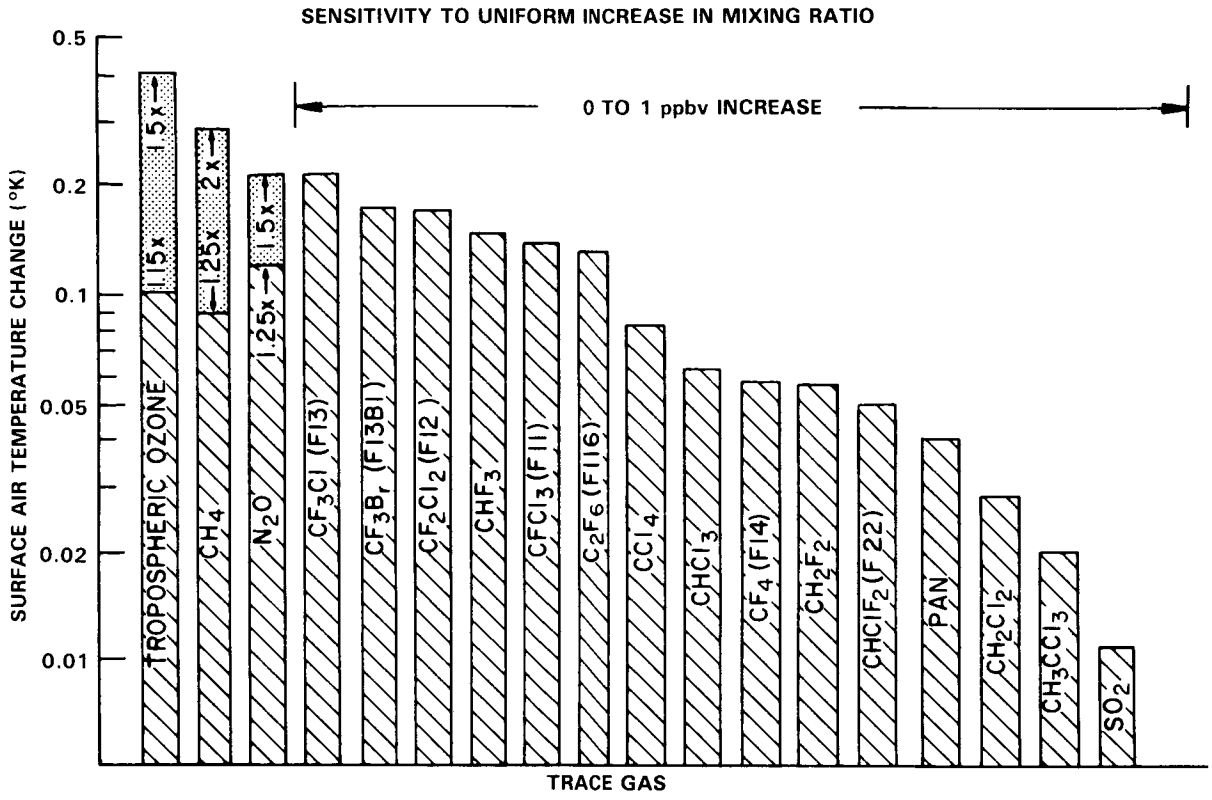

Figure 15-13. Computed surface air temperature change due to a 0 to 1 ppbv increase in trace gas concentrations. Tropospheric O_3, CH_4 and N_2O increases are also shown for comparison. For these three gases, the factor of increase is indicated in the figure. For example, for tropospheric O_3, the bottom part of the shaded region is the temperature change due to a uniform increase in O_3 from 0 to 12 km by a factor of 1.15. Source: 1-D radiative-convective model results of Ramanathan *et al.* (1985).

It is important to note that increasing levels of these gases are essentially additive and have the potential to add directly and significantly to the greenhouse effect of the present day atmosphere. Furthermore, several of the important gases shown in Table 15-8 (e.g., F13; F116; F13B1; CF_4) have lifetimes in excess of 100 years, and hence, if their use increases in the future, these gases have the potential for a substantial impact on climate on time scales of several hundred years.

15.3.2 Indirect Effects

In addition to the direct effects, many of the trace gases perturb temperatures indirectly through physical or chemical mechanisms that cause the distributions, or concentrations of other optically active constituents to be changed. The nature of some of the interactions leading to these indirect effects were shown in Figure 15-4. Most well known of these is perhaps the stratospheric destruction of O_3 due to reaction with chlorine and chlorine oxides formed as a result of stratospheric photolysis of chlorine bearing compounds (e.g., CF_2Cl_2, $CFCl_3$, CCl_4, and CH_3Cl). The altered atmospheric levels O_3 will affect both the tropospheric and stratospheric radiative budgets at both solar and infrared wavelengths. Furthermore, temperature changes can perturb chemistry through the H_2O feedback (Section 15.2). These and other examples are discussed in the following paragraphs.

15.3.2.1 H_2O-Temperature Feedback Effects on Tropospheric Chemistry

As discussed in Section 15.2.3, climate models including GCMs indicate that an increase in tropospheric humidity accompanies the computed surface/troposphere warming (due to the greenhouse effect of trace gases). For example, a 2 K tropospheric warming in the RCM (due to CO_2 doubling) leads to an increase of H_2O that ranges from about 10 to 30% (Figure 15-14). The increase in H_2O can lead to enhanced OH production through the reaction (Hameed *et al.*, 1980):

$$O(^1D) + H_2O \rightarrow 2OH \quad (1)$$

which also acts as a direct loss reaction for ozone as O(1D) is in instantaneous equilibrium with O_3. Further loss of ozone may take place through the reactions:

$$OH + O_3 \rightarrow HO_2 + O_2 \quad (2)$$

$$HO_2 + O_3 \rightarrow OH + 2O_2 \quad (3)$$

However, at high NO_x levels, ozone is efficiently produced through the catalytical cycle:

$$HO_2 + NO \rightarrow NO_2 + OH \quad (4)$$

$$NO_2 + h\nu \rightarrow NO + O \quad (5)$$

$$O + O_2 + M \rightarrow O_3 + M \quad (6)$$

The main source for HO_2 is OH reacting with CO (see discussions later under the CO section) rather than reaction (2). Hence, reactions (4) to (6) lead to a net O_3 production. However, due to the large observed variations in tropospheric NO levels, with extremely low values in some remote regions, one could expect either ozone production or ozone destruction as a result of the reactions (1) to (6).

Tropospheric CH_4 levels may also be reduced by the reaction

$$CH_4 + OH \rightarrow CH_3 + H_2O \quad (7)$$

For a doubling of CO_2, the 1-D latitudinal energy balance model (Hameed and Cess, 1983), with a ΔT_S of 3.1 K, shows a decrease in tropospheric O_3 and CH_4 of 11% and 17% respectively; the radiative-convective model, with a ΔT_S of 2 K, computes a decrease of 5-7% for tropospheric O_3 and 9-14% for CH_4. Because of the nonlinearities in the H_2O-T coupling and other nonlinearities in the chemistry, simultaneous perturbations may exacerbate the effect (e.g., see Figures 15-15 and 15-16). For example, a doubling of CO_2 with a CFC increase (due to steady state injection of CFC11 and CFC12 at the 1977 emission rate) results in a computed decrease of about 16% for O_3 (see Figure 15-15) and about 26% for CH_4 (Callis *et al.*, 1983a).

The O_3 and CH_4 changes resulting from the H_2O-T coupling have a negative feedback effect on the computed ΔT_S. For a CO_2 doubling, the computed surface warming decreases by about 10% with the inclusion of the decreases in O_3 and CH_4 (Hameed and Cess, 1983). All of the results described above

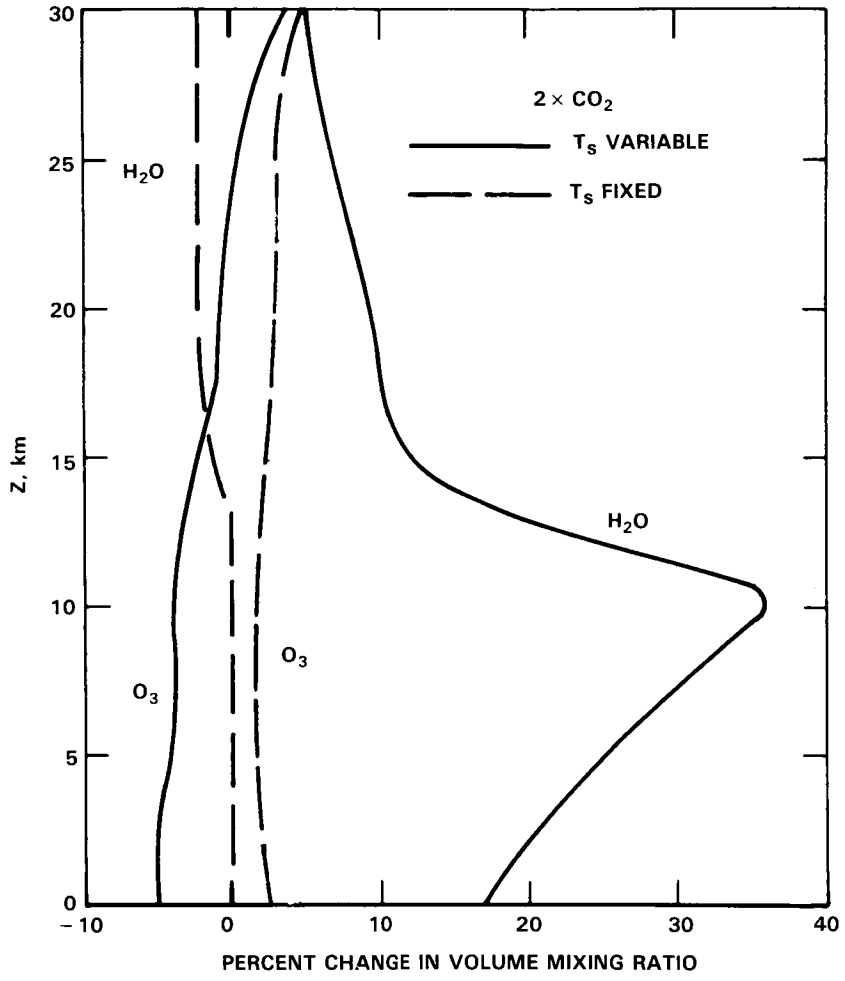

Figure 15-14. Indirect effects of CO_2 doubling on H_2O and O_3. Solid: both stratospheric and tropospheric temperatures are allowed to vary; dash: only stratospheric temperatures are allowed to vary in response to CO_2 increase. Source: 1-D model results of Callis *et al.* (1983a).

depend very strongly on the assumed background levels of NO_x (Hameed *et al.*, 1979; also see Figure 15-15), since the ozone formation as described above as well as the products in the methane oxidation scheme depend on NO concentrations.

15.3.2.2 Effects of CO_2

Carbon dioxide does not react chemically to any significant degree in the troposphere or stratosphere. However, the stratospheric temperature decrease that is computed to result from CO_2 increase (Manabe and Wetherald, 1967) will alter the reaction rates and can lead to stratospheric O_3 increases (Boughner and Ramanathan, 1975). The O_3 increase can, in turn, have a negative feedback on the CO_2-induced stratospheric cooling. Numerous coupled 1-D model studies (Boughner, 1978; Owens *et al.*, 1985) have estimated this feedback. For a doubling of CO_2, the model calculations generally indicate a column O_3 increase of 2 to 6% (see Table 6 of Owens *et al.*, 1985). This O_3 increase is mainly concentrated above 20 km where the enhanced solar heating (due to O_3 increase) reduces the stratospheric cooling due to

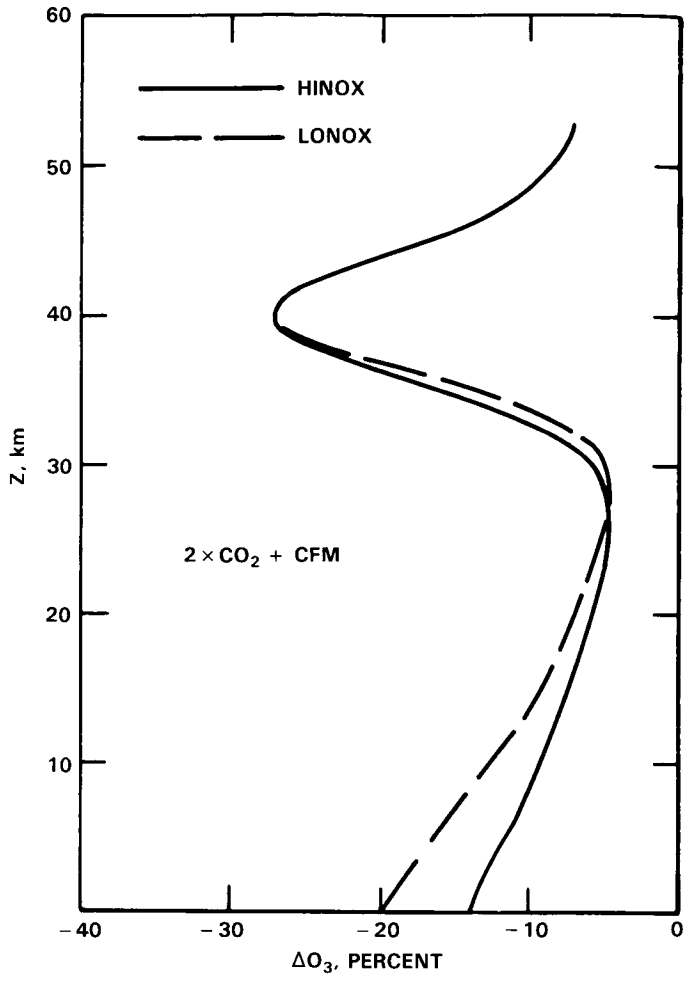

Figure 15-15. Computed changes in O_3 due to the combined effects of CO_2 doubling and CFM increase. Source: 1-D model results of Callis *et al.* (1983a). HINOX and LONOX refer to high and low concentrations of assumed background values for NO_x.

CO_2 increase by about 20% (Figure 7 of Owens *et al.*, 1985). The effect of the O_3-T feedback on surface temperature is negligible.

15.3.2.3 Effects of CH_4

Recent studies (Blake and Rowland, 1985 and Blake *et al.*, 1982) show that tropospheric concentrations of CH_4 have been increasing at a rate of about 1 percent per year over the last 4-6 years. The causes of this increase are not known at present. Both changes in the release rate of methane and in the loss rate due to changes in OH concentrations, reaction (7), affect atmospheric CH_4 levels. In addition, as the methane oxidation by reaction (7) is a main loss path of OH in the free troposphere, increases in the release rate of methane lead to a decrease in OH, and thereby to a further increase in methane levels. With continued increases in methane in the future, this positive feedback mechanism could become increasingly important. Recent 2-D model studies (Isaksen and Hov, 1985) suggest that this feedback may account for 30% of the methane increase at present. However, since the magnitude of this feedback depends on the assumed emission of NO_x, the contribution of this feedback to the observed CH_4 increase is highly model dependent

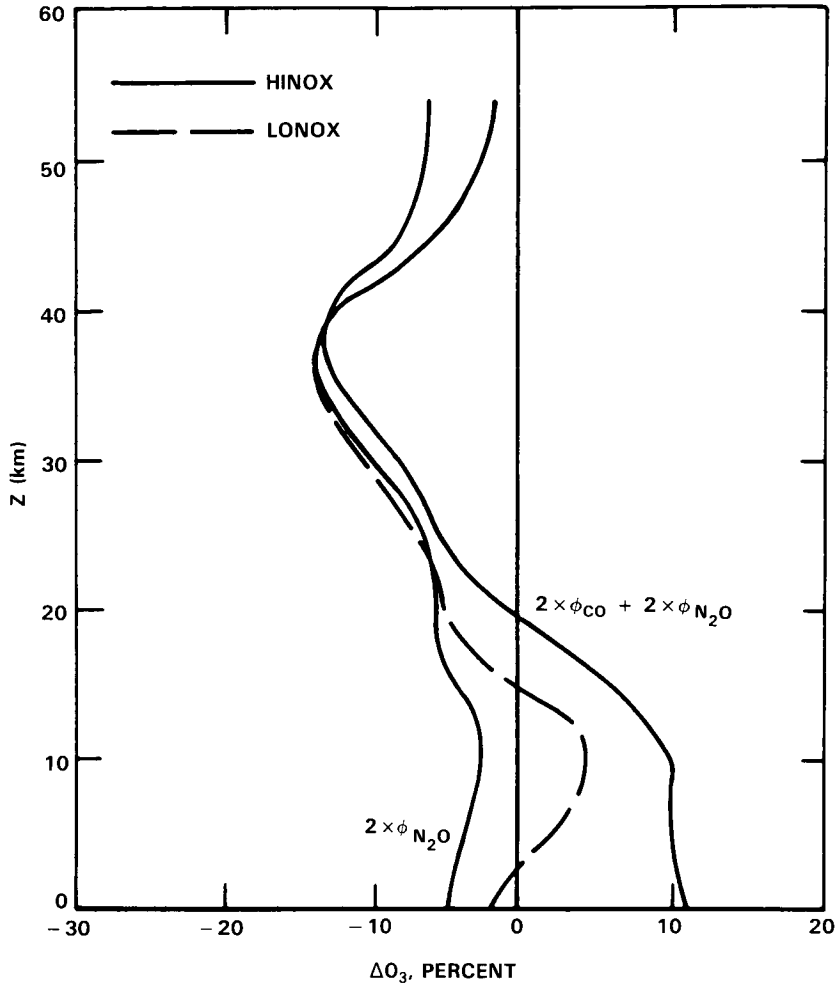

Figure 15-16. The indirect effects of increases in fluxes (ϕ) of CO and N_2O on O_3. Source: 1-D model results of Callis *et al.* (1980).

(Crutzen, private communication). A reduction of tropospheric OH levels due to CH_4 increase will also lead to reduction of the rate of scavenging (by OH) of CH_2F_2, $CHClF_2$, CH_2Cl_2, CH_3CCl_3, and SO_2 leading to increased lifetimes (and hence, concentrations) of these species with attendant perturbations to the infrared radiative balance. Increases in tropospheric methane will, provided sufficient amounts of NO_x are present, lead to enhanced ozone production through reaction (4) and the reaction:

$$CH_3O_2 + NO \rightarrow CH_3O + NO_2 \qquad (8)$$

followed by reactions (5) and (6), where productions of CH_3O_2 and HO_2 are enhanced. 2-D model estimates show that tropospheric ozone increases due to increased methane levels vary strongly with latitude, height and season (Crutzen and Gidel, 1983; Isaksen and Stordal, 1985). In 2-D models, the most pronounced ozone increase is obtained at equatorial latitudes, with ozone increases of approximately 20% in the middle and upper troposphere for a doubling of present methane levels (see Figure 15-17). In the 1-D model, the greenhouse effect of enhanced tropospheric O_3 amplifies the CH_4 greenhouse effect by as much as 75% (Table 8 of Owens *et al.*, 1985b).

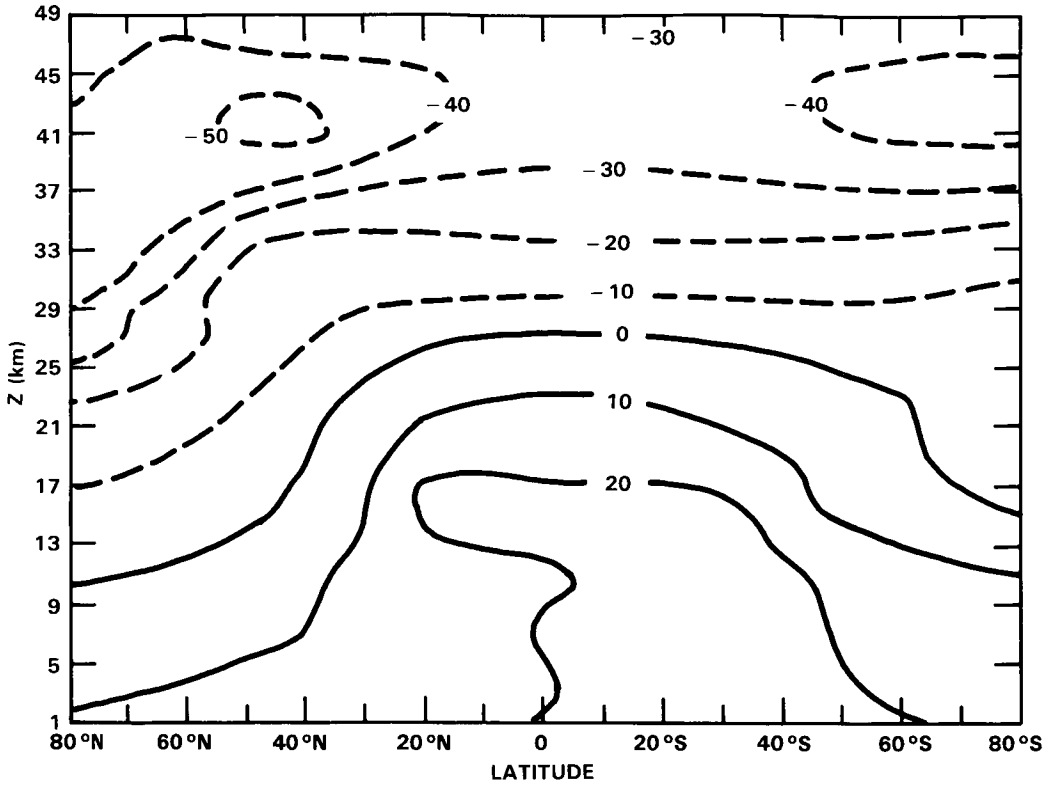

Figure 15-17. Latitudinal-height cross-section of future ozone changes (in %) due to releases of CFCs (CFC11 and CFC12), N_2O and CH_4, estimated in a 2-D diabatic circulation model (Isaksen and Stordal, 1985). The following assumptions are made with regard to future release rates and concentration rates: CFCs are in steady state with 1980 release rates, N_2O increases with a factor 1.4 from its 1980 value (300 ppb at the surface), CH_4 increases with a factor 2 from its 1980 value (1.65 ppm at the surface). The numbers given are for February.

Furthermore, increases in CH_4 are calculated to lead to similar, but less pronounced increases in lower and mid-latitudinal stratospheric ozone through their effect on HO_x, Cl_x and NO_x species (WMO, 1981). For example, CH_4 can mitigate the ozone destruction by the chlorine catalytic cycle in the middle stratosphere (around 40 km) because it can transform the Cl atoms to HCl (Brühl and Crutzen, 1984). An additional effect is that oxidation of methane may lead to substantial increases in H_2O levels in the middle and upper stratosphere (see Callis *et al.*, 1983a; Owens *et al.*, 1985b).

15.3.2.4 Effects of N_2O

Weiss (1981) has reported data that suggest that atmospheric N_2O, currently at levels of 300 ppbv, was increasing at the rate of 0.2 percent per year between the years of 1976-1980. Khalil and Rasmussen (1983) suggest an increase of 0.3 percent per year between the years of 1978-1981.

The indirect effects of increases of atmospheric N_2O arise from the reaction:

$$N_2O + O(^1D) \rightarrow 2NO \qquad (9)$$

Reaction (9) is the principal source of stratospheric NO_y (= NO + NO_2 + HNO_3 + NO_3 + HNO_4 + HNO_2 + 2 × N_2O_5 + ...). Consequently, increases in atmospheric N_2O levels will lead to increases in stratospheric NO_y and the subsequent reduction of stratospheric O_3 by catalytic destruction through the reactions

$$NO + O_3 \rightarrow NO_2 + O_2 \quad (10)$$

$$NO_2 + O \rightarrow NO + O_2 \quad (11)$$

If increases in N_2O occur at the same time as increases in the chlorine bearing compounds (e.g., CF_2Cl_2, $CFCl_3$, and CCl_4), the net effect will depend upon the details of the projected increases and their vertical distributions. Increasing stratospheric NO_y levels will provide a buffer for the stratospheric O_3 against catalytic destruction by Cl_x (= Cl + ClO + HOCl + $ClNO_3$ + ClO_2 + ...) through the reaction

$$NO_2 + ClO + M \rightarrow ClNO_3 + M \quad (12)$$

where $ClNO_3$ represents a temporary reservoir of relatively inactive chlorine. It will also affect the partitioning of chlorine species through the reaction

$$ClO + NO \rightarrow Cl + NO_2 \quad (13)$$

The chemical perturbations induced by N_2O increase are so complicated that even the sign of the tropospheric O_3 change is uncertain. For example, for a doubling of N_2O surface flux (leading to a 93% increase in surface concentration of N_2O) the computed 0-10 km column change in O_3 ranges from −2% to +4% depending upon the background levels of tropospheric NO + NO_2 (see Figure 15-16); the stratospheric O_3 column decreases by about 7%.

15.3.2.5 Effects of CO

Carbon monoxide is itself not radiatively active and therefore does not manifest any direct effects on the earth-atmosphere radiative balance. However CO does scavenge atmospheric OH through the reaction

$$CO + OH \rightarrow CO_2 + H \quad (14)$$

The reduction of tropospheric OH, as noted earlier, can, in turn, affect the abundance of numerous other species including O_3, CH_4, and hydrocarbons which are not fully halogenated (Sze, 1977; Logan *et al.*, 1978 to name a few). This has been discussed earlier in reference to CH_4 increase.

Large interhemispheric differences in the present day atmosphere are exhibited by CO due primarily to anthropogenic emissions (Logan *et al.*, 1981). In addition, increases in tropospheric CO have been suggested by recent studies (Rasmussen and Khalil, 1981; Fraser *et al.*, 1981; Graedel and McRae, 1980; and Khalil and Rasmussen, 1984). Clearly, consideration should be given to the indirect climatic effects of CO, particularly since model calculations (e.g., Hameed and Cess, 1983) have suggested the effects to be significant.

For a doubling of the surface flux of CO (leading to a factor of 2.5 increase in CO), the OH decrease through reaction (14) can lead to increases in CH_4 of about 40 to 50% and to increases in column O_3

of about 12% (Callis *et al.*, 1983a; Hameed *et al.*, 1979 and Hameed and Cess, 1983). In the model calculations (Callis *et al.*, 1983a), the increase in CH_4 also leads to stratospheric H_2O increase of about 7 to 12%.

15.3.2.6 Effects of NO_x (NO + NO_2)

As pointed out repeatedly in the earlier discussions, the indirect effects of trace gases depend critically on the tropospheric concentration of NO_x. Photochemical model calculations have also revealed the significant sensitivity of the computed tropospheric O_3 to the concentration as well as the vertical distribution of NO_x (Fishman and Crutzen, 1978; Liu *et al.*, 1980). Tropospheric NO_x has a variety of natural and anthropogenic sources (e.g., Logan, 1983): combustion and biogenic emissions are major surface sources; high flying aircraft, downward transport from stratosphere are important upper tropospheric sources. In addition, lightning may also contribute significantly in the upper troposphere. The removal of NO_x is through wet and dry deposition, mostly after its conversion to soluble species such as HNO_3 and N_2O_5. The exact removal process is not well understood and difficult to model without a realistic 3-dimensional model.

The indirect climate effect of NO_x arises because of its effect on O_3. Within the troposphere, the chemistry and photochemistry of NO_x is an important source of O_3 through reactions (4) to (6). Within the upper troposphere of the Northern Hemisphere (NH) the NO_x emission from high flying aircraft is considered to be as important a source as natural sources of NO_x (Liu *et al.*, 1980).

Although all models agree that anthropogenic NO_x emissions at the surface and by aircraft will result in the increase of tropospheric O_3, problems in modeling NO_x distribution make it difficult to obtain a reliable quantitative evaluation of the O_3 increase, particularly in the boundary layer where non-methane hydrocarbons play an important yet complex role in the photochemical production of O_3. In the upper troposphere, model calculated O_3 increase in the Northern Hemisphere ranges from a few percent (Isaksen, 1980, Derwent, 1982; Crutzen and Gidel, 1983) to as high as 30 percent (Liu *et al.*, 1980). The major difference is due to assumed natural background NO_x sources in the upper troposphere. In the lower troposphere, estimated O_3 increase in the Northern Hemisphere is about 20 percent (Isaksen, 1980).

From the above discussion, it is probably reasonable to assume a 5% increase in the Northern Hemisphere tropospheric O_3 for the decade of 1970 (e.g., Liu *et al.*, 1980; Isaksen, 1980) due to anthropogenic NO_x emissions. The Northern Hemisphere surface-troposphere radiative heating due to this O_3 increase is roughly a third of that due to the observed CO_2 increase for the decade of 1970.

15.3.2.7 Effects of Halogenated Hydrocarbons

A large number of halogenated hydrocarbons (Table 15-8) have direct effects (Figure 15-13) as well as indirect effects in both the troposphere and the stratosphere. Species not fully halogenated may be expected, at elevated concentrations, to contribute to the reduction of tropospheric OH with subsequent effects on tropospheric O_3 and CH_4 and taking place. However, this effect is expected to be small provided the concentrations of the species remain of the order of a few ppbv or less.

Some of these species released in the troposphere will be photodissociated in the stratosphere with the release of halogens which may catalytically destroy O_3. Of most concern at present and for the immediate future is the catalytic destruction of ozone by chlorine released from the photodissociation of CF_2Cl_2 and $CFCl_3$. This destruction occurs due to the reactions

$$Cl + O_3 \rightarrow ClO + O_2 \quad (15)$$

$$ClO + O \rightarrow Cl + O_2 \quad (16)$$

Recent estimates suggest that steady state emissions of CF_2Cl_2 and $CFCl_3$ may reduce the column sum of O_3 by 3-5% with local reductions of 30 to 50% between 35 to 45 km (Cicerone *et al.*, 1983a, Wuebbles *et al.*, 1983; Owens *et al.*, 1985a; to name a few). Reductions in stratospheric O_3 of such magnitudes will have a significant impact on stratospheric thermal structure (Figure 15-18). Furthermore, within the upper stratosphere, the computed cooling due to CFC-induced O_3 reduction is as large as that due to CO_2 doubling (compare the "CFCs" curve with the "2 CO_2" curve in Figure 15-18).

Since the effect of stratospheric O_3 change on surface temperature depends very critically on the vertical distribution of O_3 change, the computed surface temperature effects have fluctuated in magnitude as well as in *sign* over the years. For example, the computed O_3 perturbation profiles that were reported prior

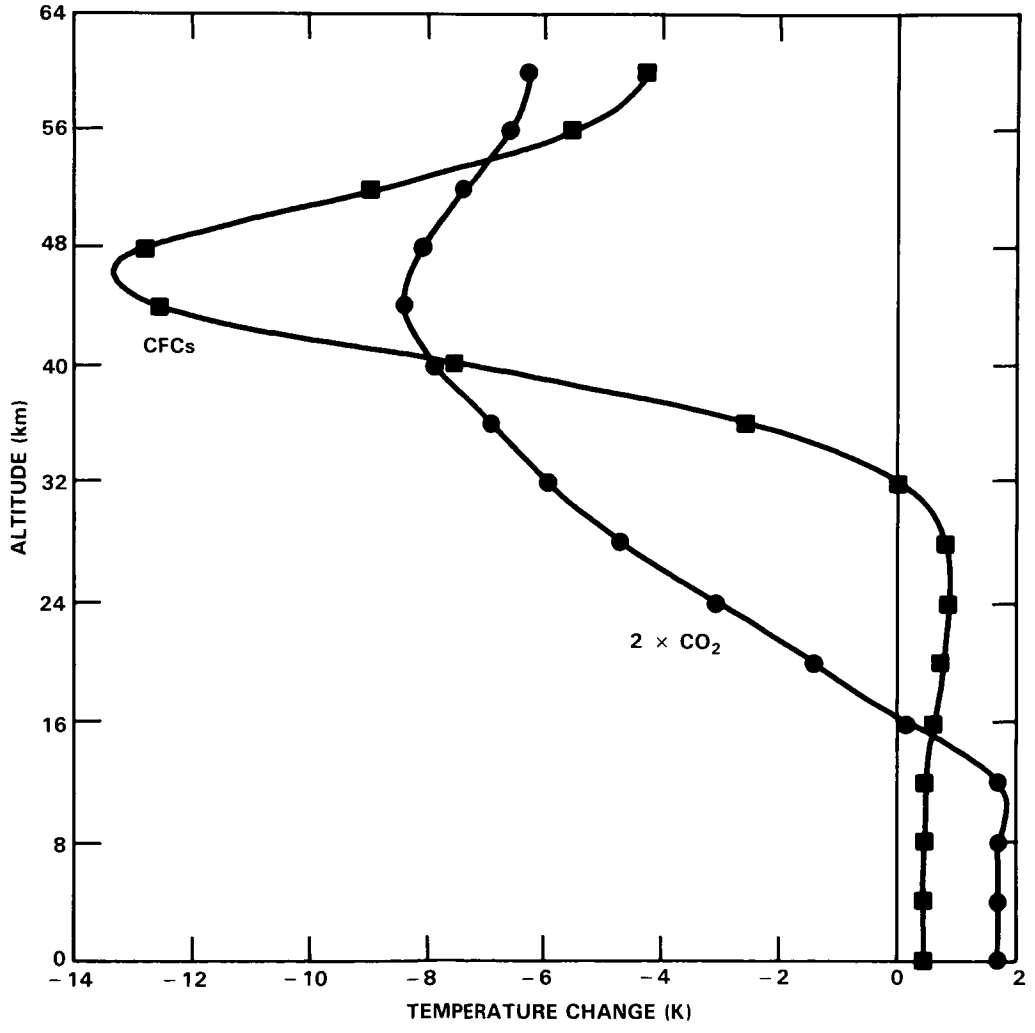

Figure 15-18. Calculated temperature changes due to releases of CFC11 and CFC12 in the steady state (open squares); solid circles: computed effect for 2 × CO_2. (Ref: Owens *et al.*, 1985a).

to the early 1980's yielded a slight surface cooling (Wang *et al.*, 1980). The more recent profiles of O_3 change yield both a surface cooling (Callis *et al.*, 1983a) and a surface warming (Owens *et al.*, 1985a; Ramanathan *et al.*, 1985). The primary source of the difference is the magnitude of O_3 changes in the upper troposphere and lower stratosphere, an issue which is somewhat unresolved at this time.

Irrespective of the sign of the computed surface temperature effect, the magnitude is non-negligible. For example, the recent studies of Owens *et al.* (1985) and Ramanathan *et al.* (1985) estimate a surface warming of 0.1 K due to O_3 change resulting from steady state injection of CFCs at constant mid-1970's emission rates which is about 25-30% of the computed warming due to the direct greenhouse effect of the CFCs. Furthermore, O_3 effects on climate depend on season and latitude (see Section 15.1.2) and both of these effects have been ignored in current climate model studies. Clearly, the O_3-climate effects resulting from the addition of chlorines to the stratosphere deserves continued study.

15.4 TRANSIENT CLIMATIC EFFECTS OF INCREASING ATMOSPHERIC CO_2

15.4.1 Observed Increases In CO_2

Measurements taken at Mauna Loa, Hawaii show that the CO_2 concentration has increased from 315 ppmv in 1958 to 342 ppmv in 1983 (Elliott *et al.*, 1985, see Figure 15-19), an 8% increase in 25 years. A variety of direct CO_2 measurements and indirect reconstructions indicate that the pre-industrial CO_2 concentration during the period 1800 to 1850 was 270 $\pm$10 ppmv (WMO, 1983b). Analyses of the future usage of fossil fuels suggest that the CO_2 concentration will reach twice the pre-industrial value by 2100 (Nordhaus and Yohe, 1983). The change in surface air temperature induced by a doubling of CO_2 as simulated by climate models was discussed in Section 15.2.2. The computed changes in global mean surface air temperature ranged from 1.3 to 4.2 K with the three most recent GCM results falling near the upper end of this range (see Table 15-7). Since such a global warming represents about 25 to 100% of that which is estimated to have occurred during the 10,000-year transition from the last ice age to the present interglacial (Gates, 1976; Imbrie and Imbrie, 1979), there is considerable interest in the identification of a CO_2-induced climatic change, and in the potential impacts of such a change on the spectrum of human endeavors.

The majority of the simulations of CO_2-induced climate change have been performed to determine the change in the equilibrium climate of the earth resulting from an abrupt increase in CO_2 such as doubling from 300 to 600 ppmv. These equilibrium climate change simulations have not been concerned with the time required for the climate change to reach its equilibrium. More recent studies have focused on the transient response of climate to both abrupt and realistic increases in the CO_2 concentration.

15.4.2 Transient Effects

The equilibrium temperature increase corresponding to the CO_2 increase from the year 1850 to 1980 can be determined using Equation 1 of Section 15.2.2 with the direct radiative forcing ΔQ scaled to that for a CO_2 doubling, ΔQ_{2X}. This scaling yields (Augustsson and Ramanathan, 1977):

$$\Delta Q = \Delta Q_{2x} \left\{ \frac{\ln[C(1980)/C(1850)]}{\ln 2} \right\} \quad (1)$$

where C is the CO_2 concentration. Combining these equations and noting that $(\Delta T_s)_{2X} = \Delta Q_{2X}/\lambda$ (see Equation 1 of 15.2), yields

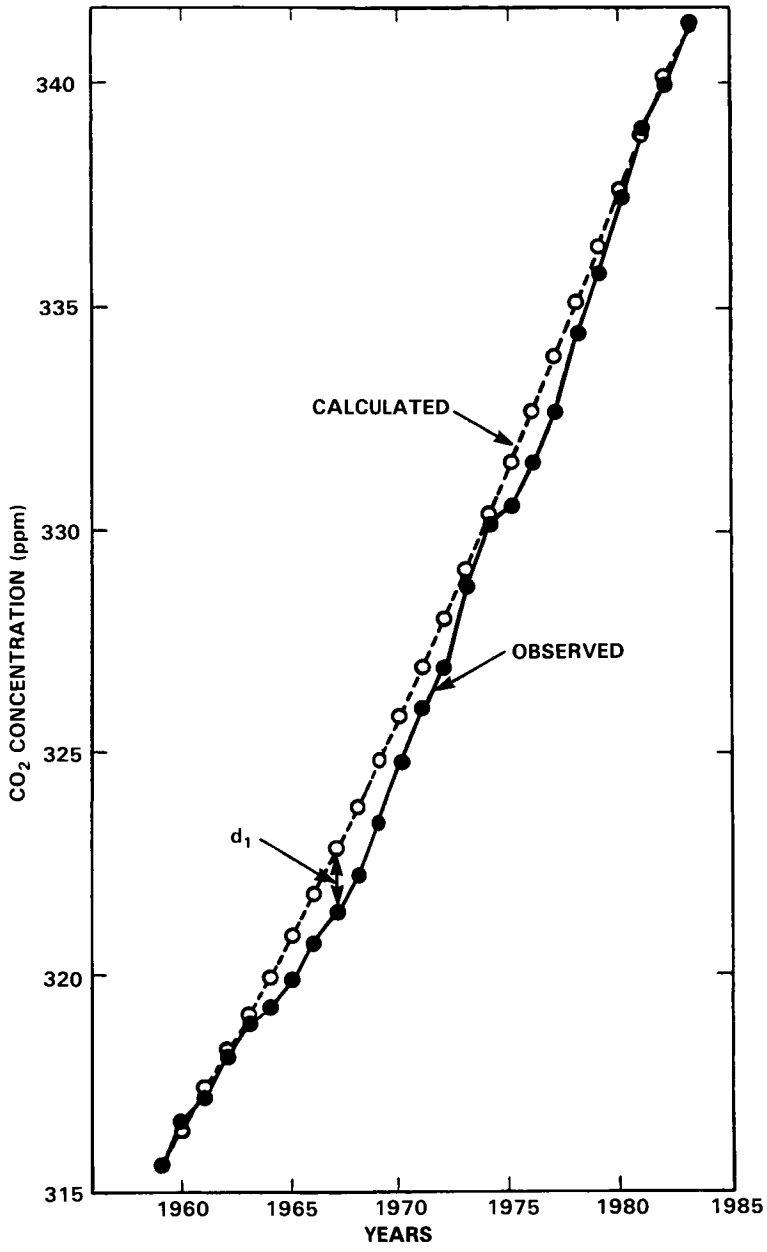

Figure 15-19. Concentration of atmospheric CO_2 at Mauna Loa Observatory, Hawaii from 1958 to 1983. The "calculated" curve is the curve used in the climate model calculations shown in Figure 15-21.

$$\Delta T_s = (\Delta T_S)_{2x} \left\{ \frac{\ln[C(1980)/C(1850)]}{\ln 2} \right\} \tag{2}$$

If we assume that $(\Delta T_s)_{2x} \approx 4$ K based on the results from the GFDL, GISS and NCAR models, then for the CO_2 concentration increase from 270 (year 1850) to 338 ppmv (year 1980), $\Delta T_s = 1.3$ K. However, the reconstructed Northern Hemisphere surface air temperature record (see Figure 15-1) indicates a warming from 1880 to 1980 of about 0.6 K. Does this difference mean that the sensitivity of the GCMs is too large by a factor of two? The likely answer is: not necessarily, since the actual reponse of the climate system

lags the equilibrium response because of the thermal inertia of the ocean. This can be illustrated by the energy balance model

$$C_s \frac{d\Delta T_s}{dt} = \Delta Q - \lambda \Delta T_s$$

where C_s is the heat capacity of the upper ocean. When equilibrium is achieved, $d\Delta T_s/dt = 0$ and $(\Delta T_s)_{eq} = \Delta Q/\lambda$. However, the transient solution

$$\Delta T_s(t) = (\Delta T_s)_{eq}(1 - e^{-t/\tau_\epsilon})$$

shows that equilibrium is approached exponentially with a characteristic "e-folding" time $\tau_\epsilon = C_s/\lambda$. In the following two sections the studies of this lag of the climate system are reviewed.

15.4.3 Results From Simplified Models

The transient response of the climate system to an abrupt CO_2 increase has been investigated with planetary energy balance, radiative-convective and simplified atmospheric general circulation models in conjunction with box-diffusion, box-advection-diffusion and two-box ocean models as well as with simplified oceanic general circulation models. The box-diffusion ocean model consists of a fixed-depth mixed layer (the box) surmounting the thermocline and deep ocean in which vertical heat transport is treated as a diffusive process with prescribed thermal diffusivity $\varkappa$. The box-advection-diffusion ocean model is a box-diffusion model with a prescribed value for oceanic upwelling. The two-box ocean model is comprised of a fixed-depth mixed-layer box and an intermediate water box which exchange heat vertically with a prescribed ventilation time.

The results from 6 studies of the transient response to abrupt heating are presented in Table 15-9. Hoffert *et al.* (1980), using a box-advection-diffusion model, and Schneider and Thompson (1981), using a two-box ocean model, obtained e-folding times of 10 to 20 years. A slightly larger e-folding time of 25 years was obtained by Bryan *et al.* (1982) and Spelman and Manabe (1984) with a simplified coupled atmosphere-ocean general circulation model in which the geographical domain was restricted to a 120°-longitude sector extending from equator to pole, with the western half of the sector occupied by land at zero elevation and the eastern half by ocean with a uniform depth of 5000 m. On the other hand, Hansen *et al.*, (1984) used a box-diffusion ocean model and obtained 27, 55 and 102 year e-folding times corresponding to assumed λ values of 2.15, 1.4 and 1 $Wm^{-2}\,K^{-1}$, respectively. Bryan *et al.* (1984) used an uncoupled global oceanic general circulation model and found an e-folding time of about 100 years in response to an imposed 0.5 K upper ocean surface warming. Lastly, Siegenthaler and Oeschger (1984) obtained a 60 year e-folding time in their study using a box-diffusion model.

The studies presented in Table 15-9 indicate that the e-folding time τ_e lies between 10 and 100 years. If $\tau_e \sim 10$ years then the actual response of the climate system would be quite close to the equilibrium response and the disparity between the latter for the 1850 to 1980 warming and that observed would mean that the climate sensitivity of recent GCMs is larger than that of nature. On the other hand, if $\tau_e \sim 100$ years, then the actual response of the climate system would be quite far from the equilibrium response, thus indicating that the sensitivity of GCMs may not be inconsistent with the observed temperature records.

Table 15-9. e-Folding Time τ_e for Abrupt Heating from Selected Climate Model Studies.

Study	Model	τ_e (Years)
Hoffert *et al.* (1980)	Planetary energy balance climate model and a box-advection-diffusion ocean model	8-20
Schneider & Thompson (1981)	Planetary energy balance model and a two-box diffusion ocean model	13
Bryan *et al.* (1982) Spelman & Manabe (1984)	Coupled atmosphere-ocean general circulation model with simplified geography and topography	25
Hansen *et al.* (1984)	Radiative-convective climate model and a box-diffusion ocean model	27 55 102
Bryan *et al.* (1984)	Global oceanic general circulation model	100
Siegenthaler & Oeschger (1984)	Planetary energy balance climate model and a box-diffusion ocean model	60

The factors that contribute to the wide range in τ_e have been investigated by Wigley and Schlesinger (1985) using their analytical solution for the energy balance climate/box-diffusion ocean model and by Hansen *et al.* (1984) using numerical solutions of the box-diffusion model and a 3-D GCM. Both studies found that τ_e depends (approximately) quadratically on λ^{-1} and linearly on the thermal diffusivity $\varkappa$. As shown in Figure 15-20, the analytic result of Wigley and Schlesinger (1985) is in close agreement with the numerical results obtained by Hansen *et al.* (1984) for $\varkappa = 1$ cm^{2}s^{-1}. However, in view of this dependence of τ_e on λ and $\varkappa$ the determination of whether τ_ϵ 10 or 100 years requires a coupled global atmosphere-ocean general circulation model (AOGCM) in which both the climatic gain (λ^{-1}) and the oceanic heat transport are self-determined. Long term integrations from a simulation with such AOGCMs are currently not available. However, preliminary results from an AOGCM indicate that an energy balance/multi-box ocean model with a self-consistent $\varkappa$ adequately describes the time evolution of the $2 \times CO_2 - 1 \times CO_2$ differences in the surface-air temperature (Schlesinger *et al.*, 1985). The required thermal diffusivity $\varkappa$ for the energy-balance climate/box-diffusion ocean model to represent the transient response of the AOGCM was determined to be 2.25 cm^{2}s^{-1} (Schlesinger *et al.*, 1985).

15.4.4 Results for a Realistic CO_2 Increase

The discussions thus far have been for the transient response of the climate system to an instantaneous doubling of the CO_2 concentration. However, the CO_2 concentration has not abruptly changed in the past, nor is it likely to in the future, at least not by an instantaneous doubling. Instead, the CO_2 concentration has increased more or less continuously over the observational period since 1958 (Figure 15-19).

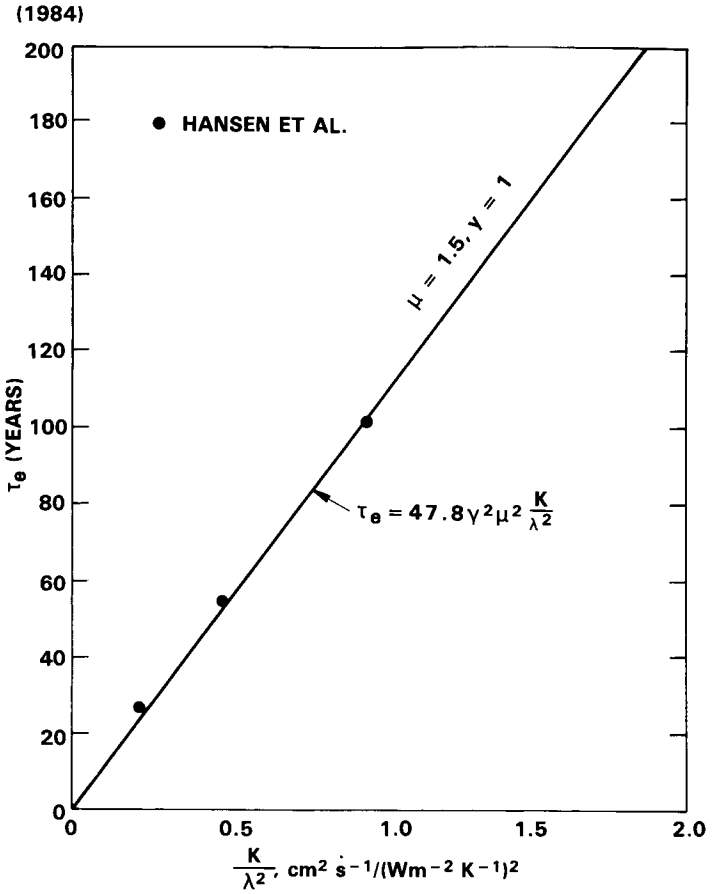

Figure 15-20. The e-folding time τ_e versus $\varkappa/\lambda^2$ for abrupt heating perturbations. The linear relation (line) is predicted by the analytical solution of Wigley and Schlesinger (1985). The data points are from the numerical computations of Hansen *et al.* (1984) for $\varkappa = 1$ cm^{2}s^{-1}.

Recently, Hansen *et al.* (1984) and Wigley and Schlesinger (1985) have estimated the temperature change from 1850 to 1980 induced by the increasing CO_2 concentration during this 130-year period. Figure 15-21, based on the study of Wigley and Schlesinger (1985), shows the 1850-1980 surface temperature change as a function of the equilibrium surface for a doubled CO_2 concentration. Let us assume that the latter is 4 K based on the recent equilibrium warmings simulated by the GFDL, GISS and NCAR atmospheric GCM/fixed-depth mixed layer ocean models. If the climate system had no thermal inertia, the 1850-1980 surface temperature change would be in equilibrium with the instantaneous 1980 CO_2 concentration, and the warming would be given by Equation (2). As shown in this figure, this instantaneous equilibrium warming would be 1.3 K. However, when the heat capacity and vertical heat transport of the ocean are considered, as shown by the curves for the oceanic thermal diffusivities $\varkappa = 1$ and $\varkappa = 3$ cm^{2}s^{-1}, the 1850-1980 warming is reduced to about 0.5 to 0.7 K. This level of CO_2-induced warming does not conflict with the temperature changes revealed in the observational record (see Figure 15-1).

Figure 15-21 also shows that even if the CO_2 concentration were to increase no further in the future, the earth's surface temperature would continue to increase by about 0.7 K (= the balance of the 1.3 K equilibrium warming for our example) in its approach to its new equilibrium value. This delayed approach to the new equilibrium surface temperature brings out the following important issue concerning the transient

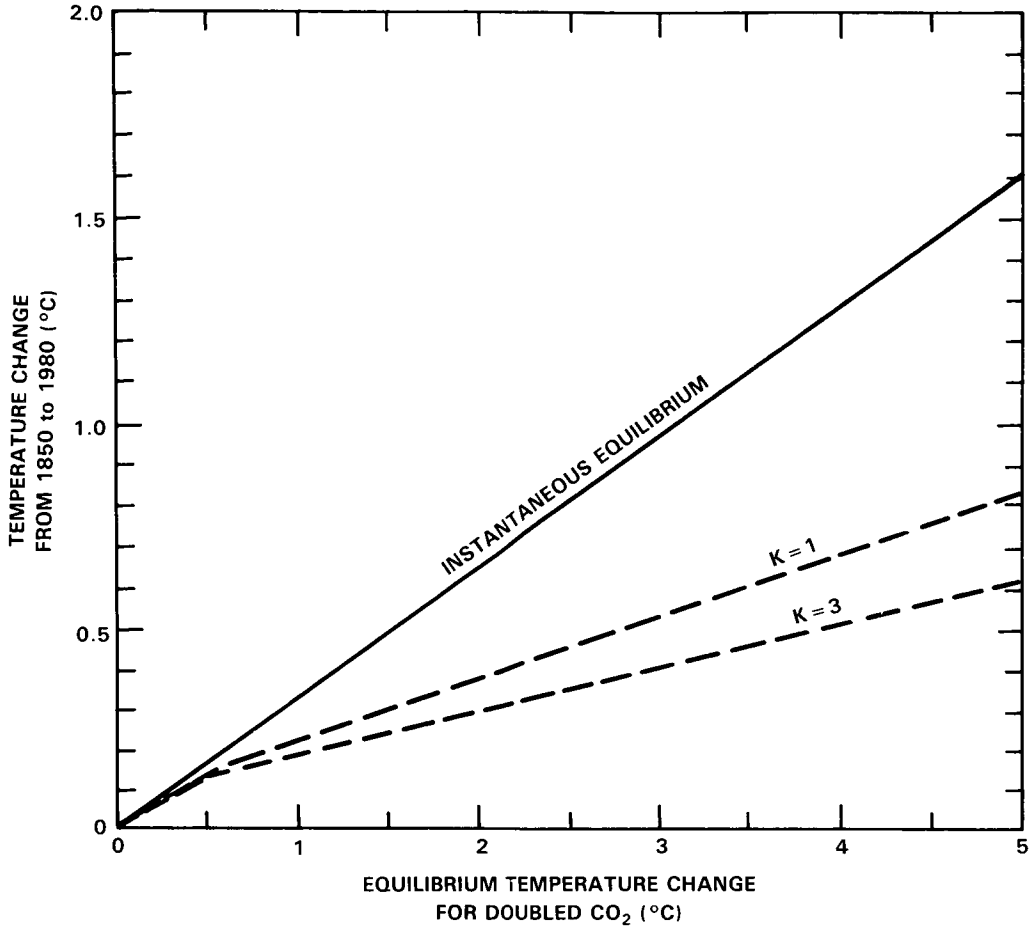

Figure 15-21. The temperature change from 1850 to 1980 versus the equilibrium temperature change for doubled CO_2. The instantaneous equilibrium curve is given by equation (2). The curves $\varkappa = 1$ and $\varkappa = 3$ are from the results of Wigley and Schlesinger (1985).

effects: the present warming is "small" and perhaps within the natural variation of climate because the ocean sequesters heat within its interior but, because of this, when the warming becomes demonstrably evident, continued future warming is inevitable, even if the CO_2 concentration were prevented from increasing further. As shown in Section 15.5, this hidden but inevitable future warming can itself increase in the future as other greenhouse gases such as N_2O, CH_4 and CFCs are added to the earth's atmosphere.

15.5 TRACE GAS EFFECTS ON OBSERVED AND FUTURE CLIMATE TRENDS

Greenhouse forcing of the climate system has accelerated in recent years due to the growth of a number of trace gases. We illustrate this quantitatively by estimating the decadal increment in greenhouse forcing for several trace gases and compare this with the forcing due to increasing CO_2 in the same decades.

15.5.1 Conceptual Framework for the Assessment

The potential effects of trace gases on past and future temperature trends have been estimated by numerous studies (Hansen *et al.*, 1984; Brühl and Crutzen, 1984; Wang *et al.*, 1985; Ramanathan *et al.*,

1985; to cite just the recent analyses). The present assessment, while it combines the salient features of the earlier work, is an independent analysis of the trace gas effects on past and future climate trends.

We do not explicitly employ a climate model but, instead, compute the zero-climate-feedback surface temperature change, $(\Delta T_S)_0$, from the radiative-convective model of Lacis (1985). The computed $(\Delta T_S)_0$ is then multiplied by the feedback factor, F (see Equation 2, Section 15.2.2.2), to obtain the expected climate forcing, ΔT_S.

The $(\Delta T_S)_0$ is the equilibrium change in surface air temperature which would occur as a result of a change in atmospheric composition in the absence of any climate feedbacks. As described in Section 15.2.2, $(\Delta T_S)_0$ is a nearly model independent measure of the radiative forcing. For example, for a doubling of CO_2, $(\Delta T_S)_0$ for RCMs is in the range of 1.2 to 1.3 K; the RCM used in this study yields a value of:

$$[\Delta T_S(2 \times CO_2)]_0 = 1.26 \text{ K} \quad (1)$$

The $(\Delta T_S)_0$ also avoids current uncertainties in *climate sensitivity*; also, since it refers to *equilibrium* response, it is independent of uncertainties in climate response time.

The next issue concerns the choice of the feedback factor, F. Climate feedbacks and climate sensitivity are discussed in Section 15.2.2. It is sufficient for our purposes to note that the estimate of equilibrium global mean climate sensitivity reported by the National Academy of Sciences (Charney, 1979; Smagorinsky, 1982) is

$$\Delta T_S\ (2 \times CO_2) = 3 \pm 1.5 \text{ K} \quad (2)$$

The above climate sensitivity range covers a factor of three, with ΔT_S ranging from 1.5 to 4.5 K. It is easier to justify the lower and the upper limits than the mean value of 3 K. For example, RCMs generally yield a value of 2 K while GCMs with seasonal cycle and realistic geography yield values ranging from 3.5 to 4.2 K (see Table 15-7). Hence, in this report, we avoid the use of a mean value for ΔT_S, but instead adopt the range recommended by the National Academy reports:

$$1.5 \leq \Delta T_S\ (2 \times CO_2) \leq 4.5 \text{ K} \quad (3)$$

Since the zero-climate-feedback forcing for doubled CO_2 is 1.26 K for the present RCM, the climate sensitivity range given by (3) corresponds to the feedback factor F[$= \Delta T_S/(\Delta T_S)_0$; Equation (2) of 15.2.2.2] of:

$$1.2 \leq F \leq 3.6 \quad (4)$$

It is because of this large range for F that we have avoided the use of a specific climate model in the present analyses. In order to account for the climate sensitivity yielded by RCMs and GCMs, we adopt the following two values:

$$\Delta T_S\ (2 \times CO_2) = 2 \text{ K; i.e., } F \approx 1.6$$

$$\Delta T_S\ (2 \times CO_2) = 4 \text{ K; i.e., } F \approx 3.2 \quad (5)$$

15.5.2 Greenhouse Forcing from 1850 to the 1980's

The sources and observed trends for the trace gases are discussed extensively in Chapters 3 and 12 of this report. Hence, only a brief summary is given in the ensuing discussions.

CO_2. The abundance of atmospheric CO_2 was 315 ppmv in 1958 when Keeling initiated accurate monitoring. Thus, since a variety of techniques indicate that the CO_2 abundance was 270 ± 10 ppmv in 1850 (WMO, 1983b), the mean decadal growth of CO_2 for the period 1850-1958 was about 4 ppmv/decade. By contrast, the current rate of growth of CO_2 is about 15 ppmv/decade. The decadal greenhouse forcing due to CO_2 growth is illustrated in Figure 15-22 for the period 1850-1960 and for recent decades.

Chlorofluorocarbons. The release rates of CF_2Cl_2 (F12) and $CFCl_3$ (F11) into the atmosphere can be estimated from production data available from the manufacturers (CMA, 1982). Under the assumption of 150 and 75 year lifetimes for F12 and F11, respectively, decadal growth rates are obtained (Rind and Lebedeff, 1984) which are in good agreement with recent atmospheric measurements (GMCC, 1983). The resulting decadal climate forcings are shown in Figure 15-22. It is apparent that these chlorofluorocarbons now add substantial climate forcing, though their contribution was negligible in the period 1850-1960.

Less abundant chlorine and fluorine compounds, such as $CHClF_2$ (F22), CCl_4, CF_4 and CH_3CCl_3 also have significant growth rates and infrared absorption strengths (see Tables 15-1, 15-1b and 15-8). However, the growth histories and absorption strengths are on the whole less well known than for F11 and F12. CCl_4 apparently had a higher growth rate in the 1960's and 1970's than it does now, while F22 and CH_3CCl have grown rapidly in recent years, with a higher growth rate than that of F11 and F12. In Figure 15-22 we include a greenhouse contribution for these other CFCs with a net radiative forcing that is 20 percent of that for F11 and F12. However, this is meant more as a reminder that these other CFCs need to be considered, rather than as an accurate estimate of their greenhouse contribution.

CH_4. Methane has been measured to be increasing for the last several years at a rate of the order of 1 percent/year (Blake *et al.*, 1982; Blake and Rowland, 1985; Rasmusson and Khalil, 1984b; Ehhalt *et al.*, 1983b). Also, measurements of air bubbles trapped in polar ice cores (Craig and Chou, 1982; Rasmusson and Khalil, 1984b) indicate that the methane abundance was about 0.7 ppmv from 25,000 years ago to 500 years ago, with an increase beginning sometime between 200 and 500 years ago. We estimate the CH_4 greenhouse forcing for Figure 15-22 by taking the abundance at 1 ppmv in 1850, 1.4 ppmv in 1958, 1.5 ppmv in 1970 and 1.65 ppmv in 1980; the growth rate is taken as 1.5 percent/year in the 1980's.

N_2O. Nitrous oxide was measured to be increasing at a rate of about 0.2 percent/year in the 1970's (Weiss, 1981). Recent measurements (NRC, 1983) suggest that the current growth rate may be closer to 0.3 percent/year. These values are used to estimate the N_2O greenhouse forcing for Figure 15-22. Although it seems likely that N_2O may have had a small rate of increase in the period 1850-1958, there are no observations providing a quantitative measure. However, in the near future, ice core data should yield a reliable pre-industrial value (Gammon, private communication).

Stratospheric H_2O. Since the abundance of water vapor in the troposphere is controlled basically by atmospheric temperature and other meteorological variables, changes in tropospheric H_2O are considered as a climate feedback mechanism rather than as a forcing mechanism. However, in the upper stratosphere H_2O is produced by methane oxidation, and therefore increase of methane may increase stratospheric H_2O. The change of stratospheric H_2O would be delayed after any increase in tropospheric

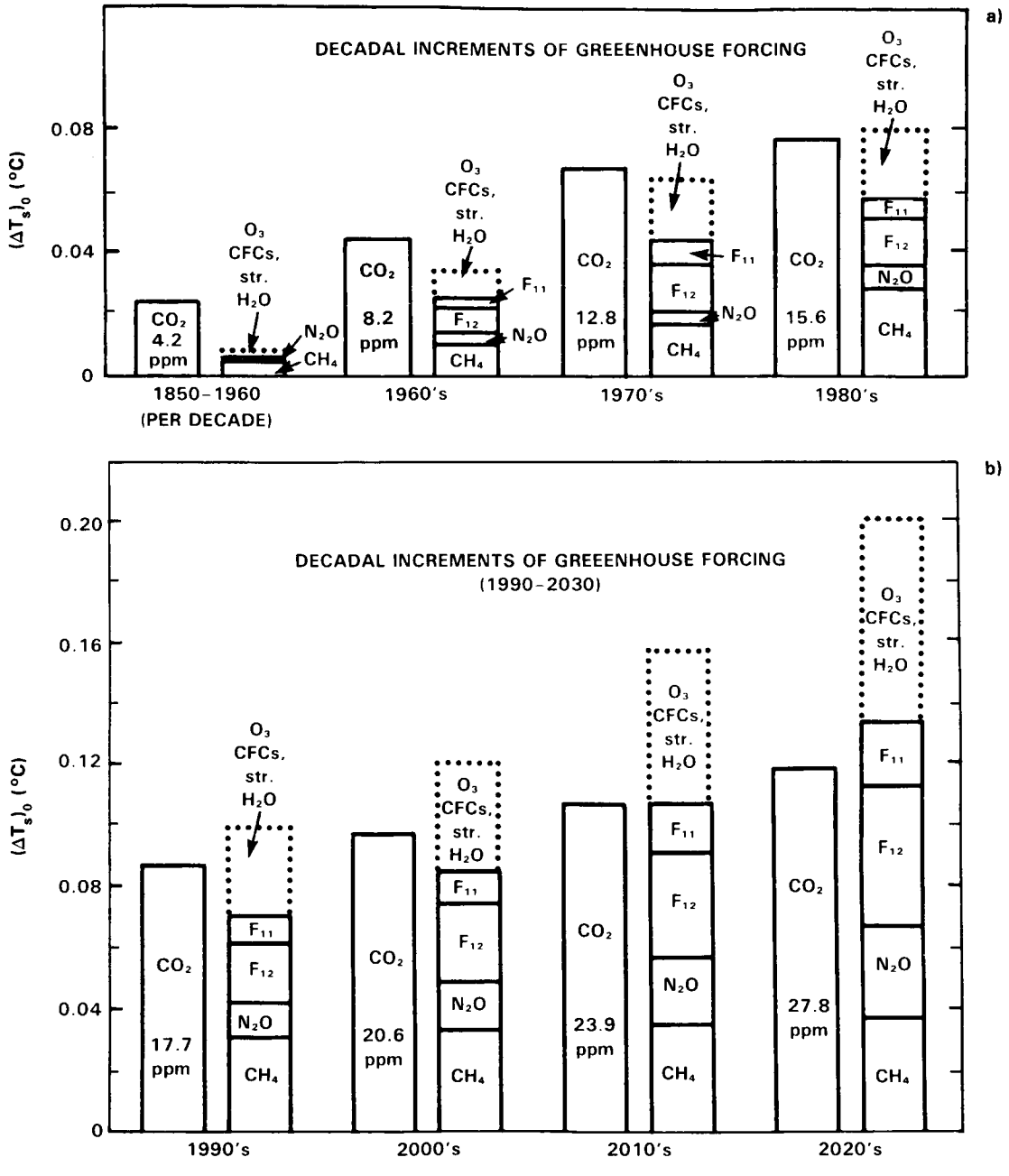

Figure 15-22. Decadal additions to global mean greenhouse forcing of the climate system. $(\Delta T_s)_0$ is the computed temperature change at equilibrium ($t \rightarrow \infty$) for the estimated decadal increases in trace gas abundances, with no climate feedbacks included. Formulas for $(\Delta T_s)_0$ as a function of the trace gas abundances are given by Lacis *et al.* (1981). (a) Past additions. Except for O_3 and stratospheric H_2O trends, the estimated trace gas increases are based on measurements as discussed in section 15.5.2; (b) Future additions. Adopts Case A scenario discussed in Section 15.5.3 and given in Table 15-10, which assumes that the sum of all trace gases other than those expressly indicated provides a forcing similar in magnitude to that of CFC11 and CFC12.

CH_4 by the time required for transport from the troposphere to the upper stratosphere. The greenhouse forcing of H_2O in Figure 15-22 is based on the added stratospheric H_2O which Wuebbles (private communication, 1985) estimates to be associated with increase of CH_4. It is apparent that the greenhouse warming from added stratospheric H_2O is about 50% as great as the direct CH_4 greenhouse warming. These estimates do not include the CH_4-O_3 feedback (see Section 15.3).

O_3. Ozone is an effective greenhouse gas because of its strong absorption band at 9.6 μm. Present understanding of atmospheric chemistry, as described elsewhere in this volume, suggests that growth of atmospheric CFCs will eventually deplete stratospheric O_3 substantially and increase tropospheric O_3, with a net column-integrated reduction of O_3. The net greenhouse effect of this would be a slight warming, because of the greater greenhouse efficiency of tropospheric ozone molecules (Ramanathan and Dickinson, 1979; Lacis, 1985; Owens *et al.*, 1985a). In addition, as discussed in Section 15.3, increases of atmospheric methane, carbon monoxide and nitric oxides tend to increase tropospheric O_3 (also see Cicerone, 1985). However, a recent 3-D transport model study (Levy *et al.*, 1985) indicates the potential importance of transport in governing the O_3 distribution. The relative importance of transport and hydrocarbon/nitrogen oxide chemistry in governing tropospheric ozone production is as yet an unresolved issue (Levy *et al.*, 1985).

Recent measurements of O_3 are not inconsistent with a long-term trend of increasing tropospheric ozone (Angell and Korshover, 1983b; Bojkov and Reinsel, 1985; Logan, 1985). For example, analyses of Northern Hemisphere ozonesonde data from 11 stations reveal a statistically significant 1.1% per year increase in the free troposphere ozone over a 15 year period; Southern Hemisphere ozone seems to have undergone very little change in the same period (Bojkov and Reinsel, 1985). These and other findings (Logan, 1985; Angell and Korshover, 1983b) based on observed ozone data are also consistent with estimates of ozone production from anthropogenically released hydrocarbons and nitrogen oxides (Isaksen, 1980; Vukovic *et al.*, 1985; Isaksen and Hov, 1985); NO_x emissions from aircraft (Liu *et al.*, 1980) and CO from incomplete combustion (Logan *et al.*, 1978). In spite of this apparent consistency between theory and observations, the large natural variability of tropospheric ozone when considered in conjunction with the poor spatial coverage of the ozone measurement stations prevents firm conclusions regarding trends.

We estimate the potential O_3 greenhouse effect by using trends for O_3 which were computed by Wuebbles *et al.* (1983) on the basis of scenarios for atmospheric methane, nitrous oxides and carbon dioxide; however, we decreased this computed $(\Delta T_s)_0$ by the factor 0.5, because much of the O_3 change would be confined to the hemispheric or smaller scale. The resulting tropospheric O_3 climate forcing, indicated by a dotted bar in 15-22, is very uncertain, but is obviously a potentially important contributor to the greenhouse effect.

The following major conclusions follow directly from Figure 15-22:

(1) Non-CO_2 greenhouse gases are now adding to the greenhouse effect by an amount at least comparable to the effect of CO_2; this is a fundamental change from the situation during the period 1850-1960.;

(2) The rate of increase of the total greenhouse forcing is now 3-10 times greater than the mean rate for the period 1850-1960, due to both increase in the growth rate of CO_2 and recent growth of other trace gases.

(3) The cumulative value of $(\Delta T_s)_0$ for the period 1850-1980 is 0.56 K; CO_2 increase contributes 0.4 K and the other trace gases contribute the balance of 0.16 K. The radiative forcing of 0.56 K would yield an equilibrium surface-air temperature change of about 0.9 K [= 0.56 × 1.6] and

about 0.6 K for CO_2 increase alone for a climate model whose equilibrium sensitivity is $\Delta T_s(2 \times CO_2) = 2$ K. These results are consistent with the earlier RCM estimates of Brühl and Crutzen (1984; 0.6 K for CO_2 alone and 1 K for all gases) and that of Ramanathan *et al.* (1985; 0.6 K for CO_2 alone and about 0.9 K for all gases) for surface-air temperature. The range in the equilibrium surface-air temperature change is 0.7 to 2 K, where we have adopted Equation (4) to multiply the $(\Delta T_s)_0$ of 0.56 K with the range in F.

(4) The computed stratospheric cooling for the period 1850-1980 is slightly under 1 K between 25-30 km and about 3 K between 35-45 K. These calculations do not include the effects of CFC-induced O_3 change which can amplify the cooling due to CO_2 increase by about 20%.

15.5.3 Greenhouse Forcing Projected Into the Next Century

We consider three scenarios (Case A, Case B and Case C) projecting trace gas greenhouse forcing into the future. The three scenarios are summarized in Table 15-10. The use of more than one scenario seems essential because of major uncertainties in our understanding of the causes of the trace gas changes and the great difficulties in projecting economic, population and other key factors. We compare these scenarios with the range of trace gas forcings estimated by Ramanathan *et al.* (1985) for 2030. The scenarios adopted by Ramanathan *et al.* (1985) are shown in Table 15-8 (see the column under the heading probable range).

The Case A scenario is an extrapolation of current growth rates for measured gases, and it includes an allowance to approximate the effect of several gases that are poorly measured and/or have uncertain absorption strengths. The resulting radiative forcing for this scenario is shown in Figure 15-22b and is near the middle of the range estimated by Ramanathan *et al.* (1985). The Case B scenario includes only five greenhouse gases that are measured reasonably well and it assumes rapidly decreasing growth rates. The resulting radiative forcing is near the lower limit of the range estimated by Ramanathan *et al.* (1985).

In Case A (current growth rates), CO_2 increases at a constant growth rate from 270 ppmv in 1850 to 315 ppmv in 1958, as observed by Keeling for the interval 1958-1984 and subsequently with a 1.5 percent growth of the annual increment. $CFCl_3$ and CF_2Cl_2 emissions are from reported rates to date and assume 3%/yr increased emission in the future, with atmospheric lifetimes for the gases of 75 and 150 years, respectively. CH_4 increases at a constant growth rate from 1 ppmv in 1850 to 1.4 ppmv in 1958, 0.6%/yr in the 1960's, 1%/yr in the 1970's and 1.5%/yr thereafter. N_2O increases according to the semi-empirical formula of Weiss (1981), the rate being 0.1%/yr in 1958, 0.2%/yr in 1980, 0.4%/yr in 2000 and 0.9%/yr in 2030. Potential effects of several other trace gases (such as O_3, stratospheric H_2O, and chlorine and fluorine compounds other than F11 and F12) are approximated by multiplying the CFC effect by a factor of 2.

In Case B (reduced growth rates) the annual increment in CO_2 is reduced from 1.5% today to 1% in 1990, 0.5% in 2000 and 0 in 2010, which compares to $\approx$4% during the period 1900-1970 and is below projected rates for population growth; the resulting ΔCO_2 is constant at 1.9 ppmv yr^{-1} after 2010. The annual growth in CF_2Cl_2 and $CFCl_3$ emissions are reduced from 3% today to 2% in 1990, 1% in 2000 and 0 in 2010; because of their finite lifetimes, the annual increments in atmospheric abundance decrease with time after 2010. The methane annual growth rate decreases from 1.5% today to 1% in 1990 to 0.5% in 2000. N_2O increases are based on Weiss' (1981) formula, but the parameter specifying annual growth in anthropogenic emissions decreases from 3.5% today to 2.5% in 1990, 1.5% in 2000 and 0.5% in 2010. No increases are included for other chlorofluorocarbons, O_3, stratospheric H_2O or any other gases.

Table 15-10. Trace Gas Scenarios.

Trace gas	Case A Current growth rate	Case B Reduced growth rate	Case C*
CO_2	1.5%/yr growth in annual CO_2 increment**	1.5%/yr growth to 1990 1.0% yr from 1990-2000 0.5%/yr from 2000-2010 0%/yr after 2010 in annual CO_2 increment	Time-dependent; averages about 2%/yr growth in annual CO_2 increment
$CFCl_3$; CF_2Cl_2	3%/yr growth in emissions	3%/yr growth to 1990 2%/yr from 1990-2000 1%/yr from 2000-2010 0%/yr after 2010	1.5%/yr growth in emissions
CH_4	1.5%/yr growth in CH_4 abundance	1.5%/yr growth to 1990 1.0%/yr from 1990-2000 0.5%/yr after 2000	1%/yr growth in CH_4 abundance
N_2O	Weiss (1981) formula 3.5%/yr growth to 1990; yields 0.2%/yr growth in abundance in 1980, 0.4%/yr in 2000, 0.9%/yr in 2030	Weiss formula with 3.5%/yr growth in emissions 2.5%/yr from 1990-2000 1.5%/yr from 2000-2010 0.5%/yr after 2010; yields 0.2%/yr growth in abundance in 1980, 0.33%/yr in 2000, 0.34%/yr in 2030	0.25%/yr growth in N_2O abundance
O_3 and other trace gases	Assumed greenhouse forcing by these gases is the same as that of CF_2Cl_2 and $CFCl_3$	None	Includes only O_3 effects. O_3 change is explicitly computed from a chemistry model

* This the same scenario used in the Model Predictions Chapter (See their Case 4; Chapter 12.)

** The CO_2 increment in 1985 was taken as 1.5 ppmv, and this increment increased by 1.5%/yr in Case A. This case is appropriate if fossil fuel use increases by 1.5%/yr and the "airborne fraction" of CO_2 remains constant, for example. Note that this growth rate is much less than the 4%/yr growth rate that existed in the 100 years before 1973.

The Case C scenario is adopted from the "model predictions" chapter (Case 4 of Chapter 13). The Case C scenarios fall in between Case A and Case B. Case C, like Case A, adopts current growth rates but chooses the lower limit of the observed growth rates. For example, it adopts 1.5%/yr growth in $CFCl_3$ and CF_2Cl_2 emissions as opposed to the 3%/yr growth assumed in Case A; the growth in CH_4 abundance is reduced to 1%/yr instead of 1.5%/yr in Case A. Furthermore, trace gases other than CO_2, $CFCl_3$ and CF_2Cl_2, CH_4, N_2O and O_3 are not included in Case C.

The Case A, Case B and Case C scenarios are summarized in Table 15-10; the time dependent concentrations for Case A and Case B are shown in Table 15-11. The computed greenhouse forcings are

Table 15-11. Trend in concentrations. From 1985 to 2100, the concentrations are derived from the scenarios A and B shown in Table 15-10.

Date	CO_2 (ppm)		CH_4 (ppm)		N_2O (ppb)		CCl_3F (ppb)		CCl_2F_2 (ppb)	
1850	270		1.00		282		0		0	
1900	290		1.17		284		0		0	
1958	315		1.40		293		.01		.03	
1970	325		1.51		297		.07		.13	
1985	346		1.79		305		.24		.40	
	A	B	A	B	A	B	A	B	A	B
2000	372	371	2.24	2.12	319	318	.42	.41	.72	.71
2015	404	400	2.80	2.28	343	335	.71	.61	1.22	1.07
2030	445	428	3.50	2.46	383	353	1.15	.78	1.99	1.41
2050	515	466	4.71	2.72	483	377	2.13	.96	3.72	1.80
2100	818	562	9.91	3.49	1432	439	9.68	1.24	17.00	2.60

illustrated in Figure 15-23 for the period 1960-2030. Case A yields a forcing that has a slightly larger forcing than the nominal scenario of Ramanathan *et al.* (see Figure 15-24). Case A yields a forcing equivalent to doubled CO_2 (with $1 \times CO_2$ defined as 315 ppmv) before 2030; Case C yields this level slightly after 2030; while Case B yields this level of forcing before 2060. The time to reach effective doubled CO_2 forcing is greatly accelerated by the non-CO_2 trace gases, which provide roughly half of the greenhouse forcing. A comparison of the forcing by CO_2 and other trace gases is illustrated clearly in Figure 15-24, taken from Ramanathan *et al.* (1985); although the relative contributions of the various trace gases in their scenario are somewhat different from either Case A or B, the results are qualitatively very similar. The following points should be noted first before comparing the Ramanathan *et al.* (1985), hereafter referred as R, results with those shown in Figure 15-23. The 1-D RCM model of R computes both surface temperature (T_g) surface-air temperature (T_s). In the R model, the computed DT_s is larger than DT_g by 10% - 13%. For CO_2 doubling, the R model yields a $\Delta T_g \sim 1.9$ K and a $\Delta T_s \sim 2.1$ K. The R model results in Figure 15-24 shows that, for the period 1980–2030, the equilibrium surface warming, i.e., ΔT_g, is 1.54 K ($\Delta T_s \sim 1.7$ K) due to all gases including CO_2 and that due to CO_2 increase alone is 0.71 K ($\Delta T_s \sim 0.8$ K). For the same period of 1980–2030, the Case A scenario in Figure 15-23 yields [for the ΔT_s ($2 \times CO_2$) = 2 K model] a ΔT_s of 1.8 K for all gases including CO_2 and a ΔT_s of 0.8 K for the CO_2 increase by itself. The cumulative ΔT_s for the Case B and Case C scenarios are respectively 1.1 and 1.25 (see Figure 15-23). The stratospheric O_3 decrease due to CFCs also causes a surface warming, and the magnitude of about 0.1 K (see Figure 15-24) is roughly 30% of the direct greenhouse effect of CFCs. Other studies (e.g., Owens *et al.*, 1985) also yield a warming of about 0.1 K due to CFC-induced stratospheric O_3 decrease.

The computed stratospheric temperature changes due to CO_2 and other trace gases are substantial (see Figure 15-25). Above 30 km, the cooling due to CO_2 increase (alone) is more than doubled by the other trace gases. The primary contribution to the enhancement in stratospheric cooling is the (computed) O_3 decrease due to CFC increase. To the extent that trace gases (other than CO_2) cause a large

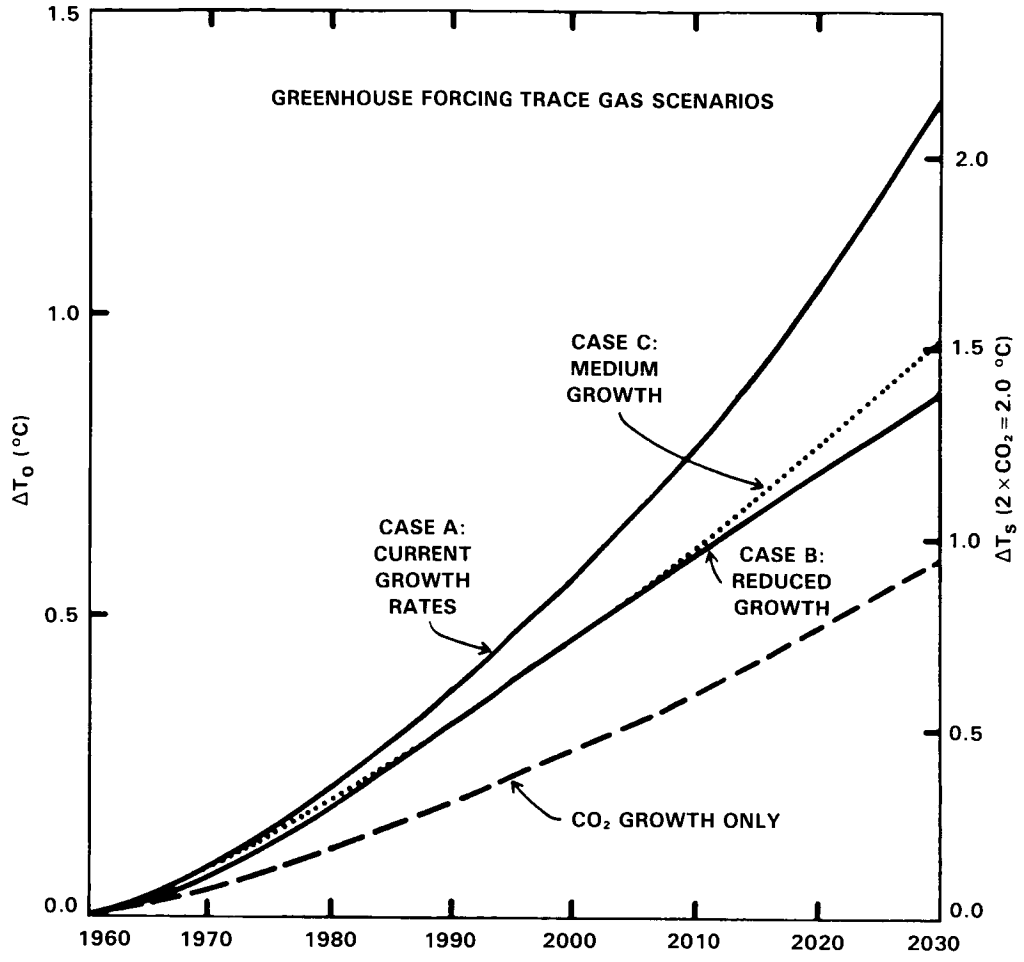

Figure 15-23. Greenhouse forcing for three trace gas scenarios: Case A, which uses current growth rates, and Case B, which assumes substantial reductions in growth, as described in the text. Case C is similar to Case A but with medium growth rate. The "CO_2 growth only" curve applies to Case A scenario. See Table 15-10 for further details. ΔT_0 is the equilibrium greenhouse warming for no climate feedbacks. The "doubled CO_2" level of forcing occurs when the CO_2 and trace gases added subsequent to 1958 provide a radiative forcing equivalent to doubling of CO_2 from 315 ppm to 630 ppm.

surface/troposphere warming and a much larger stratospheric cooling, their direct climatic effects are virtually indistinguishable from those of CO_2.

15.5.4 Regional Effects

There is general agreement that climate sensitivity is not globally uniform. Both empirical evidence from past climate changes and global climate models indicate that the surface air temperature response is magnified at high latitudes and thus somewhat muted at low latitudes, in comparison to the global mean response. This high latitude enhancement is expected on theoretical grounds, because the ice-snow albedo feedback only operates at high latitudes and because the relative stability of the atmosphere there tends to confine surface warming or cooling to low altitudes. The high latitude enhancement of the warming is illustrated in Figure 15-26, which shows model results for the annual mean surface air temperature increase from the 4 × CO_2 experiment of Manabe and Stouffer (1980). Qualitatively similar results are obtained with other general circulation models (Hansen *et al.*, 1984; Washington and Meehl, 1984).

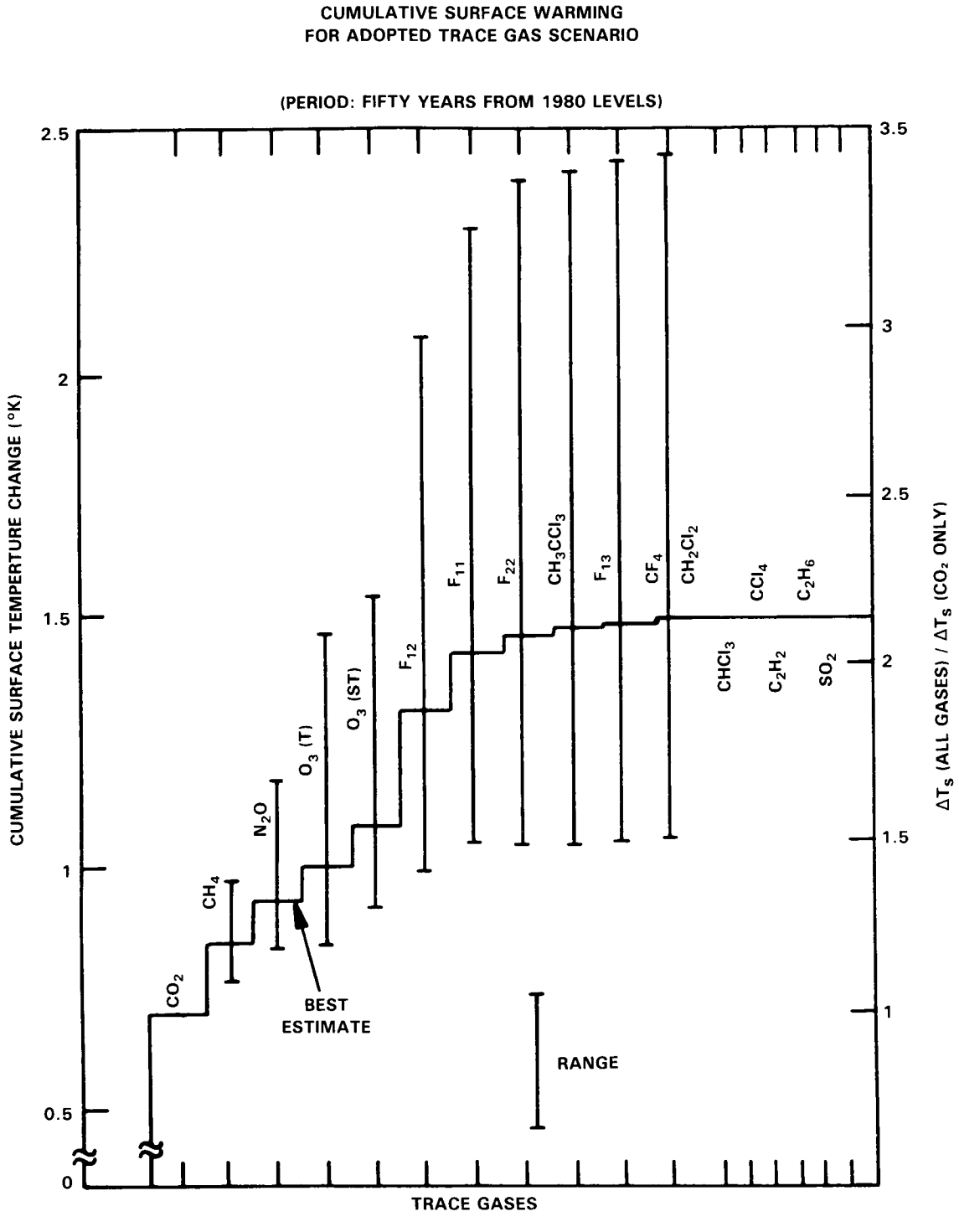

Figure 15-24. Cumulative equilibrium surface warming resulting from the trace gas scenario of Table 15-8 (source: Ramanathan *et al.,* 1985). In this 1-D model, the surface-air temperature change is larger than the surface temperature change by about 10%. The $(\Delta T_s)_0$ can be obtained by dividing the indicated surface temperature change by a feedback factor (F) of about 1.5.

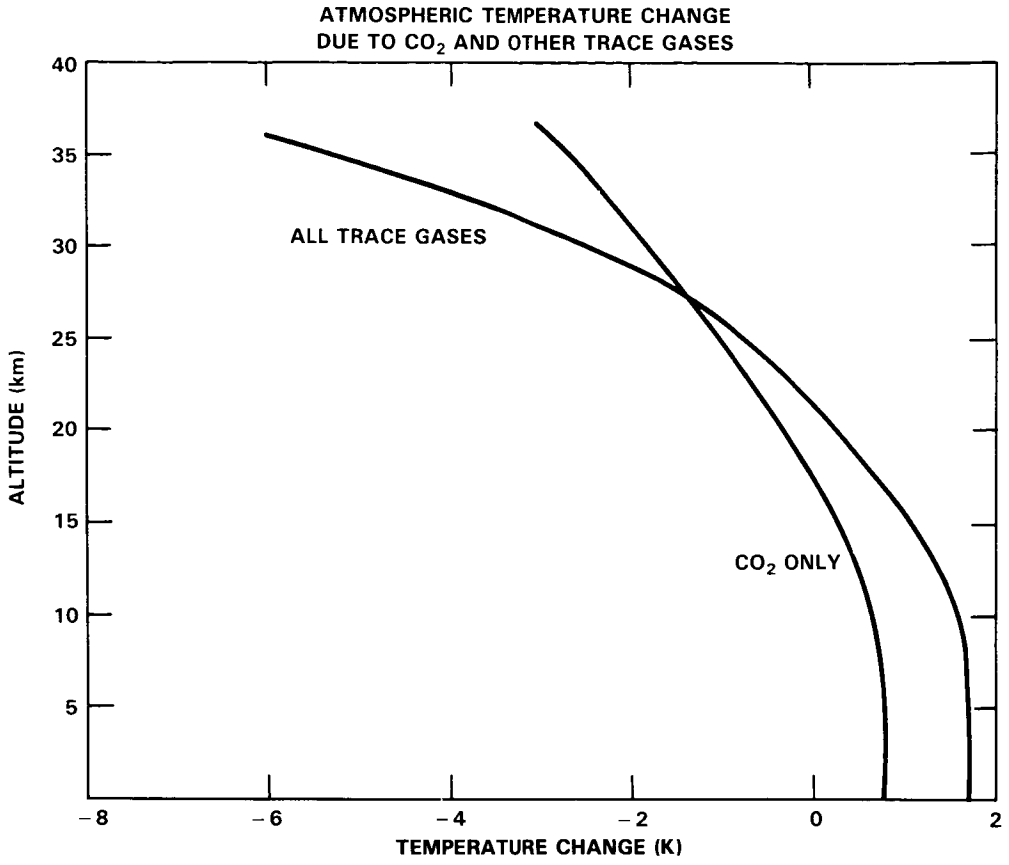

Figure 15-25. Atmospheric temperature change due to CO_2 and other trace gases. Radiative-convective model results employing the scenario in Table 15-8. (Source: Ramanathan *et al.*, 1985).

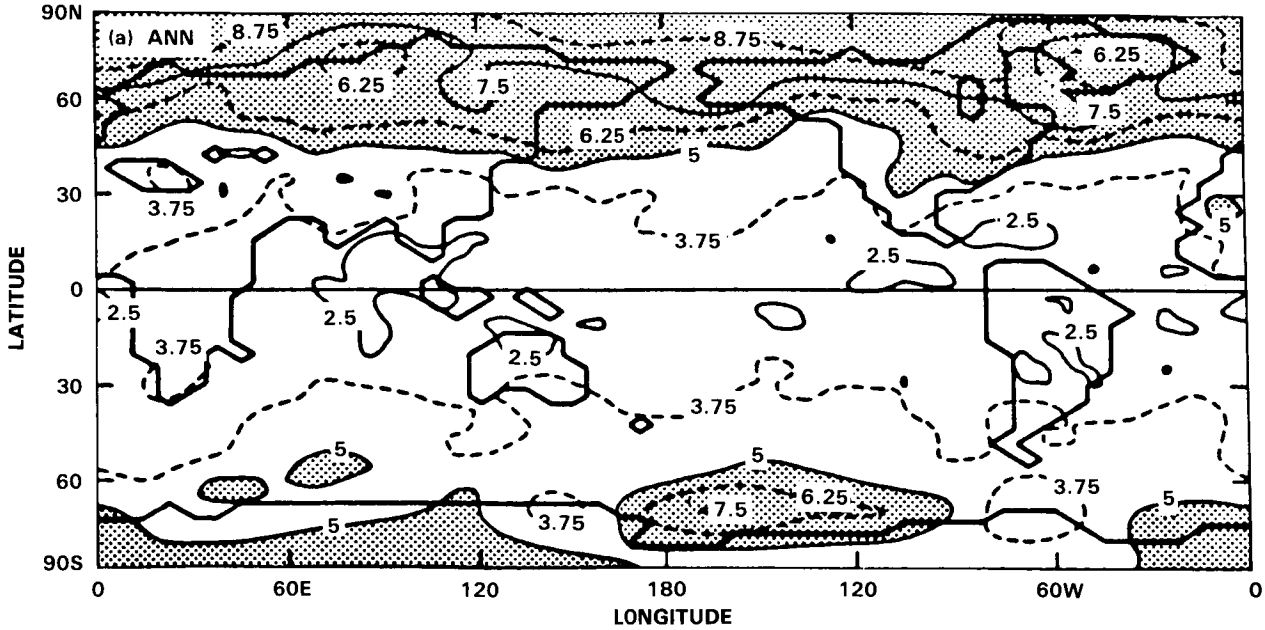

Figure 15-26. Geographical distribution of the annual mean surface air warming (°C) in the 4 × CO_2 experiment of Manabe and Stouffer (1980).

15.5.5 Equilibrium and Transient Temperature Response

The climate forcings discussed above are given in terms of the equilibrium ($t \rightarrow \infty$) response with no climate feedbacks. In order to convert these forcings to an expected temperature response, it is necessary to account for (1) climate feedback mechanisms, and (2) the finite response time of the climate system. As explained in Section 15.4, these two effects are not independent; a greater positive climate feedback leads to a longer climate response time. Also note that, although climate forcings usually can be computed with an accuracy of the order of 20 percent for a given change in atmospheric composition, the uncertainties in the strength of climate feedbacks and in the climate response time are much greater.

The transient temperature response involves additional complications because of the difficulty in properly accounting for the climate system's thermal inertia, which is due mainly to the large effective heat capacity of the oceans. Ocean circulation and mixing are not yet adequately observed, and ocean general circulation models are just reaching the point at which they can be applied to the transient climate problem. However, the essence of the ocean's effect in delaying the greenhouse warming can be demonstrated with a simple "box diffusion" model for the ocean (Oeschger *et al.*, 1975; Cess and Goldenberg, 1981; Hansen *et al.*, 1981). In this model, it is assumed that heat perturbations are rapidly mixed as a passive tracer into the deeper ocean in a way that can be approximated as one-dimensional diffusion. Although this model does not account for the buoyancy effects of sea-surface temperature changes in modifying the penetration depth of the radiative forcing, it provides a reasonable fit to the globally averaged results of a coupled ocean-atmosphere GCM (see Bryan *et al.*, 1984 for further elaboration of this issue). The effective diffusion coefficient is estimated from measurements of transient tracers to be κ = 1-2 $cm^2\ s^{-1}$ (Oeschger *et al.*, 1975; Ostlund *et al.*, 1976; Broecker *et al.*, 1980). The resulting relationships between equilibrium climate sensitivity, vertical diffusion coefficient and ocean response time have been illustrated in Section 15.4 above.

The expected warming of the ocean mixed layer is shown in Figure 15-27a for the trace gas scenario Case A (current growth rates for CO_2, CH_4, N_2O, CF_2Cl_2 and $CFCl_3$ plus an allowance for other trace gases) and in Figure 15-27b for the trace gas scenario Case B (reduced growth rates, only CO_2, CH_4, N_2O, CF_2Cl_2 and $CFCl_3$ included). In both cases, results are shown for two values of equilibrium climate sensitivity [$\Delta T_s(2 \times CO_2)$ = 2 K and 4 K] and for two values of the vertical diffusion coefficient (κ = 1 $cm^2\ s^{-1}$ and 2 $cm^2\ s^{-1}$).

In order to facilitate interpretation of the transient results, the equilibrium ΔT_s results are summarised below for the model with ΔT_s ($2 \times CO_2$) = 2 K. For the 1850–1980 period, both Case A (Figure 15-27a) and Case B (Figure 15-27b) have an equilibrium ΔT_s of 0.9 K (see major conclusion no. 3 in Section 15.5.2). For the 1980-2030 period, the equilibrium ΔT_s for Case A and Case B are about 1.8 and 1.1 K respectively (as inferred from Figure 15-23). Hence the range in equilibrium ΔT_s, in view of the range in climate sensitivity given by Equation (3), is 0.7 to 2 K for the 1850 - 1980 period while for the 1980 - 2030 period the range is 0.8 to 2.4 K for Case B and is 1.4 to 4.1 K for Case A.

These models show a warming of the mixed layer between 0.4 and 0.8 K for the period 1850-1980. This range is not inconsistent with the estimated increase of 0.54-0.6 K in Northern Hemisphere surface air temperature in that period (Kelly *et al.*, 1984; also see Figure 15-1). While the agreement with observed temperature trends is encouraging, it is difficult to conclude much from this comparison because (1) other climate forcings are likely to have operated over this time scale; for example, variations in stratospheric and tropospheric aerosols, changes in ground albedo due to desertification and changes in forest cover, and possible variations of solar irradiance are some of the other important radiative forcings; (2) the observations of surface air temperature are uncertain because of poor spatial coverage, especially in the nineteenth

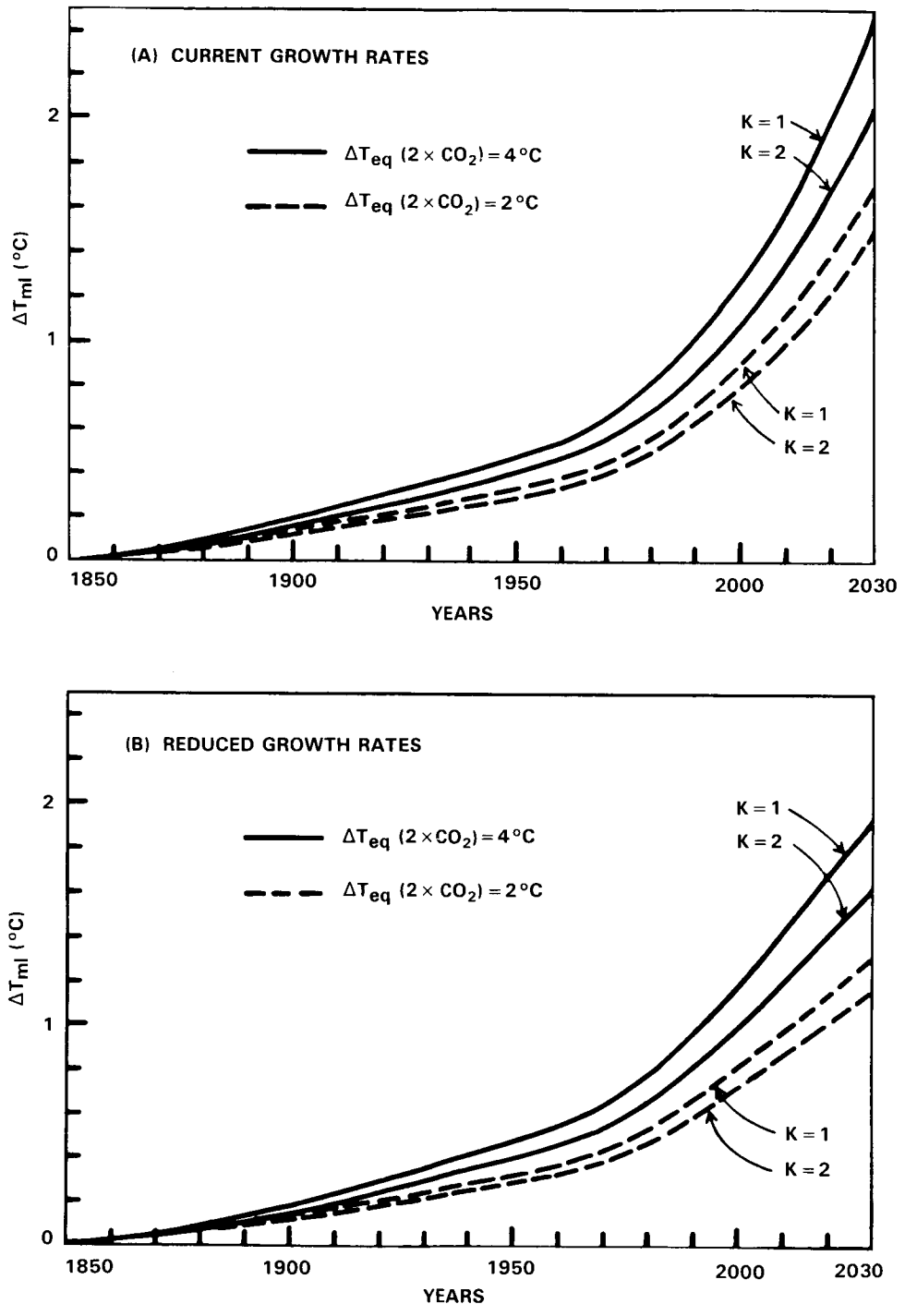

Figure 15-27. Ocean mixed layer temperature response to the two trace gas scenarios in Table 15-10 in a 1-D radiative/convective model with a box-diffusion ocean: (a) Case A (current growth rates for CO_2, CH_4, N_2O, CF_2Cl_2, and $CFCl_3$ plus an allowance for other trace gases), and (b) Case B (reduced growth rates with only CO_2, CH_4, N_2O, CF_2Cl_2, and $CFCl_3$ included). Results are shown for two values of the equilibrium climate sensitivity and two values of the vertical diffusion coefficient (in cm^2s^{-1}).

century; (3) these model calculations refer to the ocean mixed layer, while observations are of surface air over land and ocean; this surface air temperature may be more sensitive than the mixed layer temperature; for example, in three-dimensional doubled CO_2 experiments with fixed ocean temperature the global surface air temperature increased by about 0.3 K.

The computed surface-air temperature change for the period from 1850 to 2030 is in the range of 1.2 to 2.4 K (see the lowest estimate in Figure 15-27b and the largest estimate in Figure 15-27a). The equilibrium change for the cases shown in Figure 15-27 is in the range of 2 to 5.4 K and the difference between the two ranges reflect the potential influence of the oceans in delaying the "signal." If the oceans indeed have a significant delaying effect on the equilibrium warming, and if the decadal rates of increase in trace gas concentrations continue unabated (at the present rates) for the next several decades, then the climate system would be increasingly in a state of disequilibrium with the radiative forcing by the trace gases (Hansen *et al.*, 1984).

15.5.6 Conclusions

The assessment presented here reveals the following features:

(a) From the pre-industrial era to the 1950's, the greenhouse effect of CO_2 was the major source of anthropogenic impact on climate; this picture changed drastically since the early 1960's. During the last two decades or so, trace gases other than CO_2 have begun to contribute as much as the CO_2 increase to the upward trend in anthropogenically induced radiative forcing.

(b) The cumulative effect of the increase in CO_2 and other trace gases for the period from 1850-1980 is an equilibrium surface warming of 0.7 to 2 K, where the threefold uncertainty is due to current uncertainties in climate sensitivity. The contribution of the non-CO_2 trace gases to the cumulative equilibrium surface warming is about 30% (see the results cited under major conclusion no. 3 in Section 15.5.2). Time dependent calculations with a box-diffusion ocean model suggest that about 0.4-0.8 K of the (0.7 to 2 K equilibrium value) surface warming should have occurred during 1850 to 1980.

(c) A variety of scenarios that employ the upper and lower range of the observed growth rates of trace gas concentrations or their emission rates, show that if the current growth rates of trace gases continue unabated for the next several decades, trace gases other than CO_2 can have as much impact as CO_2 on future trends of surface-troposphere-stratosphere temperatures. For the various trace gas scenarios considered in this study, the equilibrium surface warming for the period 1980 to 2030 range from 0.8 to 4.1 K. This wide range is due to the range in the assumed scenario as well as that due to the uncertainty in climate model sensitivity.

(d) Thus for the 180 year period from 1850 to 2030, our assessment suggests a trace gas induced cumulative equilibrium surface warming in the range of 1.5 to 6.1 K. Because of the huge thermal inertia of the world oceans, only about 40 to 50% of the above equilibrium warming will be realized by the year 2030. Consequently, if the current rate of increase in trace gas concentrations continue unabated for the next several decades the climate system would be increasingly in a state of disequilibrium with the radiative forcing by the trace gases.

(e) In addition to CFC11, CFC12, CH_4, N_2O and O_3, radiatively active gases with long lifetimes of the order of 100-500 years (F13, F114, F115, F14, F13B1; see Table 15-8) may also become important

if their growth rates increase for the next several hundred years. The current concentrations of these gases are so small that they are projected to have a negligible impact on a 50-100 year time scale.

15.6 SCIENTIFIC CHALLENGES FOR THE FUTURE

The basic theme that emerges out of the discussions thus far is that the climatic effects of trace gases other than CO_2 are largely determined by the interactions between radiation, air-chemistry, transport of gases and large scale dynamics. The primary challenge then is to improve our understanding of the role of the above interactions in governing the observed distributions of temperatures and trace gases; and more importantly, improve our insights into their role in governing the sensitivity of the climate system to anthropogenic perturbations. Our current understanding of the above interactions is largely derived from globally averaged 1-D models or from highly parameterized zonally averaged 2-D models.

In what follows, the discussions will focus more on the challenges that are unique to trace gases other than CO_2. Hence, we do not cover some fundamentally important modeling issues such as cloud-feedback and the role of oceans; these issues are covered in ample detail in documents related to the CO_2-climate problem.

15.6.1 Theoretical and Modeling Issues

15.6.1.1 Interactions in the Troposphere

Additions of both chemically active gases (e.g., CO, NO_x) and radiatively active gases (e.g., CH_4) were shown to lead to substantial increases in tropospheric O_3 and CH_4 which in turn enhance the greenhouse effect. This indirect climate effect was shown to be as large as the direct radiative effect (Section 15.3). Furthermore, CH_4 and O_3 concentrations were also modulated by the feedback between temperature and H_2O. The principal constituents that are responsible for these chemistry-climate interactions in the troposphere are the radicals OH and HO_2. These interactions, which are illustrated schematically in Figure 15-28, are not only important for understanding climate sensitivity to trace gases but are also important for understanding the causal mechanisms for the observed trends in CH_4 and O_3. Many of the gases shown in Figure 15-28 have strong spatial and temporal variations. Hence, current analyses of these interactions, which are largely based on 1-D models, should be viewed merely as illustrative of the potential importance of the interactions (shown in Figure 15-28).

As a first step towards a more quantitative understanding of the interactions, the following key issues should be addressed:

(i) The relative role of transport and chemistry in governing the behavior of O_3, NO_x, CO (and others in Figure 15-22) should be determined. The transport processes include: downward transport of O_3 and NO_x from the stratosphere, upward transport of pollutants (e.g., CO) from the boundary layer, and lateral transport. A quantitative study of this issue requires not only interactive transport-chemistry models, but also simultaneous measurements of O_3, NO_x, CO and H_2O (as a minimum set) at a few selected locations to verify the model assumptions and simulations (Levy *et al.*, 1985).

(ii) Since the T-H_2O feedback is an important issue for the chemistry involving OH and since the temperature change (due to the trace gas greenhouse effect) is expected to be a strong function of latitude, attention should be given to the latitudinal and seasonal dependence of the interactions in Figure 15-22.

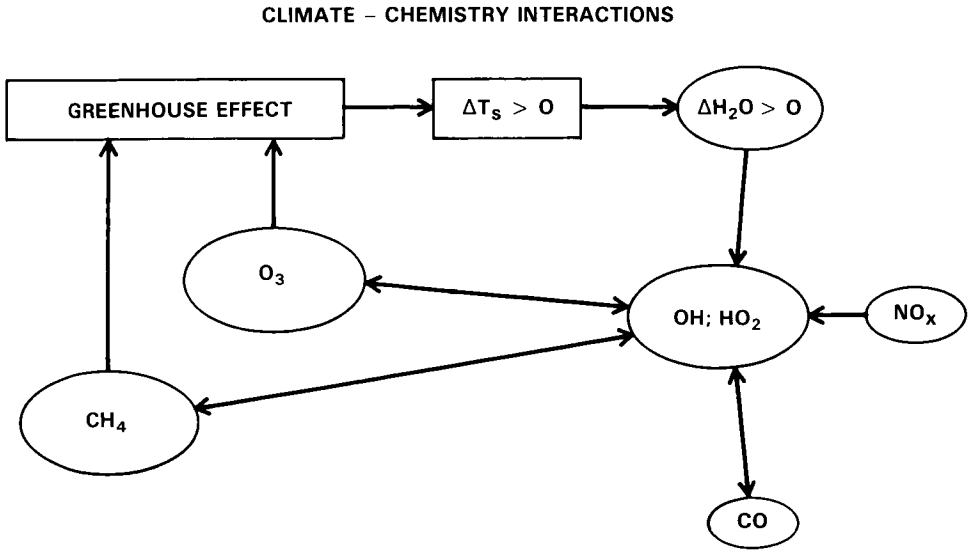

Figure 15-28. Schematic of the climate-chemistry interactions involving OH and HO_2 chemistry in the troposphere. Surface temperature increase ($\Delta T_S > 0$) due to the greenhouse effect of trace gases (including CO_2) leads to an increase in H_2O which contributes to an increase in OH. The addition of NO_X, CO and CH_4 reacts with OH and HO_2 to alter CH_4 and tropospheric O_3 which in turn modulates the greenhouse effect.

(iii) The response of biogenic source molecules such as CH_4 and N_2O to surface temperature changes are not well known and should be examined for their potential role as a feedback mechanism.

15.6.1.2 Sensitivity of Stratospheric H_2O

An important issue that has repeatedly come up during the last five years but still has not received a careful scrutiny concerns the sensitivity of stratospheric H_2O to perturbations in tropical tropopause temperatures. As discussed in earlier sections, GCMs and other models reveal the tropical tropopause temperatures to be quite sensitive to perturbations in CO_2, CFCs and O_3. However, current studies have focused largely on zonal average temperatures, whereas the entry of low levels of H_2O into the stratosphere may depend on the extreme (cold) tropical tropopause temperatures rather than the zonally averaged value. Model studies with a special emphasis on the geographical regions where H_2O enters the stratosphere in conjunction with special observational programs (for determining H_2O, temperature and cloud distribution) are needed to shed new insights on this problem.

15.6.1.3 Interactions in the Stratosphere

The continued growth of halogenated hydrocarbons in the troposphere presages reduced O_3 in the stratosphere. The subsequent effects of such changes on atmospheric opacity, thermal and dynamical structure in the stratosphere, and stratosphere-troposphere exchange bear directly on concerns about climate-chemistry issues. For example, the radiative effect of stratospheric O_3 perturbation due to CFCs can add as much as 30% to the surface warming due to the direct greenhouse effect of CFCs. Furthermore, latitudinal effects of the O_3 change on thermal structure are important. To date, most of the coupled radiative-chemical calculations of O_3 change have been performed with 1-D models. There is a strong need to develop coupled radiative-chemical-dynamical models (both 2-D and GCMs) and to examine the full scope of the climate-chemistry impact on tropospheric climate.

15.6.2 Observational Challenges

One of the most challenging issues on the observational front is the accurate determination of the long term (decadal) trends in CH_4, N_2O, CO, HO_x, NO_x, tropospheric and stratospheric O_3 and finally, tropospheric and stratospheric H_2O. As mentioned repeatedly in this report, there are significant uncertainties in our current estimates of the rate of growth of CO, O_3 and NO_x. The main source of the problem is the significant spatial and temporal variation of CO, O_3 and NO_x. The primary challenge is to design a strategy that will minimize the sampling errors, and such strategies can only evolve from active interactions between modeling and observational groups. The measurements of the above gases are also crucial for validating coupled transport-chemistry models.

Another equally challenging issue is the determination of trends in the radiative forcing (of the climate system) and the constituents that contribute to the radiative forcing. Included in this category are: solar radiation and its spectral variation at the top-of-the atmosphere, planetary albedo and its spectral distribution in 2 or 3 wavelength regions (e.g., UV, visible and IR), stratospheric aerosols, tropospheric aerosols including arctic haze, and important radiatively-active trace gases including CO_2, CH_4, N_2O, O_3 vertical distribution, F11, F12, F22, CH_3CCl_3, and stratospheric H_2O. Since the effects of aerosols, cloud-feedback and ice-albedo feedback are manifested in the planetary albedo, accurate determination of the planetary albedo should be one of the fundamental goals of future observational programs. The measurements described above are crucial for inferring the causal mechanisms for climate change. Of equal importance is continued monitoring of stratospheric, tropospheric and surface temperatures. These measurements, if they are made with high quality, excellent calibration and redundancy checks, can provide perhaps the only attractive approach for verifying the climate sensitivity of the models.

Finally, we have to develop and maintain an adequate spectroscopic data base for trace gases. For all of the CFCs and for a number of other compounds (e.g., CH_3CCl_3; PAN; CF_3Br) which have strong greenhouse effects, spectroscopic line parameters are either unavailable or unpublished. Furthermore, for the available data, there are significant discrepancies in the measured band strengths (e.g., F11 and F12 band strengths differ by 20 to 30% between different measurements). Moreover, current measurements do not separate out the contribution of the hot bands in the spectra; such identifications are crucial for incorporating the temperature dependence of the opacity in climate models. The availability of such measurements will promote line-by-line calculations which can then serve as a basis for treatment of the radiative effects of trace gases in climate models.

In preparing the ensuing assessment, the panel benefitted significantly from consultations with the following scientists: Dr. J.T. Kiehl for computing radiative heating due to trace gases; Dr. S. Liu for contributing to the subsection on NO_x and Drs. M. Geller, S. Manabe, F.S. Rowland, P.J. Crutzen, R.E. Dickinson, R. Gammon, A. Ghazi, N. Husson, M.A.H. Smith, N. Sundararaman, D. Wuebbles and R.T. Watson for their comments on the text. The panel thanks G. Escobar for preparing and proofreading the chapter.

ANNEX 1: ACCURACY OF BAND MODEL APPROACHES FOR CH_4

Band models may be divided into two categories: narrow-band models in which the longwave spectrum is divided into spectral intervals ranging from 1 cm^{-1} in width, and broad band models which employ analytical expressions either derived from theory or laboratory data to treat the absorption within the entire band. In the evaluation of a band model, two issues are involved: (1) the ability of the band model to accurately characterize the total band absorptance for a homogeneous optical path through the

gas (i.e., constant temperature and pressure), and (2) the ability of the band model to characterize absorption and emission along inhomogeneous paths (i.e., atmospheric applications). In order to treat inhomogeneous paths, a scaling approximation must be invoked in the band model.

The second item above is of particular importance with respect to broad-band models. Although several broad-band scaling approximations have been suggested (Chan and Tien, 1969; Cess and Wang, 1970; Edwards and Morizumi, 1970), there has not been a definitive examination of their accuracies.

The strategy of the present section is as follows. A reference line-by-line calculation will first be described, followed by the presentation of narrow-band and broad-band models that are tuned, for a homogeneous gas, to the line-by-line calculation. Thus, a hierarchy of band models is obtained, with these band models yielding virtually identical homogeneous band absorptances for the homogeneous case. The scaling approximations for the narrow-band and broad-band models are evaluated by applying the models to atmospheric profiles (the inhomogeneous case). Accompanying this will be a brief discussion concerning pitfalls associated with the use of narrow-band models.

The line-by-line calculations used the line locations and intensities from a JPL data tape (Orton and Robiette, 1980), with the line intensities being renormalized to a total band intensity of 129 $cm^{-2}atm^{-1}$ at 296 K (e.g., Varanasi *et al.*, 1983). The Lorentz half-width per unit pressure, γ^0, was taken to be

$$\gamma^0(cm^{-1}\ atm^{-1}) = 0.06\ (296/T) \tag{1}$$

for all lines, based upon Varanasi *et al.* (1983) who obtained a nitrogen-broadened value of 0.063 (with a standard deviation of 0.003) for 77 lines within the wavenumber interval 1300-1353 cm^{-1}. In that there are roughly 12,500 lines on the JPL tape, this comprises a rather extensive extrapolation. Although the line-by-line calculations serve as a reference, there are still some uncertainties associated with line-by-line model results because our knowledge of line half-widths is meager at best.

The narrow-band model is a modification of the Goody random band model (Goody, 1952), for which the transmittance of a spectral interval $\Delta\omega$ is given by

$$T_{\Delta\omega} = \exp\{-(S_{\Delta\omega}/\Delta\omega)[1 + (S_{\Delta\omega}\ w/\pi\gamma)]^{-1/2}\} \tag{2}$$

where $S_{\Delta\omega}$ is the sum of the line strengths within the interval, w is the absorber amount, and γ is defined by

$$S_{\Delta\omega}\gamma = C[\Sigma(\gamma S_{JK})^{1/2}]^2 \tag{3}$$

where S_{JK} denotes the individual line strengths and the summation is over all lines within $\Delta\omega$. Conventionally, $C = 4/\pi$ to be consistent with the limit of strong nonoverlapping lines (e.g., Goody, 1964). But if there is a significant number of coincident or near-coincident lines, $C < 4/\pi$ since coincident lines would be linearly summed. For present purposes, $\Delta\omega = 5\ cm^{-1}$, with elaboration on this choice to be given later.

Turning next to the broad-band model, that due to Ramanathan (1976) is adopted, for which the total band absorptance is expressed by

$$A = 2A_0 \ln\left[1 + \Sigma \frac{u}{\sqrt{4 + u(1 + 1/\beta}}\right] \tag{4}$$

where $u = Sw/A_0$ with S the total band intensity, A_0 is the bandwidth parameter, β is proportional to the ratio of a mean line half-width to a mean line spacing, and here the summation refers to the two overlapping $^{12}CH_4$ and $^{13}CH_4$ isotope bands.

The relevant coefficients appearing within both the narrow-band and broad-band models have been evaluated through regression fits to homogeneous-gas line-by-line calculations, with the result that

$$C = 0.762 \tag{5}$$

$$A_0(cm^{-1}) = 102.8(T/300) \tag{6}$$

$$\beta = 0.0838(300/T) \tag{7}$$

As discussed above, one would anticipate that $C < 4/\pi = 1.273$ if coincident lines are a factor, which may indeed be the case for the ν_4 band due both to line splitting and the presence of a Q branch. But the considerable difference between Equation (5) and $C = 4/\pi$ might include other factors as will shortly be discussed.

A comparison of both the narrow-band and broad-band models with the line-by-line results is illustrated in Figure 15-29. A single curve is used for both band models since there is no distinguishable difference between them. Similar agreement with the line-by-line results exists for temperatures spanning the range from 220 K to 300 K.

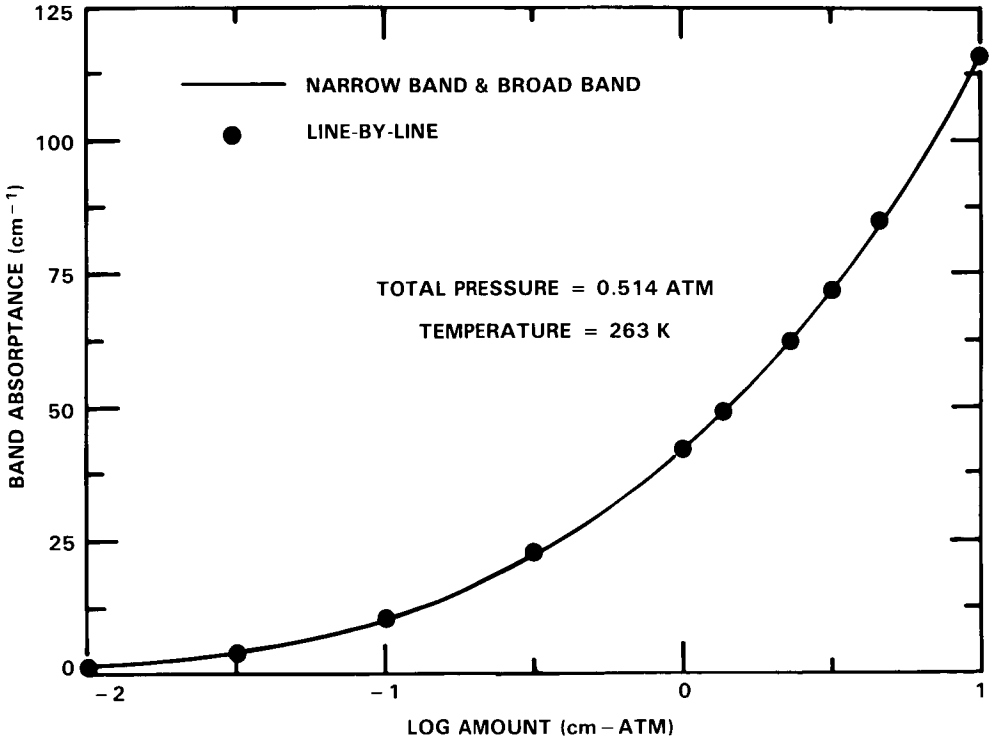

Figure 15-29. Comparison of narrow-band, broad-band and line-by-line determinations of the CH_4 total band absorptance. The CH_4 amount in cm-atm refers to STP.

As discussed in more detail by Cess *et al.* (1985), the virtual equivalence of the band models with the line-by-line calculations allows an evaluation of band-model scaling approximations. For this purpose the McClatchey *et al.* (1971) midlatitude summer atmosphere has been employed, neglecting overlap with water vapor and clouds. Table 15-12 summarizes calculations for the reduction in infrared flux at the top of the model atmosphere (25 km), at the tropopause (13 km), and at the surface, for an increase in methane volumetric mixing ratio from 1.75×10^6 to 3.5×10^6.

The use of Curtis-Godson scaling within the narrow-band model is as described by Rodgers and Walshaw (1967). Although this two-parameter scaling is exact in the weak-line and strong-line limits, the present atmospheric methane abundance lies between these two asymptotic limits. Thus, methane serves as a good test of Curtis-Godson scaling, and Table 15-12 confirms the validity of this often-used scaling approximation.

For the broad-band model, three different three-parameter scaling approximations are compared in Table 15.12 (Chan and Tien, 1969; Edwards and Morizumi, 1970; Cess and Wang; 1970). All three scaling approximations overestimate the flux reduction at the surface, with Chan-Tien scaling producing the smallest errors for the three flux reduction calculations.

On a similar point, several band models which have been employed in atmospheric radiation calculations are compared in Table 15.13 with the line-by-line results. These include the conventional random band models of Goody (1952) and Malkmus (1967), the broad-band model of Donner and Ramanathan (1980), and a broad-band model due to Cess and Chen (1975) which they developed for Jovian applications, but which was utilized for terrestrial applications by Hameed *et al.* (1980). The primary failing of the latter band model can be traced to the assumption by Cess and Chen (1975) that individual multiplets could be treated as a single Lorentz line; i.e., they neglected line splitting.

Returning to the narrow-band model, the present CH_4 example serves to illustrate certain pitfalls associated with random band models. Consider first the present choice of 5 cm^{-1} intervals. As pointed out by Kiehl and Ramanathan (1983) for CO_2, significant errors occur if one employs spectral intervals greater than 10 cm^{-1}. This is due to the statistics of the band, as manifested by the averaging procedure of Equation (3), being variable throughout the band. One way of minimizing this effect is to choose small

Table 15-12. Comparison of model calculations for the change in infrared flux due to an increase in CH_4 mixing ratio from 1.75×10^6 to 3.5×10^6. The respective scaling approximations are listed in brackets, while the numbers in parentheses denote the percentage differences from the line-by-line values.

Model	Flux Reduction (W/m^2) Top	Tropopause	Surface
Line-by-Line	1.78	1.78	2.40
Narrow Band [Curtis-Godson]	1.79 (0.6)	1.78 (0.0)	2.41 (0.4)
Broad Band [Chan-Tien]	1.77 (−0.6)	1.78 (0.0)	2.61 (8.8)
Broad Band [Edwards-Morizumi]	1.79 (0.6)	1.79 (0.6)	2.63 (9.6)
Broad Band [Cess-Wang]	1.85 (3.9)	1.83 (2.8)	2.67 (11.3)

Table 15-13. Comparison of model calculations for the change in infrared flux due to an increase in CH_4 mixing ratio from 1.75×10^6 to 3.5×10^6. Curtis-Godson scaling is used for the Malkmus and Goody models, while Chan-Tien scaling is employed for the Donner-Ramanathan and Cess-Chen models. The numbers in parentheses denote the percentage differences from the line-by-line values.

Model	Flux Reduction (W/m^2) Top	Tropopause	Surface
Line-by-Line	1.78	1.78	2.40
Malkmus	1.99 (11.8)	1.97 (10.7)	2.61 (8.8)
Goody	2.05 (15.2)	2.04 (14.6)	2.72 (13.3)
Donner-Ramanathan	1.55 (−12.9)	1.57 (−11.8)	2.17 (−9.6)
Cess-Chen	1.00 (−43.8)	1.00 (−43.8)	1.44 (−40.0)

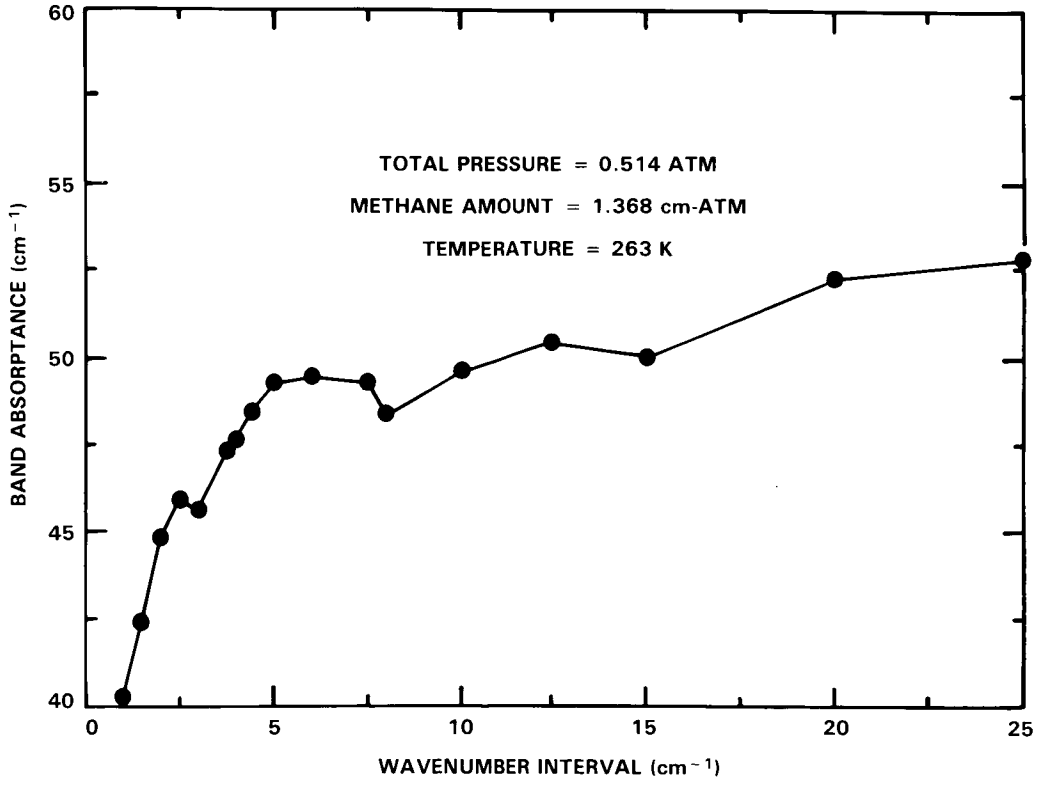

Figure 15-30. Narrow-band CH_4 total band absorptance as a function of wavenumber interval ($\Delta\omega$) as employed within the narrow band model. The methane abundance of 1.368 cm-atm (at STP) coincides with the atmospheric column abundance for a CH_4 mixing ratio of 1.75×10^{-6}.

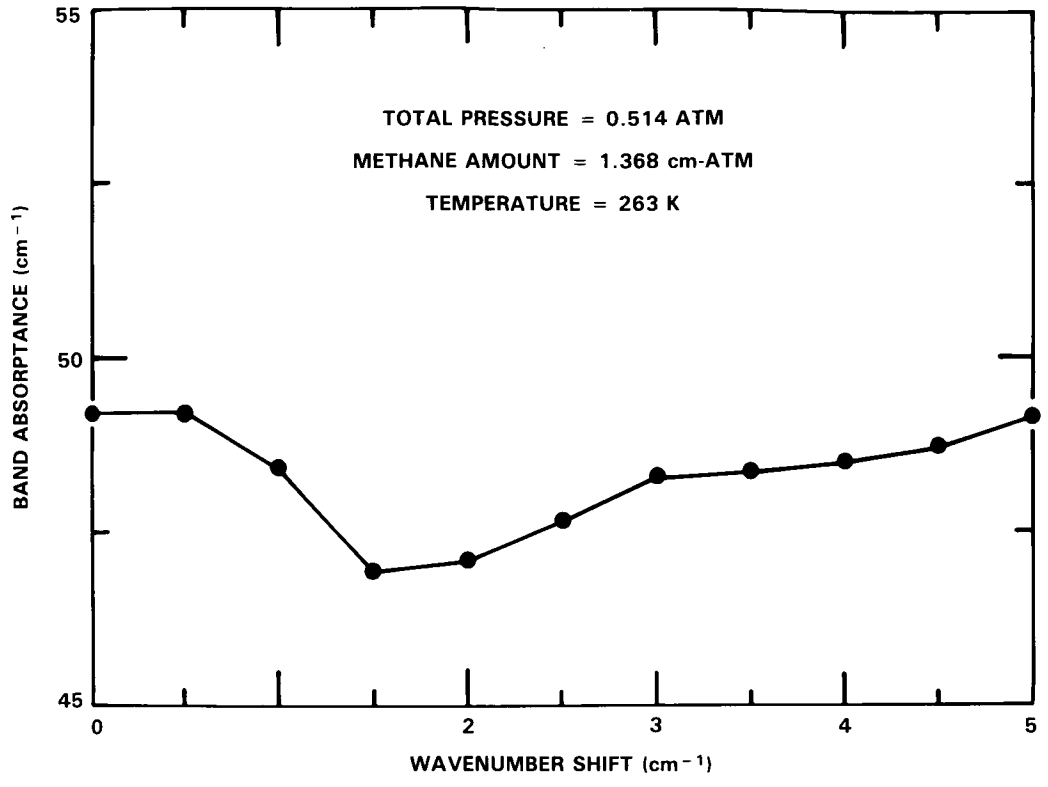

Figure 15-31. Narrow-band CH_4 total band absorptance for $\Delta\omega = 5 cm^{-1}$ and as a function of wavenumber shift of the interval spacing. The methane abundance of 1.368 cm-atm (at STP) coincides with the atmospheric column abundance for a CH_4 mixing ratio of 1.75×10^{-6}.

intervals with the hope that this will produce near-uniform statistics within each interval. But if the intervals are too small, there will not be a sufficient number of lines within each interval to yield meaningful statistics.

Ideally, one would anticipate that there should be an interval range over which the computed band absorptance is invariant to the choice of interval size, with the intervals being sufficiently large so as to contain a statistically meaningful number of lines, but at the same time sufficiently small so that Equation (3) produces meaningful statistical averages. However, as illustrated in Figure 15-30, CH_4 does not produce such a clearly defined range of intervals. The small plateau from roughly 5 to 8 cm^{-1} was the sole motivation for our choice of a 5 cm^{-1} interval size.

A second issue concerns the location of the intervals. Figure 15-31 illustrates a band absorptance calculation in which the locations of the interval spacings ($\Delta\omega$ = 5 cm^{-1}) are progressively shifted, with a shift of 5 cm^{-1} denoting a return to the original interval locations. For example, wavenumber shift = 0 corresponds to interval locations of 1200-1205 cm^{-1}, etc., while for wavenumber shift = 1 cm^{-1} these are 1201-1206 cm^{-1}, etc. As may be seen in Figure 15-31, this can result in a 5 percent variation in band absorptance, an effect that is again related to a variation in band statistics within the 5 cm^{-1} intervals as the interval positions are shifted.

In addition to the problem of coincident or near-coincident lines, as previously discussed with respect to Equation (3), the effects portrayed within Figures 15-30 and 15-31 additionally influence the evaluation

of C as given by Equation (5). For this reason, the present narrow-band models should not be applied to conditions well removed from those for which Equation (5) was evaluated.

As a final point, it must be emphasized that CH_4 represents an extreme case concerning the points raised with respect to Figures 15-30 and 15-31, since the ν_4 band possesses both line splitting and a Q branch. Experience with vibration-rotation bands of other gases (D.P. Kratz and R.D. Cess, private communication) indicates that these problems are somewhat less severe in the absence of line splitting, and are considerably less severe in the absence of both line splitting and a Q branch.